

Investigation of Electrochemical Combustion Plant
for Rural Water Disinfection
and Industrial Organic Effluent Removal

by

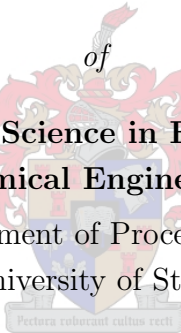
Martin Cronje

Thesis submitted in partial fulfillment
of the requirements for the Degree

of

**Master of Science in Engineering
(Chemical Engineering)**

in the Department of Process Engineering
at the University of Stellenbosch



Supervised by

Prof. J.H. Knoetze

Prof. R.D. Sanderson

Stellenbosch

April 2004

Declaration

I, the undersigned, hereby declare that the work contained in this thesis is my own original work and has not previously in its entirety or in part been submitted it at any university for a degree.

Signature

Date



Abstract

Recent years have seen the development of various treatment methods for the purification of industrial waste waters due to the increased demand for reduced pollutant effluents. Aqueous waste streams containing toxic organic compounds are of special interest, since conventional treatment methods such as biological waste treatment can not always be used. Other popular treatment methods are often ineffective. Catalytic oxidation of organic wastes has been investigated since the 1960s with varying degrees of success. A major problem associated with this method is the high temperatures and pressures required to improve the activation energies involved. Electrochemical oxidation has become a popular method in the literature of treating these wastes, since the applied voltage determines the activation energy, and therefore the process can often be performed at ambient conditions.

This thesis investigates the capability of a unique reactor system in the treatment of these wastes. The reactor utilises proton-exchange membrane technology to eliminate the requirement of conductivity in treated waste streams; thus the membrane serves as a solid electrolyte. The reactor system has therefore been referred to as a solid-polymer-electrolyte reactor. Novel metal oxide anodes are responsible for the oxidation of the organic molecules. These metal oxide catalysts show promise in the treatment of a wide variety of organic wastes. A SnO_2 catalyst doped with ZrO_2 is used as anode in this study. Dopants are added to the catalyst to improve properties such as catalytic activity and conductivity.

Kinetic data was obtained on a wide range of values for the chosen experimental parameters (current density and flow rate). Phenol, an organic molecule often referred to in the literature as model contaminant due to its resistance to oxidation,

was also used as contaminant in this study. The use of the reactor system in the disinfection of water containing selected pathogens, were included in the experimental work. This kinetic data served in the development of a simple model of the process, and provided the basis for a full analysis regarding potential scale-up and economic feasibility.

A requirement of the study was the accurate determination of the various oxidation breakdown products of phenol. This led to the refinement of an HPLC analytical method in order to quantitatively determine these products.

The full analysis showed that the current reactor system would not be economically viable — mainly due to very long reactor lengths required for the complete removal of all organic material. Both mass transfer and charge transfer at the chosen experimental conditions influenced the electrochemical oxidation of phenol. High pressure drops, causing low flow rates in the reactor, accounted for this because of the narrow flow channels required in the reactor. Some catalyst deactivation was also suspected to affect the overall reaction, but the full extent of the deactivation was not investigated thoroughly.

There is still room for improvement in the electrochemical oxidation of organic wastes. The design of the flow channels, a factor that was not investigated, can significantly improve efficiency. Another aspect that was not investigated was the catalyst type. The catalyst has been identified in the literature as the main contributing factor to the success of the oxidation reaction. A wide variety of metal oxide catalysts are currently being researched and may improve the kinetics of the process even further. Further improvement needs to be made on the membrane/electrode assembly to improve current density distribution.

Every improvement of the process in terms of the reactor design and catalyst will impact on the economics of the process, thus making the process more competitive with current treatment technologies.

Opsomming

In die afgelope paar dekades, is daar 'n wye verskeidenheid metodes ontwikkel wat gebruik kan word om industriële afvoer strome te behandel. Hierdie ontwikkeling het plaasgevind as gevolg van die verhoogde eis aan skoner afvoerstrome. Wateragtige afvoerstrome wat organiese verbindings bevat, is van besondere belang omdat hierdie tipe strome soms besonders moeilik kan wees om te behandel. Gebruiklike metodes is in die meeste gevalle ongeskik vir behandelings-doeleindes. Katalitiese oksidasie is sedert die 1960's gebruik, maar hierdie prosesse benodig dikwels hoë drukke en temperature om suksesvol te wees. Elektrochemiese oksidasie het intussen 'n populêre behandelingsmetode geword, aangesien die aktiveringsenergie vir die oksidasieproses hoofsaaklik afhanklik is van die aangewende potensiaal en dus kan die proses by atmosferiese toestande gebruik word.

In hierdie tesis word die geskiktheid van 'n unieke reaktorstelsel vir water-suiwering ondersoek. Die reaktor gebruik 'n proton-uitruilings-membraan om die behoefte vir konduktiwiteit in die water uit te skakel. Die membraan dien dus as 'n tipe soliede elektroliet en as gevolg hiervan word na die reaktorstelsel verwys as 'n soliede-polimeer-elektroliet reaktor. Nuwe metaal-oksied anodes word in die reaktor gebruik aangesien hulle belowende resultate toon in die oksidasie van organiese verbindings. In die navorsing, is 'n SnO_2 katalis wat klein hoeveelhede ZrO_2 bevat gebruik. Oksiede soos ZrO_2 word dikwels gebruik om die aktiwiteit en konduktiwiteit van hierdie kataliste te bevorder.

Kinetiese data is oor 'n wye bereik van parameter waardes ingesamel. Die hoof parameters in die eksperimentele werk was stroom digtheid en vloeitempo. Fenol, 'n komponent wat volgens die literatuur in hierdie tipe van werk gebruik word, is

as die besoedelende komponent gekies. Die doeltreffendheid van die reaktor in die ontsmetting van water, wat met 'n verskeidenheid skadelike mikro-organismes besmet is, is ook getoets. 'n Eenvoudige model is opgestel m.b.v. die kinetiese data, waarna 'n volledige analise met betrekking tot grootskaalse bedryf en ekonomiese uitvoerbaarheid gedoen is.

'n Vereiste van die studie was om die konsentrasie van die afbreek-produkte van die oksidasie akkuraat vas te stel. As gevolg hiervan is 'n hoë-druk-vloeistof-chromatografie analitiese metode verfynd.

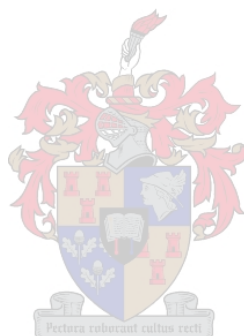
Die analise het getoon dat die reaktorstelsel nie ekonomies sou wees nie. Een van die hoofredes hiervoor is die onrealistiese reaktorlengtes wat benodig sou word. Resultate het getoon dat die reaksie deur beide massa-oordrag en lading-oordrag beïnvloed word. Hoë drukvalle in die reaktor wat gelei het tot lae vloeitempo's was hiervoor verantwoordelik. Die deaktivering van die katalis beïnvloed waarskynlik die reaksie, maar die deaktiveringsverskynsel is nie ten volle ondersoek nie.

Die reaktorstelsel kan verder verbeter word deur verskeie elemente van die reaktor te ondersoek. Die ontwerp van die vloeikanale in die reaktor is nie ondersoek nie en kan die werkverrigting van die reaktor verhoog. Uit die literatuur is gevind dat die tipe metaaloksied wat as katalis gebruik word, die reaksie direk beïnvloed. Dus kan navorsing wat tans op die kataliste gedoen word nuwe kataliste na vore bring wat meer doeltreffend sal wees. Laastens, is die huidige membraan/elektrode samestelling nog oneffektief en kan die reaktor-opstelling dus nog verbeter word.

Elke verbetering wat op die bogenoemde faktore van die reaktor ontwerp verkry word, sal die ekonomiese uitvoerbaarheid van die proses beïnvloed. So, sal die proses al meer kompetend met huidige behandelingsmetodes word.

Contents

Declaration	i
Abstract	ii
Opsomming	iv
Contents	vi
List of Tables	ix
List of Figures	xi
Nomenclature	xiii
Glossary	xvi
Acknowledgements	xvii
1 Introduction	1
1.1 Background	1
1.2 Motivation for Research	4
1.3 Objectives	4
2 Theoretical Principles and Literature Review	7
2.1 Electrochemical Reactors	7
2.1.1 Electrochemical Reaction Rates	9
2.1.2 Cell Potential	11
2.1.3 Electrode Kinetics	17
2.1.4 Electrode Mass Transfer Phenomena	19
2.1.5 Analogy to Chemical Kinetics	20
2.2 Reaction Mechanics	24
2.2.1 Overview of Reaction Mechanism	24
2.2.2 Phenol Oxidation	26
2.2.3 Electrode Passivation	28
2.3 Principles of the SPE Reactor	29
2.4 Electrode Preparation	33



2.4.1	Spray Pyrolysis	33
2.4.2	Thermal Decomposition	34
2.4.3	Sol-gel Dip-coating	34
2.5	Review of Previous Work	38
2.5.1	Grimm's Research	38
2.5.2	Other Research	39
2.5.3	Analysis of Literature Review	42
3	Materials and Methods	44
3.1	The Solid-Polymer-Electrolyte Reactor	44
3.1.1	Electrode Preparation	45
3.1.2	Proton Exchange Membrane	47
3.2	Reactor Layouts	49
3.2.1	Initial Work	49
3.2.2	Laboratory-scale Reactor	52
3.3	Microbiological Method	56
3.3.1	Introduction	56
3.3.2	Pathogen Selection	56
3.3.3	Experimental Method	57
3.4	Sample Analysis	59
4	Phenol Oxidation – Results and Discussion	64
4.1	Initial Work	65
4.2	Laboratory Experiments – Galvanostatic	69
4.2.1	Effect of Current Density	70
4.2.2	Effect of Flow Rate	73
4.2.3	Effect of the MEA Compression Factor	75
4.2.4	Anolyte-Catholyte Separation	76
4.2.5	Summary	78
4.3	Laboratory Experiments – Potentiostatic Operation	79
4.4	Laboratory Experiments – Titanium Current Collectors	85
4.4.1	Reaction Order Experiments	88
4.5	Conclusions	90
5	Microbiological Experiments	92
5.1	High-concentration Experiments	92
5.2	Low-Concentration Experiments	93
6	Application of Experimental Data	97
6.1	Reactor Model	97
6.1.1	Reservoir	98
6.1.2	Reactor	98
6.2	Discussion of Experimental Work	100
6.3	Scale-up Calculations	103
6.4	Economic Evaluation	107

7	Conclusions and Recommendations	113
	References	116
A	Model derivations	122
A.1	Reactor model	122
A.2	Scale-up Calculation	125
B	Miscellaneous Calculations	127
B.1	Reaction Rate Constants	127
B.2	Differential Method of Rate Analysis	127
B.3	Reactor Cost	128
C	Growth Curves	132
D	Technical Drawings	135
E	Experimental Measurements	142
E.1	Initial Work	142
E.2	Laboratory-Scale Experiments – Nickel	143
E.3	Laboratory-Scale Experiments – Titanium	150



List of Tables

2.1	Summary of method for determining reaction order	23
3.1	HPLC retention times for the phenolic compounds	61
3.2	Retention times for the aliphatic acids	63
4.1	Experimental parameter values for initial experiments	66
4.2	Rate constants for initial experiments	68
4.3	Summary of experimental parameters for galvanostatic experiments .	70
4.4	Experimental parameters for current density experiments	71
4.5	Reaction rate constants for current experiments	72
4.6	Experimental parameters for flow rate experiments	73
4.7	Reaction rate constants for flow rate experiments	73
4.8	Experimental parameters for MEA compression experiments	75
4.9	Reaction rate constants for stack pressure experiments	76
4.10	Reaction rate constants for separated electrolytes	77
4.11	Reaction rate constants for separated electrolytes	78
4.12	Reaction rate constants for potentiostatic experiments — with and without polarity change	85
4.13	Typical potential values for different currents	86
4.14	Reaction orders determined from the differential method	89
5.1	Reaction rate constants for microbiological experiments	96
6.1	Comparison of experimental reaction rate constants for different ex- periments	101
6.2	Calculated reactor lengths – nickel-plated current collectors	104
6.3	Calculated reactor lengths – titanium current collectors	104
6.4	Calculated reactor lengths – potentiostatic and microbiological exper- iments	105
6.5	Estimated capital costs of reactor (June 2003)	108
B.1	Data for the derivation of reaction orders (60 ppm)	128
B.2	Statistical data for polynomial fits	129
E.1	Initial experiments – total organic carbon values	142
E.2	Experimental readings (Re = 650, 20 mA, 15 lb-in, unseparated) . . .	143

E.3 Experimental readings (Re = 650, 35 mA, 15 lb-in, unseparated) . . . 143

E.4 Experimental readings (Re = 650, 50 mA, 15 lb-in, unseparated) . . . 144

E.5 Experimental readings (Re = 650, 50 mA, 15 lb-in, separated) 146

E.6 Experimental readings (Re = 1516, 50 mA, 15 lb-in, separated) . . . 147

E.7 Experimental readings (Re = 1516, 50 mA, 25 lb-in, unseparated) . . 148

E.8 Experimental readings (Re = 1516, 50 mA, 25 lb-in, unseparated) . . 149

E.9 Experimental readings (37.2 L/h ,20 mA) 150

E.10 Experimental readings (37.2 L/h, 30 mA) 151

E.11 Experimental readings (37.2 L/h, 40 mA) 152

E.12 Experimental readings (37.2 L/h, 50 mA) 152

E.13 Experimental readings (25.7 L/h, 20 mA) 153

E.14 Experimental readings (25.7 L/h, 30 mA) 154

E.15 Experimental readings (25.7 L/h, 40 mA) 154

E.16 Experimental readings (25.7 L/h, 50 mA) 155

E.17 Experimental readings (11.5 L/h, 20 mA) 156

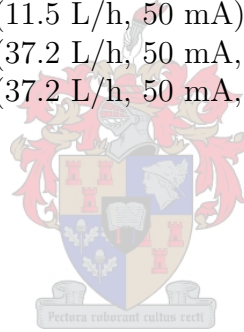
E.18 Experimental readings (11.5 L/h, 30 mA) 156

E.19 Experimental readings (11.5 L/h, 40 mA) 157

E.20 Experimental readings (11.5 L/h, 50 mA) 158

E.21 Experimental readings (37.2 L/h, 50 mA, 60 ppm) 158

E.22 Experimental readings (37.2 L/h, 50 mA, 40 ppm) 159



List of Figures

2.1	Parts of an electrochemical cell	8
2.2	Voltage components in an electrochemical cell.	12
2.3	Semilogarithmic plot for determination of i_0 and the Tafel slope.	19
2.4	Determination of reaction rate constants for different reaction orders.	23
2.5	Proposed phenol oxidation to carbon dioxide and water (ref. [5])	27
2.6	Phenol oxidation and polymerization pathways (ref. [29])	30
2.7	Parts of an SPE reactor	31
2.8	Normalised experimental data reported from the literature	43
3.1	SEM photograph of catalyst (2500x)	47
3.2	SEM photograph of catalyst (5000x)	48
3.3	Reactor flow system used in the initial work	50
3.4	Experimental set-up for the laboratory scale experiments.	53
3.5	Photographs of the laboratory-scale electrochemical cell.	55
3.6	HPLC chromatogram of the standards for phenolic compounds	60
3.7	Chromatogram of acid standards	61
3.8	HPLC chromatogram of initial acid sample (1)	62
3.9	HPLC chromatogram of initial acid sample (2)	62
3.10	HPLC chromatogram of final acid sample	62
4.1	Breakdown curve for 500 L/h experiment	66
4.2	Breakdown curve for 600 L/h experiment	67
4.3	Breakdown curve for 700 L/h experiment	67
4.4	Effect of current density	72
4.5	Effect of flow rate on reaction rate	74
4.6	Effect of MEA compression on reaction rate	75
4.7	Effect of electrolyte separation on reaction rate	77
4.8	Results of potentiostatic experiments	80
4.9	Normalised potentiostatic experimental results	80
4.10	Theoretical vs practical conversion	81
4.11	Potentiostatic breakdown curve (polarity changed)	83
4.12	Normalised potentiostatic breakdown curve (polarity changed)	83
4.13	Theoretical vs practical conversion (polarity change)	84
4.14	Concentration vs time curves for a flow rate of 37.2 L/h using titanium current collectors	87

4.15 Concentration vs time curves for a flow rate of 25.7 L/h using titanium current collectors	87
4.16 Concentration vs time curves for a flow rate of 11.5 L/h using titanium current collectors	88
5.1 Disinfection of high concentration samples	93
5.2 Disinfection of various micro-organisms	94
5.3 Disinfection of <i>Salmonella</i>	95
5.4 Disinfection of <i>E. Faecallis</i>	95
6.1 Reaction rate constants for titanium and nickel-plated current collectors	102
6.2 Proposed flow diagram for pilot plant	106
6.3 Reactor conversion versus reactor length	107
6.4 Reactor length versus recycle ratio for $X = 0.75$	111
6.5 Cost of various parts of a typical reactor (June 2003)	112
A.1 Nomenclature used in model derivation	122
A.2 Nomenclature used for reactor	124
B.1 Determination of reaction order – example	130
C.1 Growth curve for <i>E. Faecallis</i> : Absorbence and cell count	133
C.2 Growth curve for <i>E. Faecallis</i> at various TSB concentrations	133
C.3 Growth curve for <i>Salmonella</i> at various TSB concentrations	134
C.4 Growth curve for <i>E. Coli</i> at various TSB concentrations	134
D.1 Technical drawing showing initial reactor current collector	136
D.2 Technical drawing of initial reactor anodic frame	137
D.3 Technical drawing of initial reactor cathodic frame	138
D.4 Technical drawing showing all parts of the laboratory reactor	139
D.5 Technical drawing of laboratory reactor current collector	140
D.6 Technical drawing of laboratory reactor current collector frame	141

Nomenclature

General

Symbol	Description	Units
a	activity coefficient	$\left[\frac{\text{kmol}}{\text{m}^3}\right]$
$a(t)$	catalytic activity	$[\]$
A	surface area	$[\text{m}^2]$
C	concentration	$\left[\frac{\text{kmol}}{\text{m}^3}\right]$
d_e	equivalent diameter	$[\text{m}]$
D	diffusivity	$\left[\frac{\text{m}^2}{\text{s}}\right]$
e_0	charge of single electron	$[\text{C}]$
f	friction factor	$[\]$
F	Faraday's constant	$\left[\frac{\text{C}}{\text{mol}}\right]$
G	free energy	$\left[\frac{\text{kJ}}{\text{kmol}}\right]$
i	current density	$\left[\frac{\text{A}}{\text{cm}^2}\right]$
I	total current	$[\text{A}]$
k	reaction rate constant	varies ¹
k_m	mass transfer coefficient	$\left[\frac{\text{m}}{\text{s}}\right]$
L	length	$[\text{m}]$
m	mass	$[\text{kg}]$
M_R	molecular weight	$\left[\frac{\text{g}}{\text{mol}}\right]$
n	number of moles	$[\text{mol}]$
N_A	Avogadro's number	$[\text{mol}^{-1}]$
p	pressure	$[\text{Pa}]$
Q	charge passed	$[\text{C}]$
r	reaction rate	$\left[\frac{\text{kmol}}{\text{s}\cdot\text{m}^3}\right]$
$r^{ }$	reaction rate per unit electrode area	$\left[\frac{\text{kmol}}{\text{s}\cdot\text{m}^2}\right]$

¹Depends on the reaction order and type of reaction

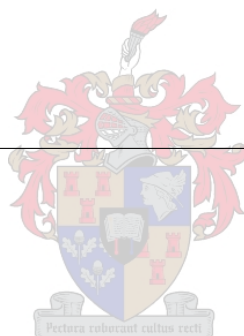
Symbol	Description	Units
R	Universal gas constant	$\left[\frac{\text{kJ}}{\text{kmol}\cdot\text{K}}\right]$
Re	Reynolds number	\square
Sc	Schmidt number	\square
Sh	Sherwood number	\square
t	time	[s]
T	temperature	[K]
V	potential	[V]
\dot{V}	flow rate per unit area	$\left[\frac{\text{m}^3}{\text{m}^2\cdot\text{s}}\right]$
v	volumetric flow rate	$\left[\frac{\text{m}^3}{\text{s}}\right]$
X	conversion	\square

Greek Symbols

Symbol	Description	Units
α	charge transfer coefficient	\square
γ	aspect ratio	$\left[\frac{\text{m}}{\text{m}}\right]$
ε	current efficiency	\square
η	overpotential	[V]
Θ	electrode bubble coverage fraction	\square
μ	chemical potential	$\left[\frac{\text{kJ}}{\text{kmol}}\right]$
ν_e	stoichiometric number of electrons	$\left[\frac{\text{mol } e^-}{\text{mol}}\right]$
ρ	density	$\left[\frac{\text{kg}}{\text{m}^3}\right]$
τ	residence time	[s]

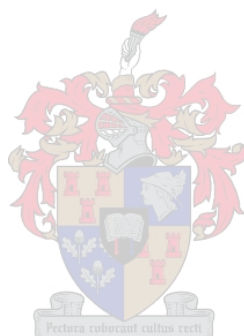
Subscripts

Subscript	Description
0	initial value
a	anode
b	bubble
c	cathode
e	electrode
in	inlet, reactor
j	specific reaction
out	outlet, reactor
p	product
Ph	phenol
R	reacor
r	reactant, recycle
t	value at time t
T	total



Glossary

- emf : Electro-motive force
EOI : Electrochemical oxidation index
MEA : Membrane electrode assembly
PEM : Proton exchange membrane
PEMFC : Proton exchange membrane fuel cell
SPE : Solid polymer electrolyte
TOC : Total organic carbon



Acknowledgements

I wish to thank the following people:

The Water Research Commission for their financial support and guidance for the duration of the project. The work conducted in this thesis formed part of the WRC Project #1196 – a combination of the research done by the author of this thesis and Mrs. P.G.L. Baker [20].

Prof. J.H. Knoetze, Mr. C. Nel (Department of Process Engineering, University of Stellenbosch) and Prof. R.D. Sanderson (Polymer Science, Department of Chemistry, University of Stellenbosch) for their guidance and advice as study leaders.

All the technical and administrative staff at the Department of Process Engineering (University of Stellenbosch) for their expertise, especially Mrs H. Botha for her help regarding the analytical method, and the workshop staff for their help in the construction of the reactor system.

Prof. L.M.T. Dicks (Department of Microbiology, University of Stellenbosch), for his assistance in making chapter 5 possible.

Prof. A.M. Crouch and Mrs. P.G.L. Baker, for their valuable inputs and stimulating discussions regarding the electrochemistry involved.

My family for their support, especially my sister, who had to read through the entire thesis.

My friends, especially Taryn Fraser, for encouragement and support.

Chapter 1

Introduction

1.1 Background

The need for reduced or zero-pollutant effluents from chemical and petrochemical industries have increased in the last few decades due to increasingly stringent legislation and pressure from environmental groups. Many of these industries have effluent streams containing quantities of organic compounds that are too low in concentration to recover economically, but high enough in concentration to be harmful to the environment. Thus, the need for a reliable system for the removal of such organics has resulted in a large amount of research focussing on water purification, especially in the electrocatalytic oxidation of organics in dilute aqueous systems.

Various methods of water treatment have been developed with different levels of success. Apart from chemical oxidation [1, 2, 3] (such as the use of ozone), the most popular of these methods are photo-assisted catalytic oxidation [4], thermal liquid-phase wet-air oxidation [5] and oxidation with the application of high-frequency ultrasound [6]. Most of these methods require the presence of metals, metal oxides or metal salts that act as catalysts in the oxidation reaction. In the last two to three decades significant advances have also been made in the field of electrocatalysts — they are used as a popular treatment method in the literature for the oxidation of dilute aqueous organic wastes.

In electrocatalysis the success of the process seems to depend largely on the type of catalyst that is used, and therefore a wide variety of catalysts have been tested in

other studies in an attempt to improve the catalytic activity. Traditional catalysts such as the noble metals Pt, Pd and Ir show limited use for the oxidation of aromatic compounds (see section 2.2), since they promote the reaction only up to the formation of quinones. These metals have thus been used as substrate materials for the more exotic metal oxide films that show a much higher selectivity toward the complete combustion of organic molecules. Due to the cost of these noble metals, they are often substituted by titanium substrates. Titanium is known as a valve-metal, which gives it the required properties for good catalyst adhesion, among other things.

Tin dioxide has been a very popular metal oxide catalyst [7, 8, 9, 10], since it shows promise in the complete breakdown of organic molecules to carbon dioxide and water (the desired final products of combustion). Additional reasons for the use of tin dioxide can be summarised as follows [11]:

- high chemical and electrochemical stability
- high electric conductivity when combined with selected dopants
- high overpotential for the oxygen evolution reaction

Lead dioxide has shown similar activity [12, 13, 14], but the possible leaching of toxic lead ions into treated drinking or natural water makes it unfavourable. It has been shown that adding dopants as metal oxides can improve the catalytic activity of the catalyst film [15]. SnO₂ powders doped with a wide variety of dopants such as Cu [16], Ir, Mb [17], Mn [18], Pd, Rh, Ru, Sb [19] and Zr [16] have been produced and tested.

This work follows on from the work of Grimm that employed Ti/SnO₂/Sb₂O₅ electrodes [15]. In conjunction with this project, another project was run to address issues regarding the electrochemical properties of a variety of electrocatalysts [20]. It was found that the Ti/SnO₂/ZrO₂ system showed the best catalytic activity and was therefore chosen as the catalyst for this project.

The need for lowering energy cost requirements has also been a main driving force in the development of these novel metal oxide catalysts, since they show promise in

lowering the activation energies. Therefore, the total energy expenditure of converting a toxic molecule to either less toxic molecules, or completely destroying the molecule to carbon dioxide, would require significantly less energy. A disadvantage of this is the high cost of some of the precursors needed to prepare the metal oxides.

Most of the work that was done with these catalysts was based on systems that contain supporting electrolytes, either in the form of altered pH or salinity. The main problem with a practical implementation of these technologies is the requirement of regular maintenance to resupply the reactor system with additional supporting electrolyte. It would be ideal if a system could be designed that does not require post-treatment to restore original pH and salinity conditions.

Therefore, a new system was developed in which the requirement of the supporting electrolyte was eliminated and substituted with a solid polymer electrolyte (SPE) that served as conductive medium for proton transfer. A disadvantage of these systems is the contacting of the electrodes to the membrane in order to obtain an evenly distributed current density. Some work has been done (especially in the development of fuel cells) on impregnating the membrane with catalyst particles, although catalyst loading then becomes a factor, as well as the lifetime of the membrane-catalyst assembly.

The work reported in this dissertation focuses mainly on the investigation of such a system to determine its feasibility in two fields of water treatment. The primary focus was, as explained above, the removal of unwanted organic compounds from water. Phenol, or some substituted form of phenol, has almost exclusively been used as model contaminant in all the literature to date and will also be used here. Since the active agent in the breakdown of the organic molecules is a hydroxyl radical, it was realised that this system could potentially be used in the disinfection of especially rural water sources in disadvantaged communities. The secondary focus of this project therefore deals with disinfection.

1.2 Motivation for Research

As mentioned, this research follows on from the work of Grimm [15], whose research focused mainly on the electrochemical aspects of the metal oxide catalysts. Principally, the same reactor was used for this research — with the exception of the flow channels. Grimm’s work showed promise in the removal of high concentrations of phenol, but the experiments included showed only the breakdown curves (concentration-time data). No additional analyses were performed and therefore no information was given about the actual rates of combustion. These values are considered to be critical in the accurate design of larger reactors.

Encouraged by the initial results of Grimm [15], a WRC project was initiated to investigate the process of electrochemical combustion from an engineering perspective. The main objectives of the WRC project were as given below:

1. Development of a multi-family water-treatment system that sterilises waters and removes undesirable organics.
2. Obtaining a water treatment system that should also be capable of treating industrial effluents.
3. Investigation of different types of cell designs as alternatives to current cell design for efficiency improvements.

These objectives were refined, to produce the set of main objectives for this research project, as discussed in the section 1.3.

1.3 Objectives

Although proton-exchange membrane (PEM) cells are extensively used in the fuel cell industry, the processes involved when they are used for electrochemical oxidation are fundamentally different. In the fuel cell industry, the reactants are both gaseous and the product is water. Depending on the cell design of the proton-exchange-membrane fuel cell (PEMFC), the water flooding can be controlled to such an extent

that it does not influence the process. Therefore the reactant concentrations may be assumed to be pure or very concentrated. In water treatment, very dilute organic solutions are often encountered (as low as 10 ppm), which already puts the kinetics at a disadvantage.

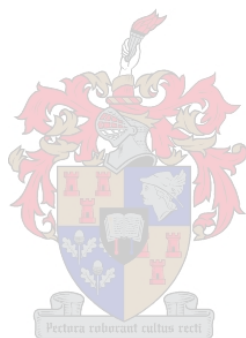
Reactants must diffuse to the reaction sites, and water, carbon dioxide and oxygen form as products. The development of a reactor system that can be used for the above-mentioned uses would, therefore, require the development of a model based on the experimental analysis of the reactor. This model can then be used in the design of larger reactor systems, which can be practically implemented. The aims that were set out for this project were:

1. Investigate the possibility of using an electrochemical combustion water-treatment system to sterilise water, to and remove undesirable organics without the addition of any supporting electrolytes.
2. Investigate whether the available PEM technology is capable of treating industrial effluents.
3. Investigate different types of cell designs as alternatives to current cell design for efficiency improvements.

From an engineering point of view, the shortcomings of Grimm's work led to the following being the main objectives of this Masters' project. The major parts of this study are the following:

1. As a limited amount of information is available on the exact kinetics of the process, additional data regarding this aspect of electrochemical combustion are to be gathered or obtained. The necessary model parameters could then be extracted from this data.
2. As in the literature, only current density and catalyst type have been investigated as process variables, the effect of other major parameters such as flow rate, necessary for a robust model, was to be determined.

3. A simple kinetic model for the breakdown of the organic contaminants was to be formulated. This would then be incorporated into the reactor model.
4. A typical water treatment unit for both the industrial and sterilisation applications, based on the model, was to be designed.
5. A full economical evaluation to determine the feasibility of the reactor systems was to be performed.



Chapter 2

Theoretical Principles and Literature Review

2.1 Electrochemical Reactors

An electrochemical reactor is defined as any device in which chemical reactions occur directly due to the input of electrical energy [21]. A schematic representation of an electrochemical cell is given in figure 2.1. A typical electrochemical reactor consists of two electronic conductors or electrodes immersed in some conducting liquid, namely the electrolyte. The electrodes are connected externally to a d.c. power supply. When a suitable electro-motive force (emf) is applied, current flows in the external circuit and chemical reactions take place at each electrode. This process is termed electrolysis.

Electrical conduction in the electrolyte is mainly due to the movement of charged species. The charged species or ions are made available from the chemical components — either by melting them or dissolving them in a suitable solvent, most commonly water. The application of a potential difference between the two electrodes causes the negatively charged species (anions) in solution to migrate towards the positive electrode (anode). Similarly, the positive ions (cations) move towards the negative electrode or cathode.

According to Pickett [21], the predominant factor in the movement of ions in an electrochemical cell can almost always be attributed to mass transfer. Since chemical reactions take place at the surfaces of the electrodes, concentration differences are

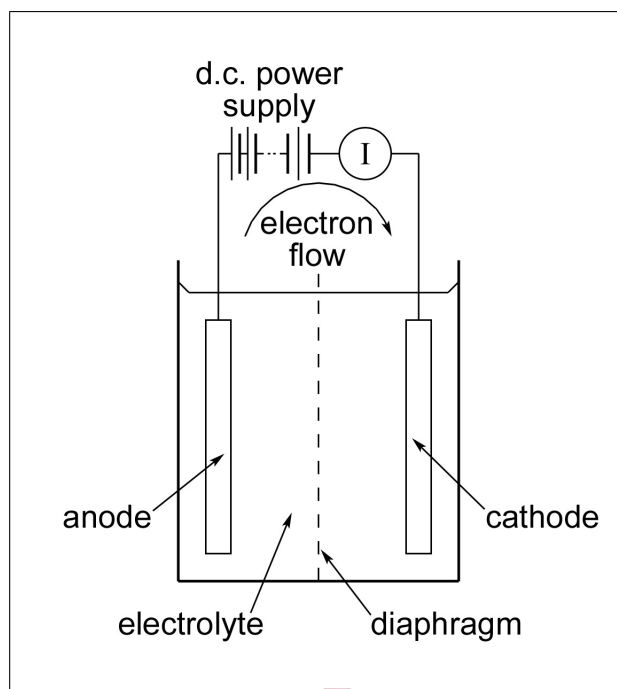


Figure 2.1: Parts of an electrochemical cell

caused between the bulk of the solution and the solution surrounding the electrode. This concentration difference then supplies the main driving force for the movement of the ions.

The discharge of ions at the electrodes results in chemical changes and causes electricity to flow in the external circuit. In this circuit, electrons flow from the anode to the cathode. In a chemical sense this implies that oxidation takes place at the anode and reduction at the cathode.

There are normally two different modes of operation for electrochemical cells. The mode of operation generally depends on the reactions taking place. Under galvanostatic operation, the cell is operated under constant current. In this case, the potential is adjusted in order to keep the applied current in the cell equal to the set value. In certain cases, especially where one or more side reactions take place, this may cause the selectivity to shift towards the unwanted side reaction. The advantage of this mode of operation is that the current density can be set to any required value.

Under potentiostatic operation, the electrochemical cell is operated under con-

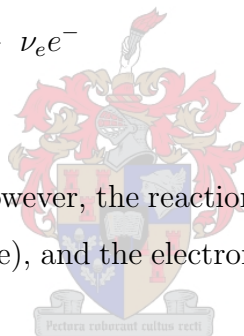
stant applied voltage. This mode of operation is sometimes necessary to force only some reactions to take place, for instance in the electrowinning of metals from a solution of several metal ions. This way, the metals can be extracted one at a time to obtain high purity metals. The disadvantage is that there is basically no control over the current — therefore, kinetically hindered reactions can give very low currents.

2.1.1 Electrochemical Reaction Rates

In a homogenous redox reaction the electrons are directly transferred from a donor molecule to an acceptor molecule. This can be summarised by the following set of equations:



In an electrochemical reaction however, the reactions are heterogeneous and occur at different sites (anode and cathode), and the electrons are transferred via the external circuit.



In equation 2.1 one can see that for one mole of product to form, a number of electrons equal to ν_e must be consumed. Faraday discovered two laws that relate the amount of product formed during electrolysis to the amount of electricity passed. These two laws can be expressed in the following statement [21] (p. 7):

The passage of 96487 coulombs through an electrochemical reactor produces in total one gram equivalent of products at an electrode.

This quantity can be calculated by taking the charge of one electron ($e_0 = 1.602 \times 10^{-19}$ C) and Avogadro's number ($N_A = 6.022 \times 10^{23}$ mol⁻¹) to give the charge of one mole of electrons ($F = 96486.69$ C·mol⁻¹) — known as the Faraday. If only one reaction takes place at the electrode and the current is constant, the following simplified relationship gives the moles of product, n , formed in an electrochemical

reaction applies:

$$n = \frac{Q}{\nu_e F} = \frac{It}{\nu_e F} \quad (2.2)$$

If the mass of product formed is required, equation 2.2 can be multiplied by the molar mass of the product to give:

$$m = \frac{M_R Q}{\nu_e F} = \frac{M_R \int I dt}{\nu_e F} \quad (2.3)$$

Here, the term Q is replaced with the integral of current over time. This is typically used if the current is not constant for the duration of the electrolysis.

According to Wendt and Kreysa [22], for the more general reaction scheme,



Faraday's law can be written as

$$m_p = \frac{\nu_p M_{R,p}}{\nu_e F} \int I dt \quad (2.5)$$

with respect to the product, or with respect to the reactant:

$$-m_r = \frac{\nu_r M_{R,r}}{\nu_e F} \int I dt \quad (2.6)$$

The differential form of equation 2.5 can be obtained by differentiation with respect to t :

$$\frac{dn_p}{dt} = \frac{\nu_p I}{\nu_e F} \quad (2.7)$$

Normally, for heterogeneous electrochemical reactions, the reaction rate is proportional to the surface area of the electrode, and therefore equation 2.7 can be normalised,

$$\frac{1}{A_e} \frac{dn_p}{dt} = \frac{1}{A_e} \frac{\nu_p I}{\nu_e F} = \frac{\nu_p i}{\nu_e F} \quad (2.8)$$

where i is the current density. In practical applications, conditions are rarely this simple. Often several reactions take place simultaneously at the same electrode. For instance, in the electrowinning of metals the following reactions may take place:



In such a case, each reaction's contribution to the overall current flowing through the external circuit is given by the specific reaction's current efficiency, ε_j . By definition, the sum of all the current efficiencies must be one:

$$\sum_j \varepsilon_j = 1 \quad (2.10)$$

Using Faraday's law, the expression for an individual reaction can be determined as

$$\varepsilon_p = \frac{n_p \cdot \nu_e F}{\nu_p Q} \quad (2.11)$$

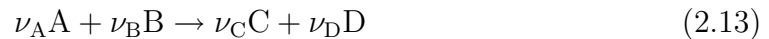
with

$$Q = A_e \int_0^t i dt \quad (2.12)$$

2.1.2 Cell Potential

In the case of fuel cells, which are electrochemical reactors that produce electrical energy from chemical energy, some spontaneous reaction ($\Delta G < 0$) takes place at both electrodes and an electrical current is produced in the external circuit. In the case of electrolyzers, the process is non-spontaneous, and an applied potential is required to force the reaction to take place. In this case the Gibbs free energy change is positive ($\Delta G > 0$). The applied potential is supplied by the external power supply and is termed the electro-motive force.

In order to quantify this emf, the approach as used by Pickett will be discussed [21] (p. 10). Consider a single reaction taking place at an electrode under constant temperature and pressure:



Since the reaction does not take place naturally, the free energy change, ΔG , of the reaction is positive:

$$\Delta G = \nu_C \mu_C + \nu_D \mu_D - \nu_A \mu_A - \nu_B \mu_B \quad (2.14)$$

where μ_A , μ_B , μ_C and μ_D are the chemical potentials for species A, B, C and D. The purpose of applying the external potential is to increase the free energies of A and B in order to reverse the sign of ΔG .

According to convention, the applied voltage is given by

$$V = V_+ - V_- \quad (2.15)$$

where V_+ and V_- are the electrical potentials of the positive and negative terminals of the power source. If the potential drop due to the resistance in the external circuit is ignored, the voltage can be separated into three potential drops — two that occur at the solution/electrode interface (to be discussed later) and the other due to resistance to ion transfer in the solution. This is schematically represented in figure 2.2(a).

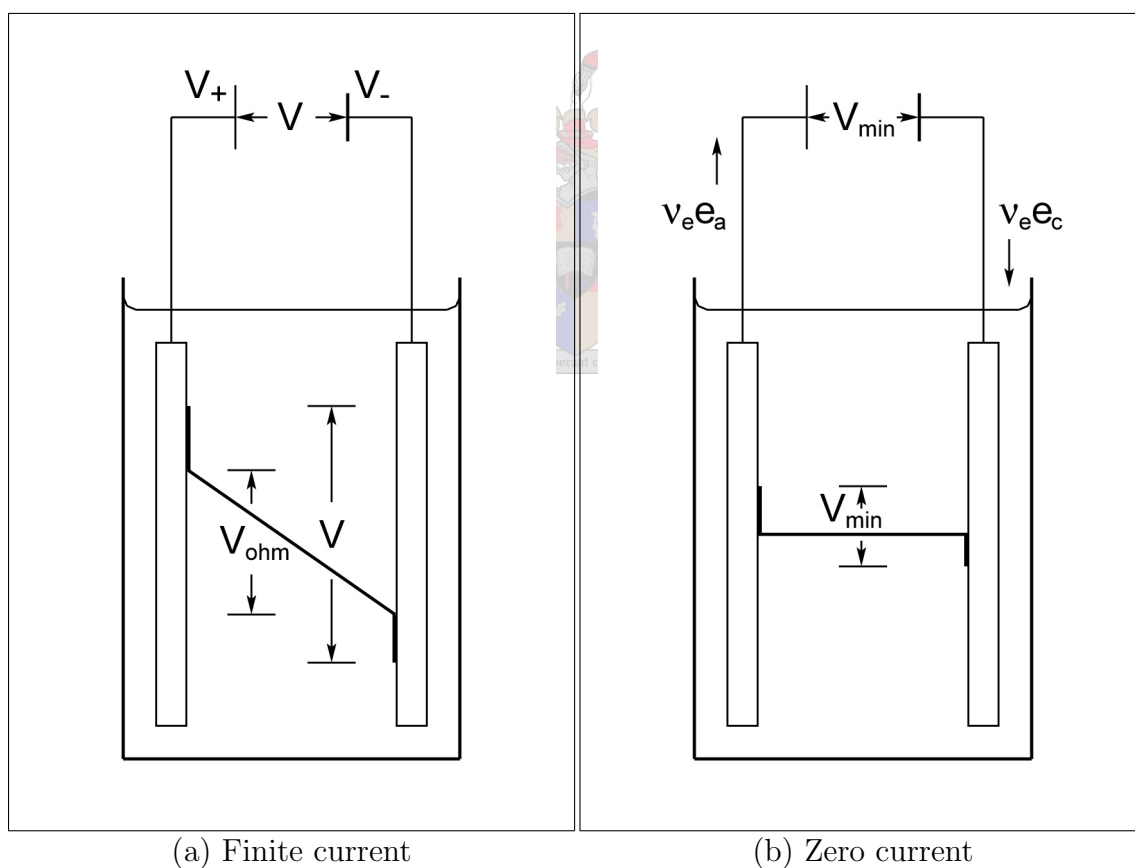


Figure 2.2: Voltage components in an electrochemical cell.

If this voltage is decreased until the solution potential drop becomes zero, this condition of zero current leaves the system in a state of equilibrium. The interfacial

potentials are still present although they are reduced in magnitude. This voltage is known as the minimum electrolysing voltage or equilibrium cell potential, and is represented by figure 2.2(b). To determine this voltage, we rewrite equation 2.13 to account for the electrons taking part in the separate electrode reactions:



(e_c and e_a being the electrons involved in the cathodic and anodic half-reactions respectively).

Since the system is in equilibrium, the free energy is at a minimum and therefore

$$\nu_e \mu_{e_c} + \nu_A \mu_A + \nu_B \mu_B = \nu_e \mu_{e_a} + \nu_C \mu_C + \nu_D \mu_D \quad (2.17)$$

Substitution of equation 2.14 into equation 2.17 then yields

$$\nu_e (\mu_{e_c} - \mu_{e_a}) = \Delta G \quad (2.18)$$

At equilibrium, the chemical potential of an electron is equal to the chemical potential of an electron in the adjacent power supply terminal, thus



$$\mu_{e_c} = \mu_{e^-}$$

and

$$\mu_{e_a} = \mu_{e^+} \quad (2.19)$$

According to Pickett [21], the difference between the chemical potentials of electrons in the two terminals can be given by

$$\mu_{e^-} - \mu_{e^+} = -F(V_- - V_+) \quad (2.20)$$

Substituting equation 2.19 and equation 2.20 into equation 2.18, one can obtain an expression for the minimum electrolysing voltage, V_{\min} :

$$\begin{aligned} \Delta G &= \nu_e F(V_+ - V_-) \\ \Delta G &= \nu_e F V_{\min} \end{aligned} \quad (2.21)$$

or, in terms of V_{\min}

$$V_{\min} = \frac{\Delta G}{\nu_e F} \quad (2.22)$$

The Gibbs free energy of any chemical reaction depends on the reaction temperature, the concentrations of dissolved species and the partial pressures of the gaseous reactants. The equations derived here should only be used at standard temperature and pressure. Concentration-related activities and fugacities are derived from actual concentrations and partial pressures, as shown in the following set of equations [22]:

$$a_i = C_i \gamma_i \quad (2.23)$$

$$p_i^* = p_i f_i \quad (2.24)$$

These coefficients account for deviations from ideal behaviour, which is described by the two limiting equations and which, in turn describes chemical potentials at low concentrations and pressures

$$\mu_i = \mu_i^0 + RT \ln \left(\frac{p_i}{p^0} \right) \quad (2.25)$$

$$\mu_j = \mu_j^0 + RT \ln \left(\frac{C_j}{C^0} \right) \quad (2.26)$$

with p^0 being the standard fugacity (0.1 MPa) and C^0 being the standard activity (1 mol·dm⁻³). The reduced quantities $\frac{p_i}{p^0}$ and $\frac{C_j}{C^0}$ are used to make the logarithm dimensionless and are often omitted in the literature. For higher concentrations and pressures, the corrected equations read

$$\mu_i = \mu_i^0 + RT \ln (p_i f_i) \quad (2.27)$$

$$\mu_j = \mu_j^0 + RT \ln (C_j \gamma_j) \quad (2.28)$$

Substituting equations 2.27 and 2.28 into equations 2.14 and 2.21 and ignoring deviations from ideality, one obtains

$$V_{\min} = \frac{\left\{ \sum \nu_{i,j} \mu_{i,j} + RT \ln \left(\prod_{i,j} C_j^{\nu_j} p_i^{\nu_i} \right) \right\}}{\nu_e F} \quad (2.29)$$

or, for the species A, B, C and D in equation 2.14,

$$V_{\min} = V_{\min}^0 - \frac{RT}{\nu_e F} \ln \frac{a_A^{\nu_A} a_B^{\nu_B}}{a_C^{\nu_C} a_D^{\nu_D}} \quad (2.30)$$

where the activities are given by equation 2.23 or equation 2.24 depending on the phase of the reactants and products. Often it is assumed that the activity and fugacity coefficients are one, especially at low concentrations. It then follows that the concentrations and partial pressures can replace the activities.

Now that the minimum voltage required to run an electrochemical process has been defined, a brief discussion of the elements of practical voltage requirements will be given. The equilibrium voltage in a typical electrochemical cell is given by the relationship

$$V_{\min} = V_a - (-V_c) \quad (2.31)$$

During non-equilibrium operation, the potential drop due to the solution resistance becomes important. Also, the electrode potentials start to deviate from their respective equilibrium values. If the electrode processes were thermodynamically reversible, one would be able to pass a large current through the solution without these potentials varying notably. The solution drop would then be

$$V = V_{\min} + V_{\text{ohm}} \quad (2.32)$$

where V_{ohm} is the solution potential drop. Such electrodes are referred to as “non-polarizable”. Most practical electrodes exhibit polarisation and this deviation in potential is referred to as the overpotential. In such a case, the electrolysing voltage can be represented by

$$V = V_a^* - (-V_c^*) + V_{\text{ohm}} \quad (2.33)$$

where V_a^* and V_c^* are the non-equilibrium electrode potentials.

To obtain an expression for the practical voltage drop in the case of polarizable electrodes, equation 2.31 is subtracted from equation 2.33, giving

$$\begin{aligned} V &= V_{\min} + (V_a^* - V_a) - \{(-V_c^*) - (-V_c)\} + V_{\text{ohm}} \\ &= V_{\min} + \eta_a - \eta_c + V_{\text{ohm}} \end{aligned} \quad (2.34)$$

where η_a and η_c are known as the anodic and cathodic overpotential. These values are defined as the difference between the electrode potential at non-equilibrium and equilibrium operation:

$$\eta_a = V_a^* - V_a \quad (2.35)$$

$$\eta_c = (-V_c^*) - (-V_c) \quad (2.36)$$

According to convention, the cathodic overpotential is generally negative, but causes an increase in the total operating voltage. Therefore, equation 2.34 is often written as

$$V = V_{\min} + \eta_a + |\eta_c| + V_{\text{ohm}} \quad (2.34a)$$

Many phenomena may be associated with the overpotential. Up to five different effects may cause this overpotential according to Kortüm [23]. The most important of these phenomena may be associated with the solution (concentration overpotential); and processes taking place at the actual site of the reaction on the electrode surface (activation overpotential).

Concentration overpotential is caused by the depletion or accumulation of species taking part in the reaction close to the surface of the electrode. The electrode is thus surrounded by a solution with a different concentration than that of the bulk solution, causing a shift in the potential away from the equilibrium value. Keeping the solution concentration as close as possible to the bulk concentration, will thus reduce the overpotential. This is typically done by increasing the mass transfer from the bulk to the electrode surface by stirring or increased flow of the solution.

Activation potential on the other hand, arises due to the phenomena associated with the electrode reaction. In any electrochemical reaction electrons are transferred across the electrode interface to the reactant molecule. This normally takes place in a sequence of steps of which adsorption and desorption of the reactants, intermediates and products, surface diffusion and surface reactions are all a part. Only one of these steps is the rate-limiting step — it is this step that requires a certain input of energy, the activation energy, to take place. This step represents the state of maximum energy of the system and is necessarily higher than the original state of

the system. Once the system has accumulated enough energy it proceeds to the final state of energy which is greater than the original state, but lower than the maximum. A portion of the original activation energy is thus lost and this irreversibility gives rise to the activation overpotential. This energy is lost at the expense of a higher potential.

2.1.3 Electrode Kinetics

The rate of an electrochemical reaction



has been shown in section 2.1.1 to be determined by the applied current. Differentiation of equation 2.2 gives

$$r = -\frac{dn_j}{dt} = \frac{\varepsilon_j I}{\nu_e F} \quad (j = A) \quad (2.38)$$

with ε_j being the current efficiency for the considered reaction. As is convention, the rate can be normalised with respect to surface area, and current density can be used to represent the reaction rate:

$$-\frac{1}{A_e} \frac{dn_j}{dt} = \frac{1}{A_e} \frac{\varepsilon_j I}{\nu_e F} = \frac{\varepsilon_j i}{\nu_e F} \quad (2.8a)$$

According to Wendt [22] (p. 41), it is an experimental fact that if mass transfer limitations are eliminated, the rate of charge transfer varies exponentially with the overpotential. For reactions that have both a forward and a backward reaction, such as the one in equation 2.37, both are changed in an opposite sense by the applied overpotential. Thus, according to the Butler-Volmer equation, one obtains the effective current density as the difference between the cathodic and anodic partial current densities:

$$i = i_0 \left(\exp \left\{ \frac{\alpha_a F \eta}{RT} \right\} - \exp \left\{ \frac{-\alpha_c F \eta}{RT} \right\} \right) \quad (2.39)$$

where i_0 is called the “exchange current density” and basically equals the current that is exchanged back and forth between the two electrodes under equilibrium. α_a and α_c

are the anodic and cathodic charge transfer coefficients and determine the response of the partial current densities towards a change in overpotential. The sum of these two charge transfer reactions must always equal the stoichiometric electrons, ν_e , of the potential-determining electrode reaction, but even this only hold for conditions close to equilibrium.

If the overpotential is high enough for one of the reactions, equation 2.39 can be simplified as follows:

$$i = i_0 \exp \left\{ \frac{\alpha_a F \eta}{RT} \right\} \quad \text{for} \quad \frac{\alpha_a F \eta}{RT} \gg 1 \quad (2.40)$$

or

$$i = i_0 \exp \left\{ \frac{-\alpha_c F \eta}{RT} \right\} \quad \text{for} \quad \frac{-\alpha_c F \eta}{RT} \gg 1 \quad (2.41)$$

Normally the Tafel equation is derived from these equations:

$$\eta = a + b \log i \quad (2.42)$$

with

$$a = -2.302 \cdot \left(\frac{RT}{\alpha F} \right) \log i_0 \quad (2.43)$$

$$b = 2.302 \cdot \left(\frac{RT}{\alpha F} \right) \quad (2.44)$$

with b known as the Tafel slope. The graphical determination of these values is schematically represented in figure 2.3.

For the system used in this study, the use of a membrane makes the system too complex to accurately derive values from the Tafel slope. The use of a membrane to separate the electrolyte in an electrochemical cell makes the system irreversible, and therefore conventional methods cannot always be used to accurately determine Tafel values in such a system. Also, due to all the breakdown products formed in the oxidation of phenol, the accuracy of the values will be suspect.

Often it is found that the value i_0 is dependent on the concentration of species in the reaction solution [22] (p. 49). Therefore i_0 can be expressed as a function of

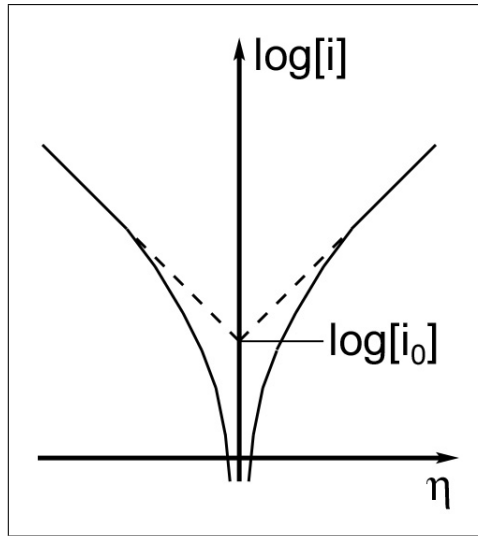


Figure 2.3: Semilogarithmic plot for determination of i_0 and the Tafel slope.

the concentration of different reactants and their respective reaction orders.

$$i_0 = i_0^0 \prod_i c_i^{n_i} \quad (2.45)$$

This approach is similar to that followed by Pickett [21] (p. 52), where the reaction rate can be directly related to current density and often assumed to have similar kinetics to chemical kinetic equations:

$$r = \frac{i}{\nu_e F} = kC^n \quad (2.46)$$

This methodology will also be assumed in this work, since very little information is available on the exact current-potential relationship. The derivation of the exact equation used in the reactor model is discussed in chapter 6.

2.1.4 Electrode Mass Transfer Phenomena

In chapter 6, a simple model is derived that takes into account the reaction taking place at the membrane-electrode interface. This reaction is quantified in terms of a reaction rate constant that is determined from the experimental results in chapter 4. Generally, there are two desired types of limiting conditions in chemical reactors: mass-transfer limited and reaction rate limited operation.

In the experimental work, in order to determine which limiting condition prevails, one needs to have some idea of the mass transfer from the bulk of the solution in the flow channel to the surface of the electrode. Several mass transfer correlations exist in the literature that describe the mass transfer coefficient in dimensionless form (Sherwood number) for a variety of electrode configurations [24]. The mass transfer coefficient for a parallel plate electrode of finite width can be calculated from the following correlation [24] (p. 80):

$$\text{Sh} = \frac{k_m d_e}{D} = 1.467 \left(\frac{2}{1 + \gamma} \right)^{\frac{1}{3}} \left(\text{Re} \cdot \text{Sc} \frac{d_e}{L} \right)^{\frac{1}{3}} \quad (2.47)$$

This correlation can then be used to determine the coefficient for external mass transfer.

Another important process that often takes place at electrodes in aqueous solutions is gas evolution. According to Wendt and Kreysa [22] (p. 103), it has been proven that an additional mass transfer element is introduced due to bubble formation. The effective mass transfer is quantitatively described by the following equation:

$$k_m = (k_{m,\text{macro}}^2 + k_{m,\text{bubble}}^2)^{0.5} \quad (2.48)$$

with the mass transfer element attributed to bubble formation given by

$$\frac{k_{m,\text{bubble}} \cdot d_b}{D} = \frac{2.76}{C} (\text{ReSc})^{0.5} (1 - \Theta)^{0.5} \quad (2.49)$$

where Θ is the degree of gas bubble coverage of the electrode and d_b is the average bubble diameter. The Reynolds number as given in equation 2.49 is proportional to the volumetric flow rate of gas evolution per unit electrode surface area, i.e.

$$\text{Re} = \frac{\dot{V}_{\text{surface}} d_b}{\nu} \quad (2.50)$$

C is a factor that accounts for the bubble shape. $C = 1.59$ for hemispheres and $C = 2$ for spheres.

2.1.5 Analogy to Chemical Kinetics

As mentioned in section 2.1.3, one can make the general assumption that an electrochemical reaction follows kinetics analogous to those observed in chemical reactors

[21]. In such a case, the rate of the reaction is given by equation 2.46.

$$r = \frac{i}{\nu_e F} = kC^n \quad (2.46)$$

In order for this equation to be used in the final model of the process, values for the reaction rate constant, k , and the reaction order, n , must be obtained. A number of methods exist that can be used to obtain these values from concentration-time data.

A method that is often used in the extraction of the reaction order is the differential method of rate analysis, as described by Fogler [25]. For a given reaction



the rate law is given by

$$-r_A = kC_A^n \quad (2.51)$$

For a constant-volume batch reactor, performing the appropriate mass balance and combining it with the rate law, one obtains

$$-\frac{dC_A}{dt} = kC_A^n \quad (2.52)$$

After taking the natural logarithms on each side of equation 2.52, one obtains

$$\ln \left(-\frac{dC_A}{dt} \right) = \ln k + n \ln C_A \quad (2.53)$$

Notice that the slope of a plot of $\ln \left(-\frac{dC_A}{dt} \right)$ versus $\ln C_A$ is the reaction order. Therefore, the concentration-time data must be differentiated, either graphically or numerically. Graphical methods can be iterative and prone to error, and thus only the numerical methods will be discussed here.

The rate of change of the concentration-time data can be obtained in two ways. The first is the three-point differentiation formulae for equally spaced data points. For a set of data containing N points:

Time	t_0	\cdots	t_m	\cdots	t_N
Concentration	C_{A0}	\cdots	C_{Am}	\cdots	C_{AN}

where m is some intermediate value ($0 < m < N$). The formulae to determine the rate of change of the concentration at various points are:

$$\left(\frac{dC_A}{dt}\right)_{t_0} = \frac{-3C_{A0} + 4C_{A1} - C_{A2}}{2\Delta t} \quad (2.54)$$

$$\left(\frac{dC_A}{dt}\right)_{t_i} = \frac{C_{A,i+1} - C_{A,i-1}}{2\Delta t} \quad (2.55)$$

$$\left(\frac{dC_A}{dt}\right)_{t_N} = \frac{C_{A,N-2} - 4C_{A,N-1} + 3C_{AN}}{2\Delta t} \quad (2.56)$$

The other popular method used is to fit a polynomial expression through the data points:

$$C_{Ph} = a_0 + a_1t + a_2t^2 + \dots + a_nt^n \quad (2.57)$$

and then finding appropriate values for the constants a_i . Once this has been done equation 2.57 can be differentiated with respect to time

$$\frac{dC_{Ph}}{dt} = a_1 + 2a_2t + 3a_3t^2 + \dots + na_nt^{n-1} \quad (2.58)$$

and used to obtain the rate of change of the concentration at any time t . The logarithm of the rate of change of concentration can then be plotted against the logarithm of concentration. The slope of a straight line fitted through the data will give the order of the reaction.

Another method is to assume a value for the reaction order. The concentration-time data is then linearised according to the assumed reaction order and a straight line is fitted through this data. If the fit is statistically sound, the correct reaction order has been assumed. This method will be described shortly with reference to typical graphs that can be obtained for each reaction order. One rarely finds reaction orders higher than two and therefore the discussion will only be extended to reaction orders of two.

With this method, one does not have to have only constant-volume batch reactor data and the kinetic expression can be directly incorporated into the reactor model, thereby accounting for other possible effects playing a role in the reactor.

If one assumes 0-th order kinetics, equation 2.52 can be written as

$$-\frac{dC_{Ph}}{dt} = k \quad (2.59)$$

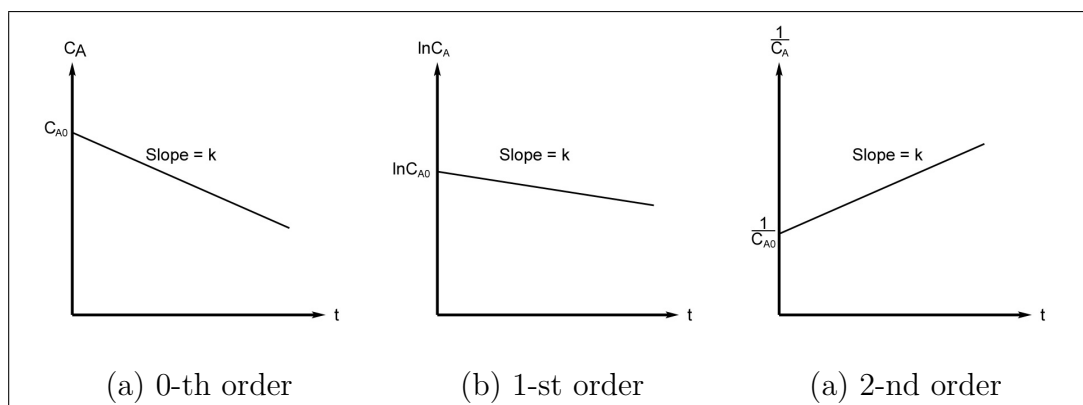


Figure 2.4: Determination of reaction rate constants for different reaction orders.

integrating yields

$$C_{Ph} = kt + K \quad (2.60)$$

In this case, one would plot values of the concentration versus time, and fit a straight-line through the data points. If the straight line fits the data well in a statistical sense of the word, the order of the reaction is zero. The slope of this line is equal to the reaction rate constant, k . K in equation 2.60 equals the intercept of the straight line at time $t = 0$. This would correspond with a calculated value for the initial concentration $C_{Ph,0}$. The procedure for obtaining the parameter values for 0-th order kinetics is shown in figure 2.4(a).

The same can be done for first and second order kinetics. The quantity used for the y -axis and the integrated equations are summarised in table 2.1.

Table 2.1: Summary of method for determining reaction order

x -axis	y -axis	Slope	Intercept	Equation
t	C_A	k	C_{A0}	$C_A = C_{A0} - kt$
t	$\ln(C_A)$	k	$\ln(C_{A0})$	$C_A = C_{A0} \exp(-kt)$
t	$\frac{1}{C_A}$	k	$\frac{1}{C_{A0}}$	$C_A = \frac{C_{A0}}{1 + C_{A0}kt}$

If none of the plots based on these three reaction orders are statistically valid, some other effect is taking place in the reaction and a more sophisticated approach

must be tried. Especially in the case of reactions on a catalytic surface, adsorption and desorption often influences the reaction kinetics.

2.2 Reaction Mechanics

There is still some uncertainty about the exact reaction mechanism that is followed in the oxidation of aromatic organic molecules, especially the ring-opening reaction (see sections 2.2.2 and 2.2.3). A possible reason for this is the reactivity of the oxidant taking part in the oxidation. Since it can react with the ring at any point, a wide variety of intermediates (whether they are unstable or not) may be formed, making the reaction pathway complicated. There does seem to be some correlation between the catalyst used and the reaction pathway followed though. A general discussion of the types of anodes, and their selectivity towards reaction pathways, will be given in section 2.2.1. This will be followed by a discussion of the actual breakdown products as observed by several researchers from the literature in section 2.2.2. Finally, Gattrell and Kirk did valuable work on the passivation effects that occur due to phenol polymerization — this will be discussed in more detail in section 2.2.3.

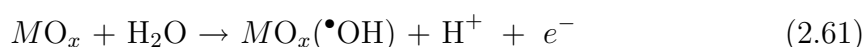
2.2.1 Overview of Reaction Mechanism

According to Comninellis [26], there are two main reaction pathways that are dependent only on the type of catalyst chosen as anode. In the electrochemical conversion method, cyclic organic molecules are converted by ring opening to aliphatic acids, which can be treated using biological methods for further purification. This method requires post-treatment to completely remove all organic carbon. Electrode materials that have a high selectivity towards organic ring opening but a low selectivity towards reaction with the formed aliphatic acids should be chosen. Typical electrode materials are Pt, Ti/IrO₂ and Ti/RuO₂.

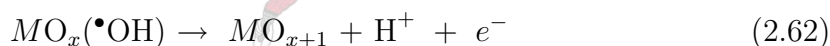
The electrochemical combustion reaction on the other hand completely oxidises the organic molecules into carbon dioxide and water. Electrode materials must have high catalytic activity towards the combustion of all organic molecules to CO₂.

Comninellis has found that Ti/SnO₂ gives the best results for this type of reaction. It also shows higher current efficiencies than the previously mentioned electrode materials.

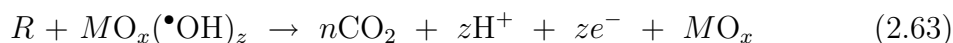
The first and most important step in the oxidation reaction pathway is the formation of the active site on the catalyst surface. The active site is formed by discharge of a water molecule on the catalyst surface to produce an adsorbed hydroxyl radical as shown in equation 2.61.



This may or may not be followed by the interaction of the hydroxyl radical with the oxygen in the metal oxide lattice. The hydroxyl radical absorbs into the lattice to form a higher oxide:



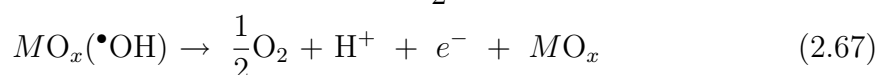
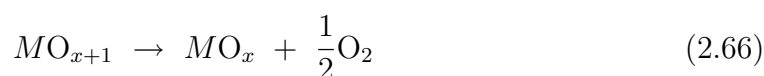
This is only possible if the metal has higher oxidation states. Therefore the “active oxygen” can take two forms: physisorbed “active oxygen” (hydroxyl radicals, $\bullet OH$) and chemisorbed “active oxygen” (lattice oxygen, MO_{x+1}). If an organic molecule is available when a reaction site is formed, the following oxygen transfer reactions can take place:



where n is dependent on the number of carbon atoms in the original organic molecule and z , to a certain extent, is dependant on the exact breakdown pathway that is followed. The corresponding acid formed in reaction 2.64 is normally treated by biological methods to convert it to carbon dioxide.



In the absence of an organic molecule, oxygen is formed as a side reaction:



If the potential of the reaction is kept below the potential for oxygen evolution by hydrolysis, equation 2.67 represents the only competing side reaction.

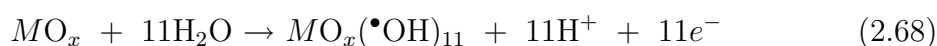
2.2.2 Phenol Oxidation

Equation 2.63 offers a very simplified view of the overall reaction mechanism. In reality, several intermediate steps take place before the phenol molecule is completely converted to carbon dioxide and water. The most complete reaction pathway reported for the oxidation of phenol has been sourced from work pertaining to the wet-air oxidation of phenol [5]. Although the process does not operate with electrodes, it still uses a catalyst and is believed to follow a free radical mechanism. The reaction scheme is presented in figure 2.5.

Researchers examining the use of electrodes for the combustion of organic molecules observed some of the breakdown products given in the reaction scheme. Using Ti/SnO₂ electrodes, Comninellis [7, 9] found the aromatic dihydroxy-benzenes and *p*-benzoquinone. *o*-Benzoquinone may have been present, but no standards for analysis could be obtained due to its instability. Maleic, oxalic and formic acid were also found in the reaction mixture, together with some unidentified intermediates. With Ti/IrO₂ electrodes, Comninellis *et al.*[27] found only the aromatic intermediates. Sharifian and Kirk [13] and Tahar and Savall [14] both detected benzoquinone and maleic acid as intermediate products.

In figure 2.5 only the breakdown products are shown, with no information on the formation of the hydroxyl radical intermediates or the number of electrons involved. In the literature, both Comninellis *et al.* [7, 27] and Petrov *et al.* [8] have found that the complete combustion of phenol requires a total of 28 electrons and the discharge of 11 water molecules.

Thus, the total hydroxyl formation reaction can be written as



The reaction for the oxidation of phenol to carbon dioxide and water may then be

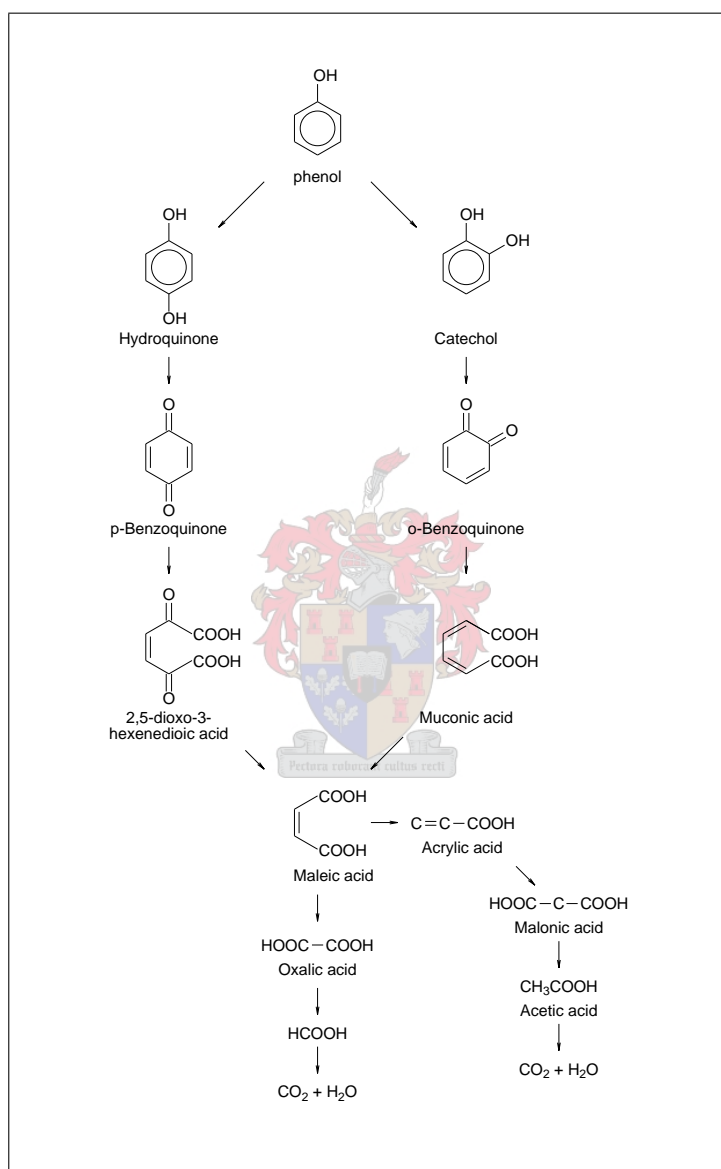
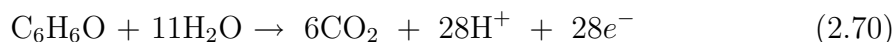


Figure 2.5: Proposed phenol oxidation to carbon dioxide and water (ref. [5])

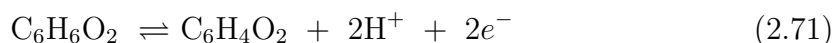
written as



Combining equations 2.68 and 2.69 the overall reaction for the breakdown of phenol can be obtained:



It must be noted that the reactions of 1,2- and 1,4 dihydroxybenzene to form *o*- and *p*-benzoquinone are reversible reactions and take place without requirement of the active oxygen:



2.2.3 Electrode Passivation

According to Gattrell and Kirk [28, 29], passivation of an electrode is the decrease in the activity of an electrode caused by the formation of an unreactive, impermeable film on the electrode surface. In some of the initial work regarding the catalysed combustion of organic molecules, it has been found that in some cases the catalyst became poisoned, causing the catalyst to lose activity rapidly. The first report of this poisoning was on the combustion of cumene using Fe_2O_3 as catalyst [30]. It was found that phenol was the poison, it being one of the breakdown products.

Gattrell and Kirk oxidised phenol using platinum electrodes. They observed the formation of a strongly adhering, defect-free polymeric film on the surface of the anode. The passive film is the result of the formation of organic tars through electropolymerization. These tars are characterised by their low rate of oxidation, low permeability and strong adhesion properties.

In figure 2.6 the reaction pathway is shown for both the polymerisation reaction as well as the first steps of the oxidation reaction. The phenoxy-radical intermediate was found to be the key intermediate — it interacted with other phenoxy-radicals to form dimers. These dimers could in turn form radicals and interact with the phenoxy radical or other dimeric radicals, forming higher molecular weight materials. Gattrell and Kirk determined that the product distribution and reaction pathways were

dependent on several factors such as phenol concentration, the electrode material, reactant adsorption characteristics, pH, current density and potential.

Gattrell and Kirk [31] suggested that an oxide-coated electrode could be used to prevent the formation of the passivating film at higher potentials, where hydroxyl radicals and peroxide intermediates are formed. Due to the oxygen evolution reaction, a fraction of the applied current will be wasted, causing a reduction in observed current efficiencies. Koile and Johnson [32] determined the effect of this oxygen evolution on the passivating film and found that significant rupturing of the film did not result in recovery of the electrode surface. However, this proved the strong adsorption characteristics of the film.

According to Comninellis, the metal oxide catalysts, especially the SnO_2 and doped SnO_2 films, are resistant to the formation of this passivating film. This theory however has not been proven yet. For instance, in this study, the phenol concentration was found to decrease with time, but none of the aliphatic acid intermediates were detected. This could imply the removal of phenol by the formation of a polymeric film.

2.3 Principles of the SPE Reactor

In an attempt to clarify the discussions that are to follow in the rest of this chapter, this section will discuss the major parts of an SPE reactor as well as the principles involved in its operation. It is not the aim of this section to discuss in detail the exact processes that take place in the reactor with reference to the oxidation of organic molecules. These processes will be referred to in subsequent sections in this chapter.

A simplified representation of a typical SPE reactor is given in figure 2.7. A cross-section of the membrane-electrode assembly and the top current collector is shown to give a view of the flow channels.

The most important part of the reactor is the membrane-electrode-assembly (MEA). This is the structure in the reactor where all of the half-reactions take place. It consists of the proton-exchange-membrane (PEM) sandwiched between the

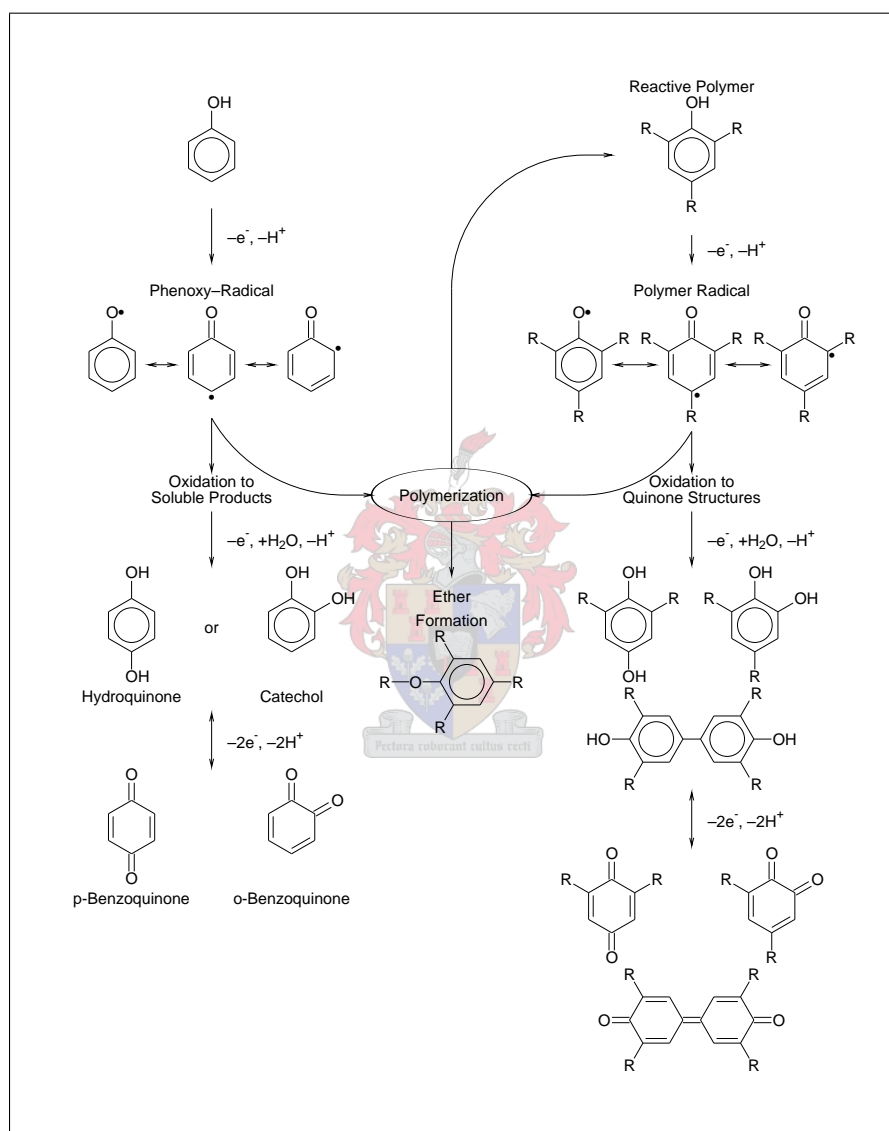


Figure 2.6: Phenol oxidation and polymerization pathways (ref. [29])

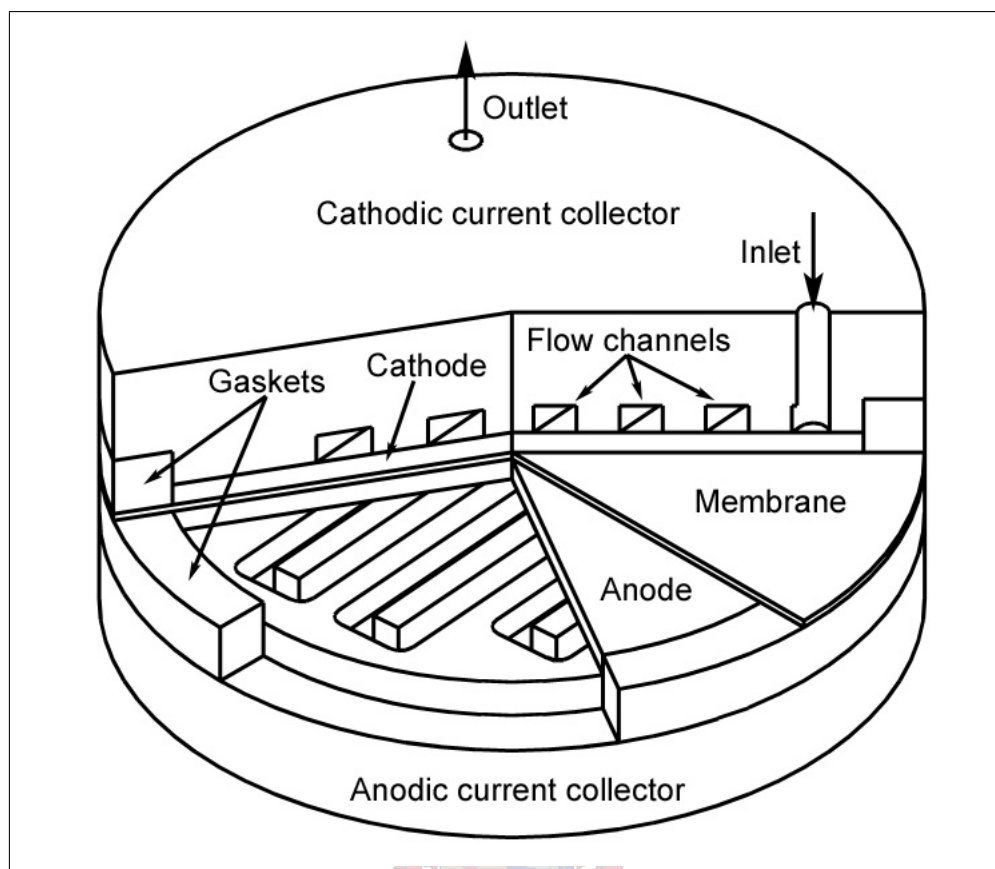


Figure 2.7: Parts of an SPE reactor

two electrodes. The literature states that in all cases, Nafion was selected as the proton exchange membrane for the SPE reactors. Nafion (a trademark of E.I. du Pont de Nemours Company) is a copolymer of tetrafluoroethylene and sulphonyl fluoride vinyl ether. Due to these constituents, Nafion contains functional SO_3^- groups that interact with the protons and allows for the proton conductivity. The characteristics that make it such a good choice for the PEM are summarised below:

1. High ionic conductivity,
2. outstanding chemical and thermal stability and
3. good mechanical strength.

Usually the Nafion membrane is used in the H^+ -ionic form, although it can also be used in other ionic forms such as K^+ and Na^+ .

As mentioned in chapter 1, the reactor system needs to operate without the need for any additional electrolytes. Typically, some form of ionising compound (in the form of acidity, salinity or alkalinity) is added to the water to improve the conductivity of the system. This has been done in almost all of the cases in the literature that has been studied. The addition of such compounds to the system, although it would eliminate the need for the PEM, would lead to the requirement for regular maintenance of practical electrochemical reactors. This can be undesirable in cases where the reactor system is used in water purification, for a number of reasons:

1. accessibility to remote areas, which can prevent scheduled maintenance checks of the treatment reactors, resulting in the reactor not being operational for periods of time,
2. the potential hazard to the environment and residents in the case of a reactor leak, and
3. the cost involved in periodically restocking a reactor with the appropriate chemicals.

The use of a PEM membrane eliminates the possible dangers and expenses involved with any of the above issues. The one disadvantage of the PEM membrane is the relatively high cost, but this is balanced against the stability and long lifetimes of these membranes.

As mentioned, protons and water molecules travel through the PEM. In this way it basically serves as a solid electrolyte, hence the name SPE. In this case, protons are generated at the anode according to the reactions given in equation 2.61 and equation 2.63. These protons then migrate into the membrane and interact with the functional SO_3^{2-} groups. The protons in the membrane at the cathode are consumed in the cathodic reaction, which in this case, is the hydrogen evolution reaction.



Electrons pass through the external circuit as they are generated at the anode and are consumed at the cathode.

The reactions take place close to or at the membrane-electrode interface. Therefore, good contacting between the membrane and electrode is vital for uniform current distribution. This is normally accomplished by bolting the two current collectors together. They are then connected to the power source via an external circuit. The cathode is connected to the negative terminal and the anode to the positive terminal.

The flow channels are machined into the current collectors. The contaminated water flows in through the inlet in the current collector, travels through the reactor, and leaves by the outlet. In this way the liquid in the cathodic and anodic sides of the reactor can be separated if desired. The water in the flow channel diffuses through the electrode to the membrane-electrode interface where the reaction will take place.

2.4 Electrode Preparation

In general, the preparation of the electrode involves the deposition of a metal oxide layer onto a substrate material. In most cases the substrate material used is titanium, because of its excellent resistance to corrosion. Another reason is that the metal oxide catalysts often lack the mechanical strength to be used as electrodes. Titanium therefore serves as the backbone for these types of electrodes. Titanium has been the substrate material most widely used and described in the literature [33].

Various methods have been developed for the formation of the oxide layer such as chemical vapour deposition, thermal decomposition, reactive sputtering, spray pyrolysis and the sol-gel technique. Since the sol-gel technique is employed for the preparation of the catalysts in this project, it is discussed in detail in section 2.4.3, while short discussions of the other techniques are given in sections 2.4.1 and 2.4.2 as background.

2.4.1 Spray Pyrolysis

With this technique [33, 11, 34, 19, 35], an appropriate solution is made with suitable precursors (exclusively inorganic salts) and solvents (typically ethanol). The solution

is then sprayed through a nozzle from a fixed distance onto the pre-heated substrate. Typical temperatures of the substrate at this stage of catalyst preparation are about 400-700°C. This is sometimes followed by a heating period of about 10 minutes after which additional coatings of the solution are applied to the substrate. After all the necessary coatings are completed, a final heat treatment is applied in some cases. It appears that 550°C resulted in films with the best electrical conductivity.

2.4.2 Thermal Decomposition

In this technique [36, 37], a paste or solution containing the desired ratios of precursor salts are prepared. When using the paste, a brush is used to apply the mixture onto the substrates, whereas in the case of a solution the coating film can be applied by brush, spray or dipping onto the substrate. This process is followed by an initial drying step at low temperature (50°C), followed by the annealing stage, which typically takes place at 400-550°C.

2.4.3 Sol-gel Dip-coating

The sol-gel method of catalyst preparation is claimed to have several advantages over the aforementioned methods. Excellent homogeneity, easy control of film thickness, ability to coat large surfaces and simple and low-cost processing are some of the most important advantages [38]. The sol-gel process has been studied extensively and has been used to prepare a wide variety of metal oxide catalysts.

According to Hench and West [39], three approaches are used to make sol-gel monoliths:

- gelation of a solution of colloidal powders,
- hydrolysis and polycondensation of alkoxide or nitrate precursors, followed by supercritical drying, and
- hydrolysis and polycondensation of alkoxide precursors, followed by ageing and drying under ambient atmospheres.

In this project, the third approach was used for the preparation of the doped tin dioxide catalyst. The first method requires the use of colloidal powders. This can be difficult to obtain in some cases, especially where the more exotic dopants are used. The second method requires the use of supercritical fluid drying, which utilises high pressure and temperature vessels. The third method is relatively easy when compared to the first two and was chosen for this reason. The precursor salts are very easy to obtain (Merck, Sigma-Aldrich) and no complicated instruments or machinery are required in the process.

Firstly, important terms in the sol-gel process need to be defined. A *sol* is defined as a dispersion of colloidal particles in liquid; *colloids* being solid particles with diameters of 1-100nm. A *gel* is an interconnected, rigid network, containing submicrometer size pores and polymeric chains with average lengths greater than a micrometer [39].

Once simultaneous hydrolysis and polycondensation form the interconnected 3-D network of the gel, the pore liquid must be removed as a vapour phase to leave behind the gel. Supercritical drying of the gel may be employed to remove the excess pore liquid [40]. Due to the supercritical conditions, the network does not collapse and a low-density *aerogel* is formed. Pore volumes as high as 98% and densities as low as 80 kg/m^3 have been reported.

When conventional drying at ambient pressure is used to remove the pore liquid, the network collapses due to shrinkage and a *xerogel* is formed. These xerogels have been termed *alcogels* if the pore liquid is primarily alcohol based. A dried gel can be obtained by removing all physically adsorbed water. This occurs between 100-180°C.

Due to the very large surface concentration of chemisorbed hydroxyls on the surface of the pores, heat treatment in the range 500-800°C is used to desorb these hydroxyls. This reduces the number of pores and connectivity substantially, due to viscous-phase sintering (*densification*). This results in a *stabilized gel*. Complete densification results in the elimination of all pores and takes place at temperatures between 1000-1500°C — it is dependent on the surface area and pore size of the gel.

In the preparation of a gel, up to seven steps may have to be followed to form a

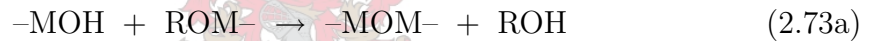
gel with the desired properties. Only the most important steps for the preparation of the tin dioxide catalysts will be presented here.

Step 1: *Mixing*. Generally a liquid alkoxide precursor is used to prepare the sol, but according to Ward and Ko [41] a wide variety of precursors may be used. The liquid alkoxide precursor ($M(OR)_n$) is hydrolysed by mixing with water. Hydrolysis and condensation reactions then take place in the solution (according to Ward and Ko [41]) as follows:

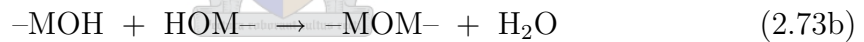
hydrolysis:



condensation:



or



These hydrolysis and condensation reactions continue until sufficient interconnected M–O–M bonds are formed, at which time they begin responding as a sol. The size of the sol particles depends on the pH and the ratio of alkoxide to water in the initial solution.

Step 2: *Gelation*. Given enough time, the colloidal particles will link together and form the 3-D network. The size of the particles and the extent of cross-linking before the gelation step determine the physical properties of the network. At this stage, the viscosity increases greatly.

Step 3: *Ageing*. Also known as *syneresis*, ageing involves the continuation of polycondensation. Localised solution and reprecipitation of the gel network also takes place, increasing the strength of the gel. Porosity of the gel network decreases with increased ageing time.

Step 4: *Drying*. During drying, whether by the conventional or supercritical technique, the pore liquid is removed from the interconnected network.

Step 5: *Densification*. Through the heating of the porous gel at high temperatures, the pores in the network are eliminated and, in the case of coated substrates, the catalyst is fused to the substrate.

Ward and Ko [41] suggest several parameters that are responsible for the final properties of the layer. Of these, the type of precursor, type of solvent, water content, acid or base content, precursor concentration and temperature are important.

In the literature, preparation of SnO₂ films has almost exclusively been done using inorganic precursor salts. These salts were always hydrated salts, i.e. SnCl₄·5H₂O [40] or SnCl₂·2H₂O [42, 43, 44, 45]. In one instance Tin(IV)ethylhexano-isopropoxide (Sn(OOC₈H₁₅)₂(OC₃H₇ⁱ)₂) was used as precursor [38]. It is assumed that the water required for the hydrolysis reaction comes from the adsorbed water in the precursor salt, since no water is added at any stage of the process. The precursor salts are then dissolved in a suitable solvent (ethanol or isopropanol) and heated under reflux at temperatures up to 80°C in a closed vessel.

Different steps are followed at this stage of the process. In some cases the solvent was evaporated until a fine powder was left behind, while some researchers allowed the solution to undergo gelation for up to 5 days. The same procedure was followed for any dopants that were to be added to the tin solution. In the case of the powders, the desired level of dopant was added and the mixture was redissolved in the solvent. This solution was then heated under reflux, in an open vessel, for 2 hours.

The substrates were then immersed in the solution and withdrawn slowly at a constant rate. This rate varied from 3 to 11 cm/min. These films were then dried in air at 60 to 110°C for between 1 and 2 hours. This process was repeated for each coating of the catalyst. The substrates were then subjected to a final heat treatment at temperatures ranging between 500 and 600°C for 10 minutes to 1 h, at a heating rate of 2°C per minute.

2.5 Review of Previous Work

Several researchers have done a significant amount of work using metal oxide electrocatalysts for the oxidation of phenol. A fair variety of catalysts and model contaminants have been tested for their activity towards the oxidation reaction. This section will be subdivided into two parts. The first is a detailed description of work carried out by Grimm, since all of the work in this study is based on his findings. The second section is a short overview of the most important research done by other authors in the field of electrocatalytic oxidation of organics. In most cases SnO_2 , PbO_2 or IrO_2 were used, sometimes with the addition of dopants. Several researchers employed the solid-polymer-electrolyte system, as used in this study, but with the addition of supporting electrolytes for improved conductivity.

2.5.1 Grimm's Research

Since this study is based mainly on Grimm's work, a detailed account of his oxidation results will be given first. All of the facts in this section were taken from his PhD thesis [15].

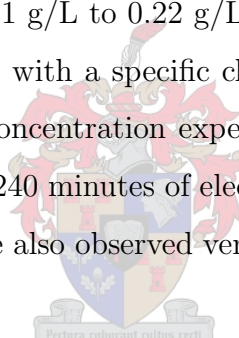
As with this study, one of the major hurdles was the determination of the phenol and intermediate concentrations. Grimm chose a simple and easy-to-use method for the determination of the compounds. The exact method is described in detail in section 3.4. The method entails the reaction of phenols with 4-aminoantipyridine to form a coloured antipyrene dye that can be analysed spectrophotometrically at 510 nm. In effect, a phenol index is obtained that is a comparative measure of the content of the phenolic compounds. Mention is made of the inherent problems in this method of analysis, since several distillation steps are required to ensure that only phenolic and substituted phenolic compounds are detected. Also, no differentiation can be made between different phenolic compounds. Several other types of interference can also affect the obtained phenol index.

The electrochemical cell utilised was identical to the one used in the laboratory-scale work in this study, with the exception of the flow channels. Grimm's reactor was

initially used for water hydrolysis and therefore the current collectors were machined to optimise the hydrogen and oxygen yields. The problem with the shape of these current collectors was that it was very difficult to characterise the flow without the use of computational methods.

Grimm conducted experiments at two different phenol concentrations. The first experiment used a very high phenol concentration (1 g/L) while the second used a very low concentration of phenol (1 mg/L). This corresponded with molar concentrations of 10.6 and 0.011 mM phenol. He used two different reaction volumes for the different experiments. In the high concentration experiment, only 100 mL was used and in the low concentration experiment, 500 mL was used.

The analysis of the results showed that for the high concentration experiment the concentration was reduced from 1 g/L to 0.22 g/L after 960 minutes of electrolysis. This reaction time corresponded with a specific charge of $320 \text{ Ah}\cdot\text{dm}^{-3}$ and a conversion of 78%. With the low concentration experiments the phenol concentration was reduced to 0.02 mg/L after 240 minutes of electrolysis. This corresponds with a specific charge of $8 \text{ Ah}\cdot\text{dm}^{-3}$. He also observed very low current efficiencies, ranging from 22.3% to 2%.



2.5.2 Other Research

Some of the first work done in the field of electrochemical oxidation of cyclic organic molecules was by Kirk *et al.* [12] using a packed bed reactor. Lead particles were converted to PbO_2 to act as anodic material and a stainless steel plate served as cathode. Aniline was chosen as model contaminant. As a result, a 98% conversion of the aniline after the passage of $25 \text{ Ah}\cdot\text{dm}^{-3}$ was obtained. Sulfuric acid (pH 2) was used as supporting electrolyte. The cell was operated at a current density of about $9 \text{ mA}\cdot\text{cm}^{-2}$ and current efficiencies in the range of 42 to 18% were obtained.

They also tested the reactor system in the electrolysis of phenol [13] and obtained a 98.4% conversion of the phenol to intermediates after the passage of $25 \text{ Ah}\cdot\text{dm}^{-3}$. The supporting electrolyte was 1.0 M sulfuric acid.

Stucki *et al.* [46] studied the performance of high overpotential anodes in the

treatment of waste waters. A wide variety of organic compounds were evaluated. These compounds were dissolved in a base electrolyte of 0.5 M Na₂SO₄ and adjusted to the desired pH by addition of either NaOH or H₂SO₄. It was found that after the passage of a specific charge of 74.7 Ah·dm⁻³ all of the TOC carbon was removed. The model contaminant in this specific case was benzoic acid. An electrochemical oxidation index (EOI), which is a measure of the reactivity of a particular compound with regards to oxidation by electrogenerated hydroxyl radicals, was calculated for each compound. This Comninellis defined this EOI as [47]

$$\text{EOI} = \frac{1}{\tau} \int_0^{\tau} \frac{\dot{v} - \dot{v}_{\text{org}}}{\dot{v}} d\tau \quad (2.74)$$

The EOI is determined by the measurement of the evolved oxygen (\dot{v}) during an experiment in the presence and absence of the organic compound. They observed the highest EOI value for the benzoic acid (EOI = 0.79). The next lowest value for the EOI was 0.8 for nitrobenzene, while the lowest EOI value was 0.02, which was obtained for triaminotriazin.

Murphy *et al.* [48] performed similar experiments using a PEM as electrolyte in an electrochemical cell. The anode (with a geometric surface area of 6.25 cm²) consisted of a platinum 10% iridium mesh that was pressed onto the Nafion 117 PEM. This membrane mesh assembly was then sandwiched between two titanium current collectors coated with platinum. Experiments were conducted on a mixture of 12 organic compounds that was being circulated through the reactor at 3 L/h. These experiments showed that at a current density of 1.2 A/cm², 97.3% of the TOC present in the solution was completely removed after the passage of a specific charge of 3703 Ah·dm⁻³. The long times required for TOC removal may be due solely to the resistance that some organic molecules have to electrochemical oxidation, especially acetic acid which had the highest TOC concentration. In these studies, using wet-air oxidation, acetic acid has been shown to be particularly resistant to oxidation [5].

Petrov *et al.* [8] prepared anodes by hot-pressing Teflon bonded (10 wt%) SnO₂ onto a fine titanium mesh. The membrane/electrode assembly was prepared using a technique employed in the proton-exchange-membrane fuel cell (PEMFC) technolo-

gies. This enhanced the energy efficiencies and power densities. The electrodes were then impregnated with Nafion solution ($0.6 \text{ mg}\cdot\text{cm}^{-2}$) and hot pressed to the Nafion membrane at 130°C , which is slightly above the glassification temperature of Nafion. The cathode material was platinum gauze. The electrodes were tested on the same cocktail of organics used by Murphy *et al.* [48]. All of the total organic carbon was removed after the passage of 1050 to $2100 \text{ Ah}\cdot\text{dm}^{-3}$, depending on experimental conditions.

Comninellis and co-workers used a two-compartment cell for the oxidation of organics. In the initial work [7, 9], SnO_2 coated titanium was used as anode and a platinum spiral was used as cathode. Oxidation of phenol was carried out in the reactor at a current density of 50 to $57 \text{ mA}\cdot\text{cm}^{-2}$, a temperature of 70°C and pH 2. The initial concentration of the phenol was 21 mM. The removal of the phenol, as well as the TOC in the solution, was measured and compared. The analysis showed that after 25 to $30 \text{ Ah}\cdot\text{dm}^{-3}$ (3.125 to 3.75 h), complete elimination of phenol had occurred. Longer oxidation times were necessary to reduce the TOC to 10% of the original value ($50 \text{ Ah}\cdot\text{dm}^{-3}$ or 6.25 h).

The effect of NaCl on the rate of removal of organics was also tested [49]. Using Ti/IrO₂ electrodes they observed an improvement in the removal rate in the presence of Cl^- . Cell conditions were the following: current density $100 \text{ mA}\cdot\text{cm}^{-2}$, pH 12.2 and temperature 50°C . After $20 \text{ Ah}\cdot\text{dm}^{-3}$, using only Na_2SO_4 as electrolyte, a 40% conversion of the phenol was obtained. For solutions with both Na_2SO_4 and NaCl, 95% conversions were obtained. The removal rate seemed independent of the Cl^- concentration (which was 433, 85 and 17 mM respectively).

Final experiments [27] involved the testing of the Ti/IrO₂ system for conventional aromatic removal. Phenol was used as model pollutant in a solution with a pH of 2. The temperature of the solution was 50°C and current densities of between 2.5 and $28 \text{ mA}\cdot\text{cm}^{-2}$ were maintained. Full conversion of the phenol to intermediate molecules was obtained after the passage of $35 \text{ Ah}\cdot\text{dm}^{-3}$.

Tahar and Savall [14] prepared PbO₂ electrodes on a tantalum surface for the oxidation of phenol. They prepared the lead dioxide by oxidation of a lead nitrate

solution. They are some of the few researchers that mention the possibility of the formation of polymeric oligomers, and they also used sulfuric acid (pH 2) to increase the conductivity of the solution. The oxidation experiments were performed at temperatures ranging from 60 to 90°C and they managed to convert all of the phenol to intermediates after the passage of between 31.6 and 15.2 Ah·dm⁻³ respectively. However, only 93.1% of the TOC carbon was removed after 100 Ah·dm⁻³ (initial TOC = 1500 ppm). It was found that maleic acid was difficult to oxidise into breakdown products.

Polcaro *et al.* [10] also used a parallel plate reactor with a SnO₂ coated sheet of titanium as anode. They used Na₂HPO₄ and H₃PO₄ as supporting electrolyte at different pH values (7 and 3). 2-chlorophenol was used as organic pollutant. In some of the experiments chlorides were added to investigate the effect on the combustion of the chlorophenols. It was found that 98.1% of the chlorophenol was removed after the passage of 2.13 Ah·dm⁻³.

2.5.3 Analysis of Literature Review

To shed some perspective on all of the data given in this section, the experimental data of some of the researchers mentioned has been converted into a normalised form and plotted. The researchers are indicated in the key of the graph. This data is presented in figure 2.8.

The x -axis of the plot is given in terms of specific charge ($[\frac{\text{Ah}}{\text{dm}^3}]$), as the extent of an electrochemical reaction is normally proportional to the amount of charge passed according to equation 2.2.

$$n = \frac{Q}{\nu_e F} = \frac{It}{\nu_e F} \quad (2.2)$$

Also, since the number of moles of reactant present in the solution determines the required charge, the charge is divided by the volume of the solution. All of the curves given in figure 2.8 are based on phenol concentration. Therefore, the number of moles of electrons that are required for the combustion of one mole of phenol is constant for all of the cases ($\nu_e = 28$). An efficient oxidation reaction will be one represented by a sharp gradient. On the other hand; lines with low gradients will represent

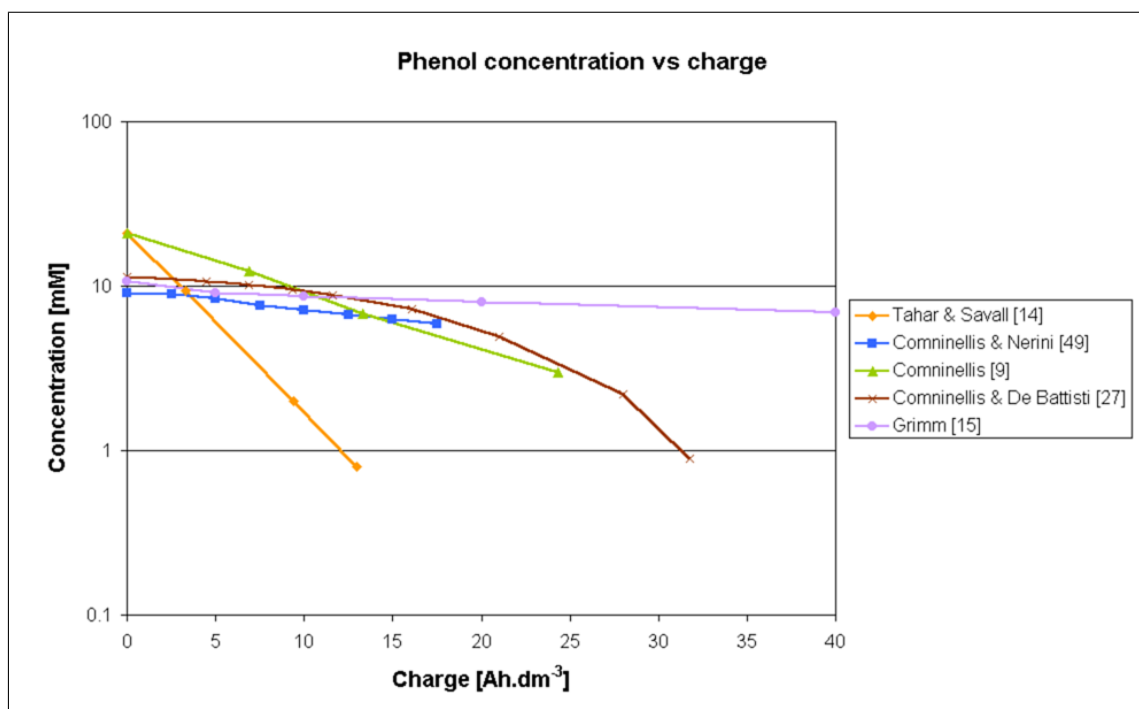


Figure 2.8: Normalised experimental data reported from the literature

an inefficient reaction. This can be explained by the specific charge. An efficient reaction will ensure that a larger fraction of the applied current is applied towards the oxidation reaction. This will in effect reduce the nominator of equation 2.2 since a smaller total current needs to be applied.

Another way of looking at an efficient process is by examining the moles of reactant that can be converted for the applied charge. If a larger fraction of the applied current is spent on converting phenol, more moles of phenol can be converted, corresponding to either a higher concentration of solution or a larger volume of solution with the same initial concentration. This in effect increases the denominator of the specific charge, leading to smaller values of the specific charge for higher conversions.

Chapter 3

Materials and Methods

3.1 The Solid-Polymer-Electrolyte Reactor

In section 1.3 the main aims of the project were set out. These aims specified the development of both industrial and residential water treatment facilities. In most industrial processes, a supporting electrolyte will normally be present in the form of salts or pH, and therefore a system can be designed that does not require the provision of supporting electrolyte. On the other hand, residential water treatment is not guaranteed of having a sufficient quantity of supporting electrolyte. The conductivity of the feed solution may have a wide range of values, depending on conditions affecting the source.

Therefore, a system that could function without the need for a supporting electrolyte was required. Such a system could not, however, be affected by the presence of high conductivity. Some researchers have used the solid-polymer-electrolyte system in their work and this system is ideal for these types of applications. An SPE reactor can function in solutions with exceptionally low conductivity (μS range) and is not detrimentally affected by the presence of even high concentrations of acids. It does have some disadvantages, but these will be discussed in section 3.1.2.

The exact method of preparation of the electrode used in this study is discussed in section 3.1.1. The different materials used and tested in the experimental work, together with the advantages and disadvantages of each, is provided, together with a description of the experimental set-ups used in section 3.2. Finally, the analytical

methods developed to determine the concentrations of the breakdown products are given in section 3.4.

3.1.1 Electrode Preparation

The method of catalyst preparation was similar to the method described by Fang *et al.* [16]. They used the sol-gel method to prepare the coating gels (see section 2.4). Baker also used this method to prepare and test zirconium-doped tin dioxide films electrochemically [20].

The organic molecules in feedwater react at the electrode-membrane interface where the protons formed in the reaction can be absorbed into the Nafion. This demands that the electrode be porous in order for the molecules to have access to that interface. The electrodes therefore consist of porous titanium electrodes (approx. 45%, Magneto Special Anode B.V., Netherlands), coated with the selected metal oxide catalyst.

The substrate metal is an important aspect in the deposition of the catalyst. As mentioned earlier, a separate project was run, parallel to this one, to address the optimisation of the catalyst materials [20]. Several different substrates were tested for suitability. Suitable adhesion of the metal oxide catalysts to the substrate material without cracking was only found on titanium. This has to do with the electron structure of the titanium metal, a so-called valve metal. Thus, if a cheaper valve metal or some alloy exhibiting similar characteristics could be found, it could also be employed as substrate.

The first step in the preparation process is the pre-treatment of the substrate material. The circular porous titanium plate used as substrate was first cleaned to ensure that no organic residues were present. This was done by boiling the substrate in nitric acid for approximately 5 minutes and then rinsing the substrate with absolute methanol.

A 150-mL round-bottom flask was used to prepare the gel. It was first cleaned by boiling a small amount of methanol (approximately 50 mL) in it, under reflux, for 30 minutes, to remove any impurities in the flask before the solution is prepared.

After discarding the methanol, the flask was rinsed again.

The tin dioxide was prepared first. A sample 7 g of $\text{SnCl}_2 \cdot 2\text{H}_2\text{O}$ (6.33×10^{-2}) was dissolved in 85 ml methanol. The solution was then well stirred and refluxed for 1 hour. The zirconium was then added to the solution. The amount added was calculated as the quantity of $\text{Zr}(\text{OC}_3\text{H}_7)_4$ required to ensure that the final film contained 1 mole% Zr — This corresponded to a total of g.

The mixed solution was once again well stirred and heated under reflux for another hour. After this stage in the preparation, the vessel containing the mixed oxide solution was sealed and allowed to age for 24 hours at ambient temperatures.

Different methods have been described by which to coat the substrate materials. The most popular methods are the following:

1. *Spin coating.* The substrates are mounted on a rotating disc and rotated at high speeds (1000 rpm). The gel is then dripped onto the substrate to create an evenly coated surface.
2. *Dip-coating.* The electrode is immersed in the gel and withdrawn at very slow speeds (1 to 11 mm/min).
3. *Drop coating.* The electrode is placed on a horizontal surface and the solution is distributed evenly over the substrate by dripping with a dropper.

The dip-coating method was used in this study. A custom-made multi-phase motor was built and used to withdraw the substrates from the coating solution. One of the disadvantages of this method is the large quantity of gel required, especially in the case of large electrodes. The advantage of this method is the homogenous surface coating that can be obtained.

The coated electrode was dried at 100°C and then coated a second time to heal any cracks in the surface. The coating was dried again and then heat-treated to create the metal oxide coating. This was done at 600°C for one hour, at a heating rate of $1^\circ\text{C}/\text{min}$. After cooling the electrode was ready to be used in the SPE reactor.

SEM photographs were taken of the surface to determine the quality of the coating. The photographs are shown in figures 3.1 and 3.2.



Figure 3.1: SEM photograph of catalyst (2500x)

Notice the cracks in the pores of the catalyst. These pictures were taken of substrates after only one coating. The substrates were coated a second time to heal these cracks.

3.1.2 Proton Exchange Membrane

One of the problems with the Nafion membrane is that impurities present in the electrolyte can have a negative influence on the functioning of the membrane. Heavy metal ions like Mg^{2+} and Ca^{2+} ions may replace the H^+ -ions in the polymer, thus changing the morphology and functionality of the membrane. These ions bond permanently with the Nafion membrane, thus reducing its capacity for protons and increasing the specific resistance of the membrane. While the electrochemical cell is operational, the membrane absorbs protons in favour of the other heavier ions. It is only when no potential is applied on the cell that any of the ions can interact with

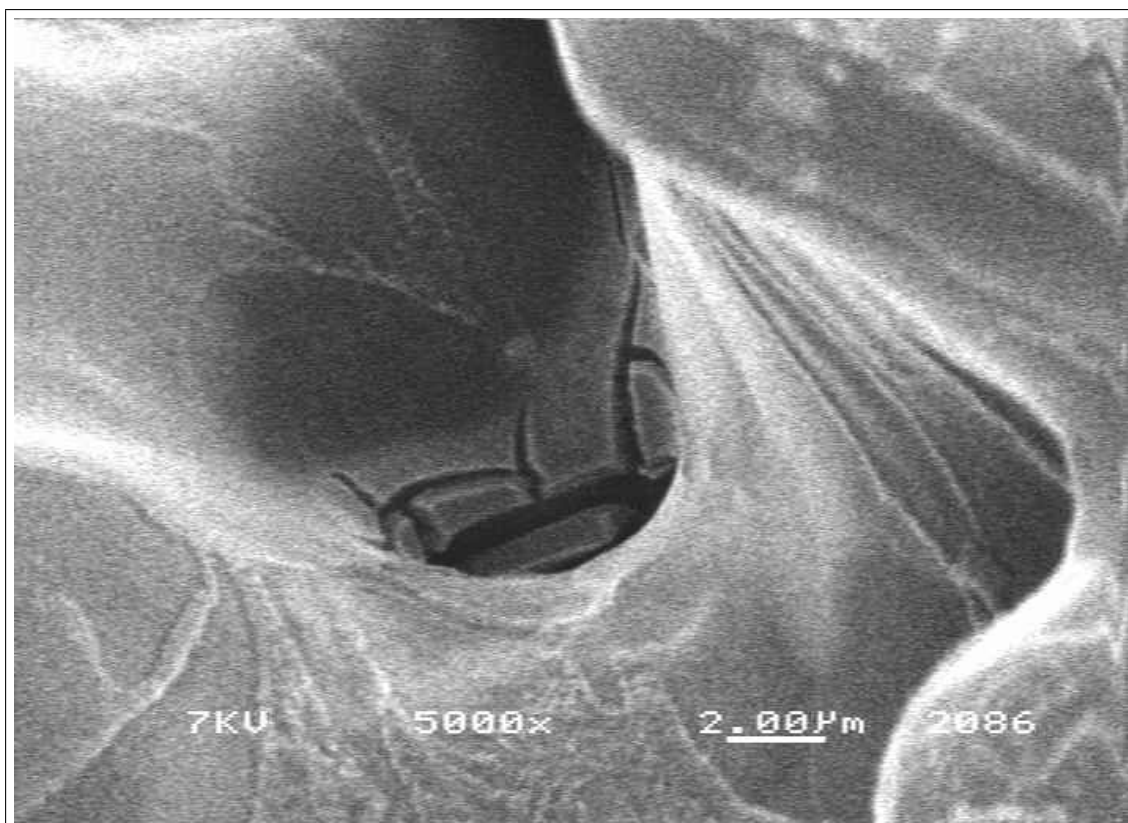


Figure 3.2: SEM photograph of catalyst (5000x)

the membrane. It has also been observed that the Nafion membrane absorbs organic molecules. This may have a significant influence on the efficiency of the membrane.

Another limitation of the membrane is the maximum current density. It has been found that high current densities can dehydrate the membrane, thereby reducing the proton conductivity and increasing the resistance to charge transfer. Very high current densities can even cause the membrane to burn causing permanent and irreversible damage. This only occurs at very high current densities, in the order of $1000 \text{ A}\cdot\text{cm}^{-2}$.

The membrane as used in the experimental work requires pre-treatment to ensure that the membrane is in the correct form and also to maximise its ionic conductivity. This is done by preparing a 0.1 N HCl solution, using distilled water to minimise the number of heavy metal ions in the solution. The membrane is then boiled in this solution for one hour, after which the membrane is ready for use in the SPE reactor.

3.2 Reactor Layouts

From the review of work done in the literature (section 2.5), it was determined that long reaction times (in the order of a number of hours) were required for the combustion of phenol, especially in cases where no supporting electrolyte is added. Also, in all of the cases in the literature, the experiments were conducted in a semi-batch way. This approach was followed due to the low conversion per pass, which makes accurate analysis of phenol and breakdown products difficult. The same approach was therefore also used in this study. The reactor system was operated under semi-batch conditions with varying degrees of recycling to provide flow control.

The major aspect of the flow system that changed as the project progressed was the design of the SPE-reactor. The design of the first system was based on an analysis of Grimm's [15] work. The reactor is discussed in section 3.2.1. A second, smaller reactor was then built due to the first reactor's shortcomings. This reactor is discussed in section 3.2.2.

3.2.1 Initial Work

Instruments and Specifications



Although both set-ups mentioned were similar in design, the scale of the two separate systems was different. In the first work with the initial set-up, the scale was significantly larger compared to the SPE reactors in the literature. It was presumed that most of the work done in the literature could be scaled up directly to make a working bench-scale reactor. A schematic of the first reactor flow system is given in figure 3.3.

The initial set-up consisted of two 50L tanks, constructed from 1.6mm stainless steel 316. Only the bottom-most tank was filled at the beginning of each experiment. The other tank was situated directly above this source tank. The purpose of this set-up was twofold. Firstly, the second tank was sealed from the environment so that any gases generated in the process could be salvaged. Secondly, the process could be run in both semi-batch and continuous fashion.

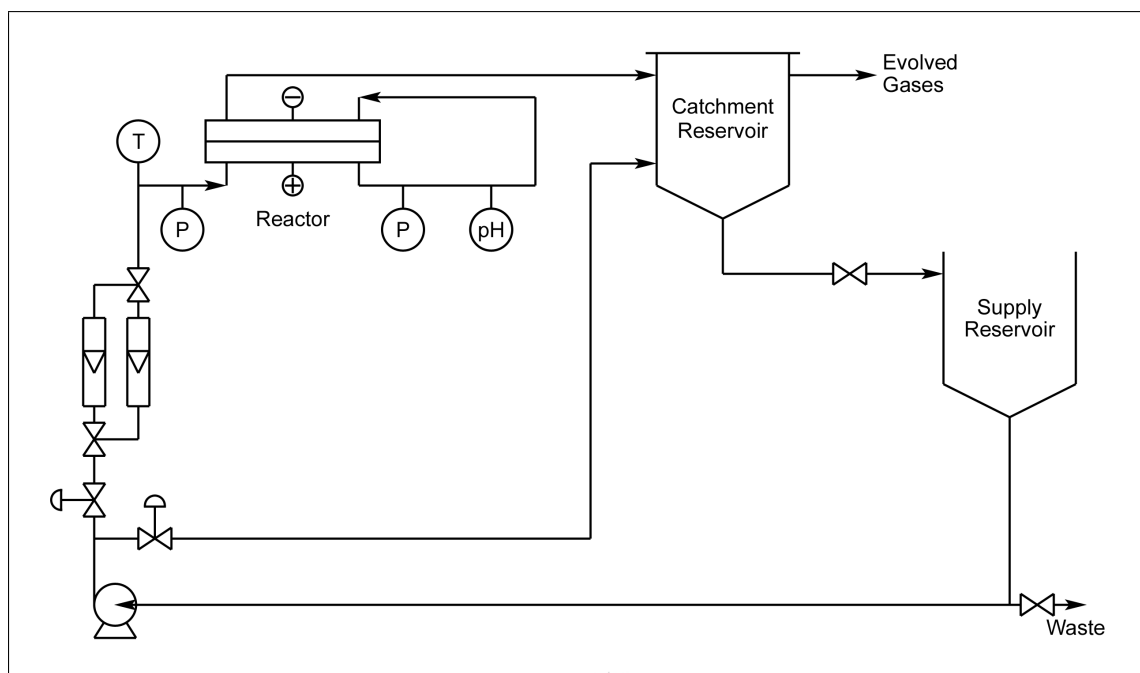


Figure 3.3: Reactor flow system used in the initial work

After a number of experimental runs were performed, the two tanks were replaced with a single 10L tank. These runs showed no conversion at all and therefore the volume to electrode area ratio was reduced. Also, no gas evolution was observed and therefore the need for the sealed tank was deemed unnecessary.

A magnetically driven centrifugal pump (Brubin, Magflo M6.1 SS 316) was used to circulate the reaction solution through the system. Downstream from the pump, the solution could be pumped through two different rotameters, depending on the desired flow. A flow range of between 60 and 2400 L/h could be monitored by the two rotameters. Both the reactor and the recycle line had a diaphragm control valve so that the desired flow rate could be obtained.

Other instruments included a temperature gauge situated on the inlet of the reactor, two pressure gauges (before and after the reactor) and a pH sensor capable of measuring the temperature on the outlet line. All of the instruments, including the rotameters were obtained from Indecx, Cape Town, South Africa. All of the tubing, fittings and valves were PVC products obtained from Astore Africa, Cape

Town, South Africa. The electrical current was supplied by a d.c. power source (GW Laboratory DC Power Supply GPR-3520H).

In the course of an experimental run, each with duration of 12 hours, samples of the contaminated water were taken every 2 hours. Since the HPLC analytical method for the determination of the phenol concentration (see section 3.4) was not developed at this stage, these samples were analysed for total organic carbon (TOC). The analyses were done at the CSIR in Stellenbosch, South Africa. Some additional information of the analyses is provided in section 3.4.

Experimental Reactor

In the design of the experimental reactor, the material of construction was a very important factor to consider. At this stage of the design it was still not known exactly what processes took place at the electrode/membrane interface. An important unknown in the design was exactly what sort of conditions was present in the reactor, especially close to the current collectors. From the general reaction mechanism given in section 2.2.1 it is seen that protons were being generated. This meant that the pH in at least the anodic compartment of the reactor should be less than 7. It was also possible that the adsorbed hydroxyl radicals could interact with one another to form hydrogen peroxide which would give a pH higher than 7.

Thus, the choice of current collector material had to be made very carefully so that the reactor would show excellent corrosion resistance over a wide pH range. Titanium was therefore chosen as the construction material for the current collectors. Titanium, upon exposure to water, forms an insoluble oxide layer that is highly resistant to chemical attack, but still allows electrical conductivity.

Straight, rectangular flow channels were then machined into the current collectors to allow fluid flow past the electrodes. The choice in length of the flow channel was unfortunately fixed due to the limited availability of the porous titanium substrates. The porous substrates used in the study were only 85mm in diameter. Larger substrates could be obtained from manufacturers in America (Mott Corporation), but the variation in the flatness of these larger substrates could lead to local variations

in the current density. Since the reactor used square current collectors, the circular discs were cut to fit the current collector, which measured 66mm on a side.

Each current collector was machined with nine square flow channels, each flow channel measuring 4×4mm in size. The titanium machining was done commercially by Allweld Marine Industrial cc. (Cape Town, South Africa). The electrode membrane assembly was then sandwiched and fitted into a PVC frame (Cape Plastics, Cape Town, South Africa). Diverging channels were machined into the PVC frame on each side of the current collector housing to attempt to reduce pressure drop in the reactor. Schematic drawings of the reactor are given in Appendix D.

Electrical contact was supplied to the current collector through five stainless steel bolts. The cathodic side was fixed to prevent the flow channels from shifting too far from being flush with the PVC frame flow channel. This was done by welding five M6 bolts onto a flat stainless steel plate. This served as the secondary cathodic current collector. The EMA (electro-membrane-assembly) rested on this plate. The anodic current collector was then pressed onto the cathodic current collector plate by fastening five M8 stainless steel 316 bolts that passed through the PVC frame and connected directly with the anodic current collector.

The reactor was sealed using a 3mm Viton o-ring that fitted in a groove around the flow channels and EMA. A total of 16 M6 galvanised mild steel bolts were used to provide the required compression to seal the reactor.

3.2.2 Laboratory-scale Reactor

Results obtained in the initial work are discussed in section 4.1. It was found that the reactor set-up (as used in the initial set-up) failed in removing any significant amount of organics from the feed solution. Even with a reduced reaction volume to electrode ratio, insufficient rates of reaction were obtained. It was therefore decided to return to a reactor scale similar to that used in the literature. In this way additional data regarding the reaction kinetics could be obtained for the design of a larger scale reactor. At this stage of development it was not yet realised that the total organic carbon analysis that was used in this study, was inadequate for the detection of

refractory organics (see section 3.4).

Also, during this period, it was decided to investigate cheaper alternatives to the titanium current collector as it was realised that the price of the titanium current collectors alone could shift the price of a unit out of the viable region.

Instruments and specifications

The experimental set-up used the same reaction volume as that used by Grimm [15]. The reservoir consisted of a 1L glass bottle that could be sealed to prevent the relatively volatile organics from escaping into the atmosphere. Flow control was maintained by a ball valve, since only three flow rates were chosen for the experimental work. The experimental set-up is shown in figure 3.4

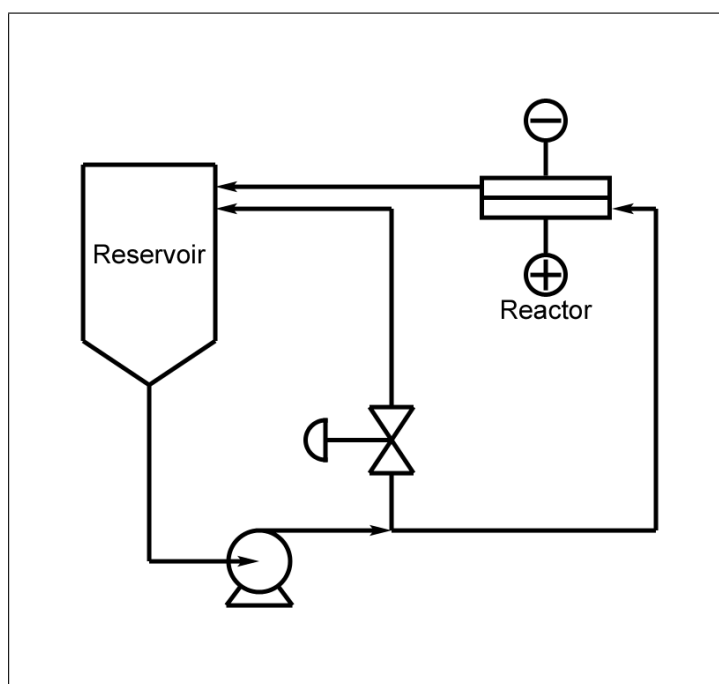


Figure 3.4: Experimental set-up for the laboratory scale experiments.

Preliminary work on the laboratory scale reactor was done using a peristaltic pump (with a maximum flow rate of 21.8 L/h). Later a small magnetically driven centrifugal pump with a maximum flow rate of 37.2 L/h was used (Schmitt-Kreisel, 7505). This does not correspond with the maximum flow rate capacity of the pump due to the high pressure drop through the reactor. Since the pH measurements in

the initial experiments remained constant over the duration of the experiments, the pH measurements were abandoned and only the phenol concentration was measured. In later experiments, pH, conductivity and temperature were measured.

The pH and temperature were measured on-line using a +GF+ Signet 2714 pH electrode obtained from Indecx, South Africa. The pH probe was connected to a pre-amplifier (+GF+ Signet 2720) and the readings were displayed with a +GF+ Signet 8750-1 transmitter. The conductivity was measured using a Genway 4071 conductivity meter.

Experimental Reactor

The materials of construction chosen for the current collectors in the laboratory scale reactor were also chosen for their relative corrosion resistance. Since the initial experiments showed that the pH of the solution leaving the reactor remained virtually constant ($\text{pH} \simeq 4.5$), it was decided that nickel, which has good corrosion resistance to mild acidic solutions, could be used as current collector material. Nickel, although possessing a relatively good electronic conductivity, has a resistance three times greater than titanium and about six times greater than aluminium.

Aluminium, upon exposure, forms an oxide layer that acts as electric insulator and could therefore not be used in pure form as current collector material. One advantage of using aluminium was its relatively easy machinability. Therefore aluminium discs were obtained (Non-ferrous Metals, Cape Town, South Africa); upon which a single flow channel of length 548 mm was machined (see schematic in Appendix D). The inlet and the outlet of each current collector were situated in the back of each current collector. Stainless steel 316 flow nozzles ($\frac{1}{8}$ " , West Beach Instrumentation, Cape Town, South Africa) were used to provide connections to the external fluid circuit. The aluminium current collectors were then electroplated with nickel to provide adequate electric conductivity and corrosion resistance. The electroplating was done by Metana Surface Coatings cc, Cape Town, South Africa.

Four nickel-plated aluminium pins attached to the back of the current collectors supplied electrical contact. On the edges of each current collector facing the opposite

current collector a lip was machined. On the edges of each current collector facing the opposite current collector a lip was machined. A Viton gasket was placed onto this edge to provide a seal for the reactor. The current collectors were once again housed in a PVC frame, which was fastened with eight M8 mild steel bolts. The nuts for these bolts were fastened using a torque meter to ensure that the stack pressure was constant for each experiment. Detailed drawings of the laboratory-scale reactor are given in Appendix D. Photographs of the various parts of the reactor are given in figures 3.5(a) to (d).



Figure 3.5: Photographs of the laboratory-scale electrochemical cell.

Although the cost of this experimental set-up was significantly less than the equivalent titanium reactor (approximately 10 times), it was found that some corrosion still took place. Most of the corrosion was believed to take place due to the anodic

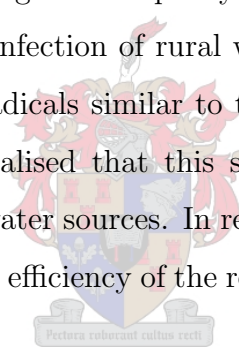
oxidation of the nickel to nickel oxide, since very high potentials (between 20 and 30 V) were required to obtain the working current densities. Another reason for the use of nickel was to ensure that sufficient funds remained for the construction of a pilot plant if the need arose.

Once it was found that the process was not economically viable (see chapter 6), a titanium reactor was constructed to see if this would have any significant effect on the observed reaction rates.

3.3 Microbiological Method

3.3.1 Introduction

The reactor system, besides being able to purify selected industrial waste waters, also had to be usable in the disinfection of rural water supplies. Since the catalyst form highly reactive hydroxyl radicals similar to the reactive intermediates formed in ozonation systems, it was realised that this system could be very effective in the treatment of contaminated water sources. In response to this, some basic experiments were conducted to test the efficiency of the reactor with selected contaminated samples.



3.3.2 Pathogen Selection

With the help of the Department of Microbiology at the University of Stellenbosch, three of the more commonly occurring pathogenic micro-organisms were chosen based on their doubling times. These pathogens included the following:

- *Enterococcus Faecallis* (strain 92) - an opportunistic pathogen with a doubling time of approximately 35-40 minutes that is generally found in most types of faecal matter. It causes diarrhoea and nausea when excessive quantities are present in the human body.
- *Salmonella Choleraesius* (strain 10398) - a pathogen with a doubling time of approximately 20-30 minutes that originally comes from the digestive tracks of

birds and can be found in raw meat (especially chicken and eggs). It causes abdominal pains, diarrhoea, vomiting and fever. It has an incubation period of 48 hours.

- *Escherishia Coli* (strain k88) - a pathogen with a doubling time of approximately 20 minutes that is generally found in contaminated water and food (especially beef). It causes severe diarrhoeal diseases, vomiting and fever, and has an incubation period of 24 hours.

The main reason the three above mentioned micro-organisms were chosen were availability, safety and ease of analysis, while the experiments would still be able to demonstrate the principle that the reactor can be used in the destruction of these and similar micro-organisms.

3.3.3 Experimental Method

In an attempt to imitate typical contaminated water from water sources, a diluted solution of tryptone soy broth was used. This is simply a solution of a specific sugar (tryptone), peptones and NaCl that is used by the above-mentioned micro-organisms to sustain life and multiply. A 1% solution was used which equates to 0.05 g/L NaCl and 0.25 g/L of other agents such as peptone and sugar. Chemical oxygen demand (COD) measurements of the solution were taken and a value of 850 mg O₂/L was found.

The experiments themselves entailed the initial setting up of growth curves for the corresponding micro-organisms to determine the required minimum duration of the experiments. It was decided that the experiments would be run until the microorganisms reached their respective stationary phases. Once a certain species of microorganism reached its stationary phase its rate of death and rate of multiplication becomes the same due to toxins formed by the microorganism and availability of nutrients. This will correspond to the maximum 'concentration' of microorganisms that can possibly survive in a certain growth medium. If the reactor has not decreased the numbers of the micro-organisms at this stage, it is most likely inefficient in the

treatment of water supplies containing these micro-organisms.

A 10 mL 100% solution of the growth medium was made up and inoculated with the pathogens. It was then left for a period of time, which corresponded with the specific pathogens' time to reach stationary phase. 1 mL of this inoculum was then used to infect the test and control volume, which consisted of 1 L of the 1% growth medium. The control volumes were used to compare the efficiency of the reactor on disinfecting the test volume.

In all the experimental results reference is made to the 'concentration' of the solution. This is a very loose term and refers to the number of living cells per unit volume. This must not be confused with chemical concentration. In the case of a solution containing these living organisms, the organisms form colonies that tend to clump together. This often causes spatial inconsistencies in the cells per unit volume. Due to this characteristic, obtaining accurate representations of the cell count at any given time in the experiment is difficult. In an effort to negate this effect the solutions were kept well stirred.

Initially, highly concentrated samples were used which created unrealistic test environments. The concentration of cells was then reduced to typical contamination levels found in the literature (typically between 100 and 10 000 cells per 100mL). At these low concentrations, analysis of the samples became difficult and a different technique had to be used. This involved filtering of entire test volume and therefore only initial and final sample points were available. One option would have been to increase the test volume, but then the risk of flooding the electrodes with too many cells was higher.

Even with this method, inaccurate results were obtained. In the end, it was decided to use the plate count method to determine the cell count. Usually 100 μ L was taken as a representative sample. If only this quantity was plated out, it would correspond to a maximum cell count resolution of 1000 cells per 100mL, which was in the middle of the typical contaminated range. It was therefore decided to increase the sample size being plated out to one mL. This would correspond to a maximum resolution of 100 cells per 100 mL, generally the maximum cell count that

uncontaminated water may have [50, 51].

Since this was still fairly inaccurate, it was decided to let the final reaction volume grow for 24 hours. If there were any living organisms left in the solution after disinfection, they would grow to a significant measurable quantity. Another sample was therefore taken 24 hours after the experiment was completed and plated out to determine if any micro-organisms were present.

Two types of electrodes were tested in the disinfection experiments: the metal oxide catalyst and graphite electrodes. The graphite electrodes are inert — they do not produce the active hydroxyl radicals, and is ideal to use to test for any other possible influences accounting for the disinfection of the test volume. The graphite electrodes were obtained from LeCarbone (Cape Town, South Africa) and had the same dimensions as the titanium substrate (85mm diameter, 1mm thick). The graphite of grade 2112 was chosen for high conductivity and mechanical strength.

3.4 Sample Analysis

Originally, a standard method [52] was used to determine the phenol concentration. The method involved the use of 4-aminoantipyridine to react with phenolic compounds to form a coloured component that can be measured using a spectrophotometer.

The major problem associated with this method is that the 4-aminoantipyridine is not specific in its reaction with phenolic compounds and may therefore also react with other benzene structures, such as the benzoquinones and di-hydroxybenzenes. Furthermore, the products formed with these other intermediates may not have the same absorbance as the equivalent amounts of product formed with phenol. Also, since a polymer film might be formed which consists of aromatic rings, the dye may also react with these polymers. Use of the dye formation method was therefore deemed inadequate for the required analysis purposes.

Since the use of total organic carbon (TOC) analysis of the samples required a large sample volume (20mL) relative to the reactor volume (1L), the use of HPLC

for the determination of the breakdown products was investigated. It was later determined that the method used by the CSIR (Stellenbosch) for TOC determination was inadequate for the determination of the TOC for the phenolic samples. The method used was ideal for TOC determination of water sources, but due to the refractory characteristics of phenol and phenolic compounds, inaccurate results were obtained. Using HPLC, it was found that two different columns could be used for the quantitative analysis of the suspected breakdown products.

The column used for the determination of the phenolic compounds was a conventional C18 column (Phenomenex, LUNA 5 μ C18(2) 150 \times 4.6mm). The column used for the determination of the aliphatic acids was a PL Hi-Plex H Ligand Exchange Column (300 \times 7.7mm). The separation and analysis were performed using a Thermo Separation SpectraSystem HPLC with an UV-detector.

The samples containing phenolic compounds were injected (10 μ L) using 50% methanol/50% water as mobile phase. The detector was set at a wavelength of 280 nm for these compounds. A chromatogram of the phenolic standards is shown in figure 3.6 and the retention times for the various compounds are given in table 3.1.

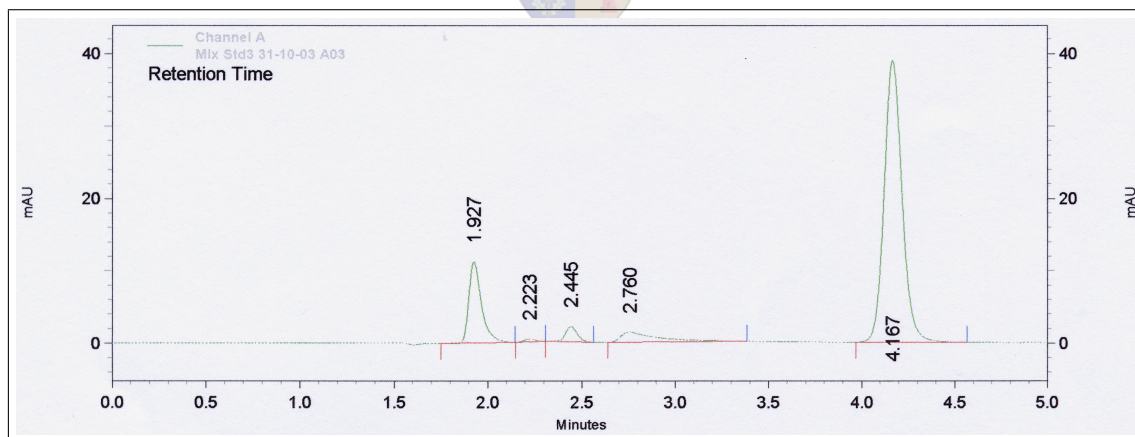


Figure 3.6: HPLC chromatogram of the standards for phenolic compounds

For the analysis of the organic acids, a 0.01 N H₂SO₄ mobile phase was used. Detection of the acid peaks was done at 210 nm. The chromatograms produced in the analysis of the organic acid standards showed tailing on all of the peaks, but the peaks so obtained were still usable. A chromatogram of the organic acid standards

Table 3.1: HPLC retention times for the phenolic compounds

Compound	Retention Time [min]
Hydroquinone	1.927
Resorcinol	2.223
Benzoquinone	2.445
Catechol	2.760
Phenol	4.167

is given below in figure 3.7. The acids tested were maleic, fumaric and oxalic acid. Formic acid was also tested, but did not show a well-defined peak. The residence times of the individual acids are given in table 3.2.

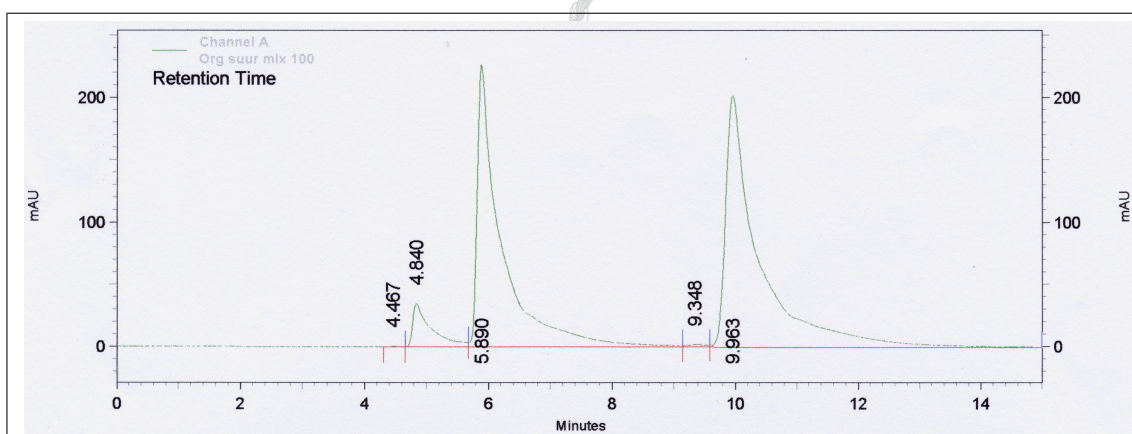


Figure 3.7: Chromatogram of acid standards

The samples taken during the experiments were analysed with both columns and examples of the chromatograms of initial and final samples are given in figure 3.8 to figure 3.10.

Two strange peaks were noted in the chromatograms obtained from the acid column figure 3.10. The initial sample was taken before the solution was pumped through the reactor and therefore should only have contained phenol as contaminant. Thus, the peak observed could be due to the presence of phenol in the sample. However, as the experiment progresses, an additional peak is observed before the

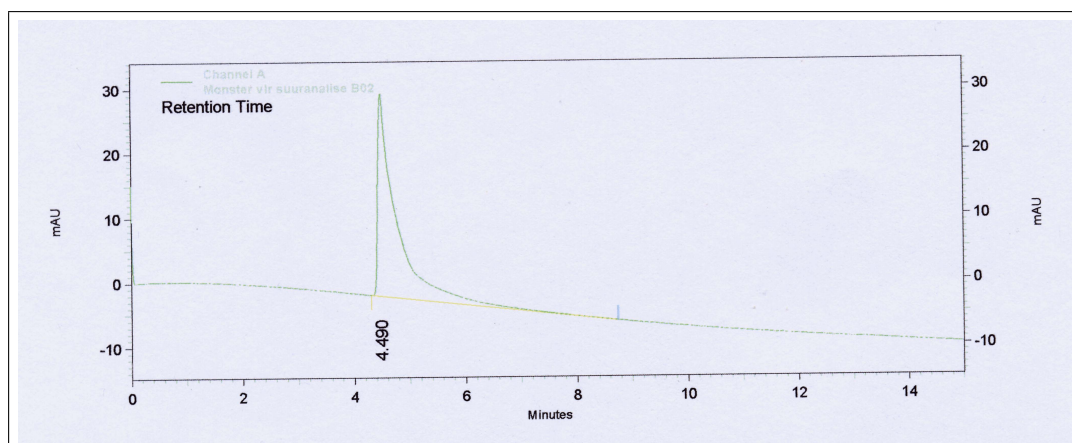


Figure 3.8: HPLC chromatogram of initial acid sample (1)

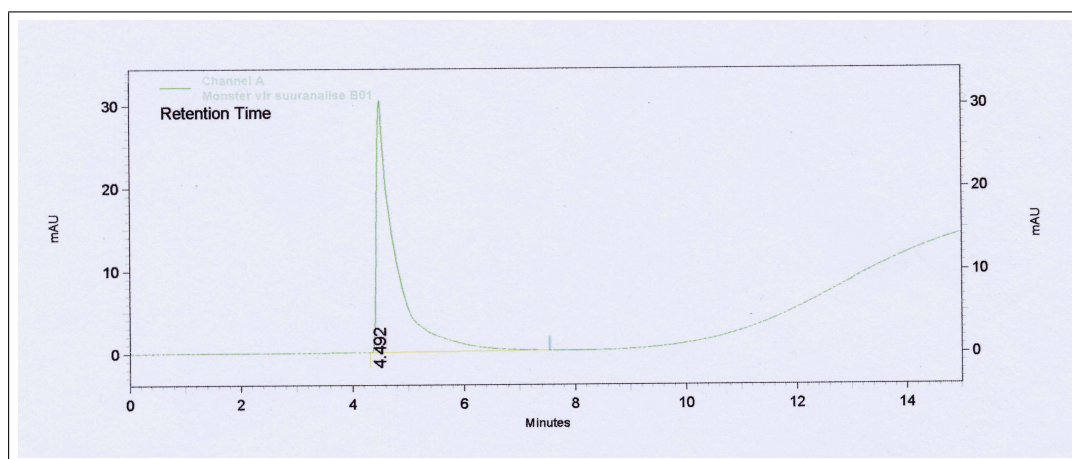


Figure 3.9: HPLC chromatogram of initial acid sample (2)

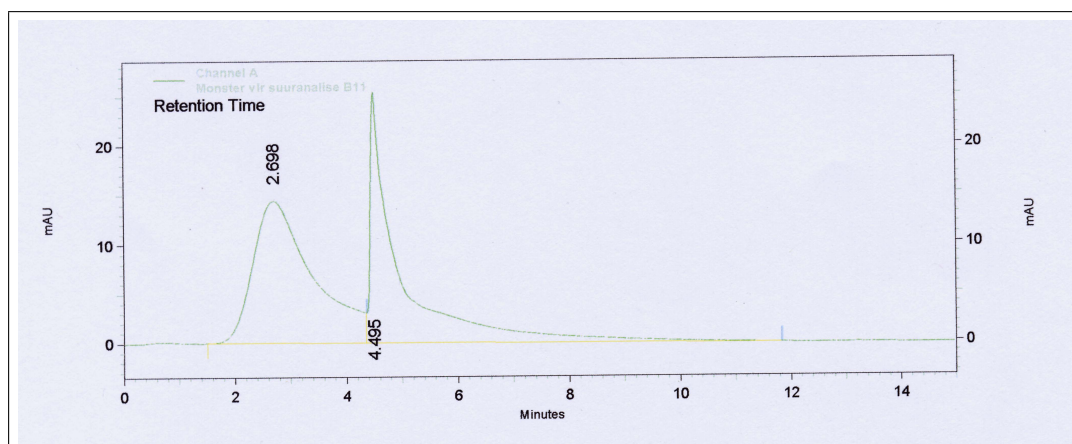


Figure 3.10: HPLC chromatogram of final acid sample

Table 3.2: Retention times for the aliphatic acids

Compound	Retention Time [min]
Formic acid	4.467 and 9.348
Oxalic acid	4.840
Maleic acid	5.890
Fumaric acid	9.963

‘phenol’ peak.

One possible explanation for the strange peaks is the formation of aliphatic organic intermediates with other functional groups such as alcohols and ketones. This is possible since the reaction involves the formation of the highly reactive hydroxyl intermediate, which can react with organic molecules in any number of ways. Note however, that none of the aliphatic intermediates that are popularly believed to be formed (oxalic, maleic and fumaric acid) are present in the samples.

Therefore, the samples can be accurately analysed by HPLC for the phenolic compounds, but total organic carbon must still be used to account for the contribution of the aliphatic intermediates.

Chapter 4

Phenol Oxidation – Results and Discussion

The experimental work relating to the electrochemical oxidation of phenol can be divided into two main parts (as seen in section 3.2). The experimental results obtained in the work done with the first reactor system are presented in section 4.1. One of the most important factors is the mode of operation of the reactor. The two options in this case were galvanostatic operation or potentiostatic operation. Both modes have distinct advantages and disadvantages as mentioned in section 2.1 and are discussed in more detail with reference to the actual results obtained in section 4.5. Therefore the results obtained with the nickel-plated laboratory scale reactor is subdivided into galvanostatic experiments (section 4.2) and potentiostatic experiments (section 4.3). The results obtained with the reactor using titanium current collectors will be presented separately in section 4.4.

In all of the experiments carried out in the study, an exponential curve is fitted through the data as a first approximation to the reaction rate constants. This is done so that some quantitative comparison of the data can be performed. The reason for selecting an exponential curve is explained in chapter 6 through the derivation of the model for the reactor. The symbol β is used for the constant in the exponent, i.e.

$$C_{\text{Ph},t} = C_{\text{Ph},0}^* e^{-\beta t} \quad (4.1)$$

where $C_{\text{Ph},0}^*$ is the calculated initial concentration based on the exponential fit.

All of the experiments with the nickel-plated reactor are represented by plotting

normalised concentration or concentration versus normalised charge. The analysis of the reaction rate constants is not based on this; it focuses on the concentration-time data, since the model derivation is based on time, not charge. The reason for presenting the data in such a way is the different reaction times required for the various current values selected. The galvanostatic experiments were run until 100% of the theoretical charge had been passed. This corresponds to times of between 8 and 24 hours, depending on the current setting. In this way the experimental data can be compared qualitatively for discussion purposes.

4.1 Initial Work

In the initial experiments, only the effect of flow rate on the reaction rate of the organic oxidation was investigated as all of the experiments were run galvanostatically. Due to the high overpotential of the reaction, relatively high current densities ($230 \text{ mA}\cdot\text{cm}^{-2}$) had to be maintained in order for the potential to be high enough. This corresponded with the maximum output for the power source and could therefore not be varied.

A 5 mM solution of phenol is used as stock solution in the experiments. This corresponds with a concentration of about 360 ppm total organic carbon (TOC). Samples were taken according to the method described in section 3.2.1 and analysed. The experimental results obtained for the initial reactor are shown in figures 4.1 to 4.3. In these graphs, the TOC is plotted versus time and an exponential curve is fitted through the data (see section 6.1).

The experimental parameters and conditions of the initial experiments are summarised in table 4.1. These conversions based on the difference between the initial and final values are also given. The conversion in this case is defined as

$$X = \frac{\text{TOC}|_{t=t_e} - \text{TOC}|_{t=0}}{\text{TOC}|_{t=0}} \quad (4.2)$$

Both the initial concentration as well as the calculated initial TOC is given. In all the cases the analyses of the initial samples resulted in values close to 250 ppm

TOC. This can be attributed to the refractory nature of phenol, which gives a lower predicted value of the TOC, as discussed in section 3.4.

Table 4.1: Experimental parameter values for initial experiments

Flow rate [L/h]	Applied Current		Initial concentration		Volume [L]	Conversion
	I [A]	i [$\frac{A}{cm^2}$]	[mM]	[TOC _{calc}]		
500	10	230	5.0	360.3	10	0.024
600	10	230	5.0	360.3	10	0.034
700	10	230	5.0	360.3	10	0.083

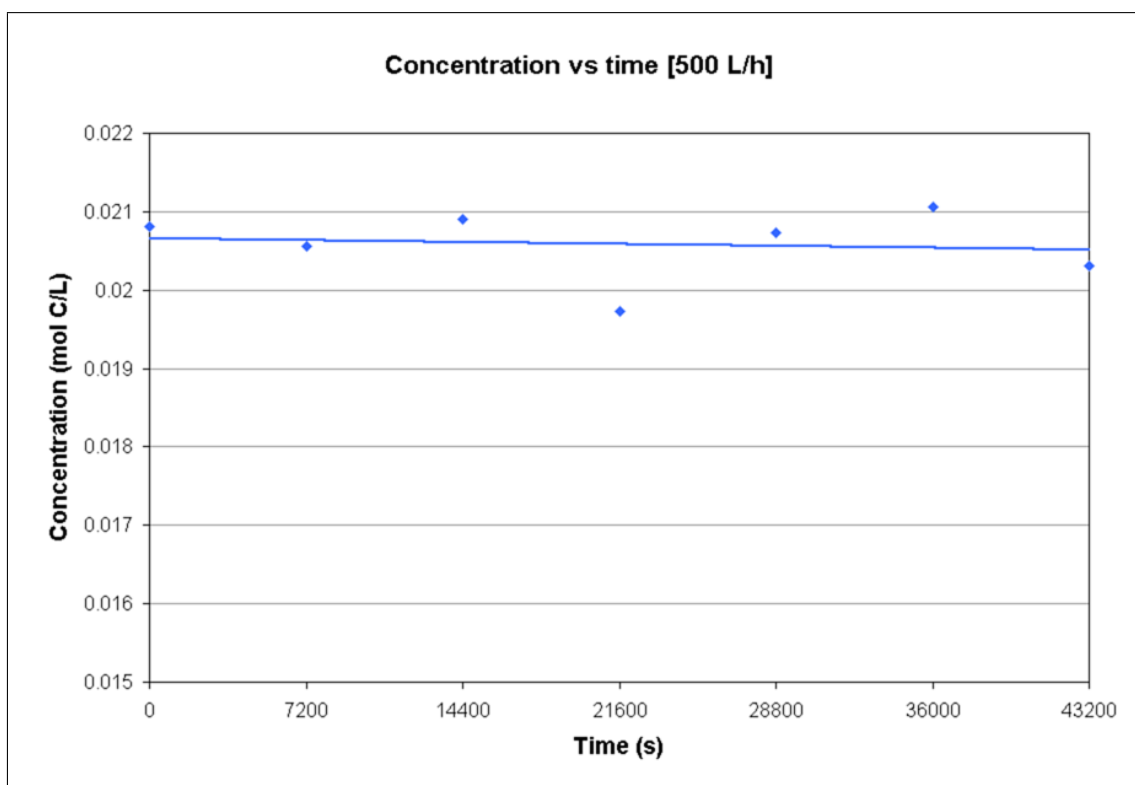


Figure 4.1: Breakdown curve for 500 L/h experiment

From the breakdown curves it can be seen that very low conversion of the total organic carbon was obtained. It was only realised at a later stage in the project that passivation of the electrode could have a major influence on the reaction rate. In these experiments, the electrode surface area to reaction volume was much smaller

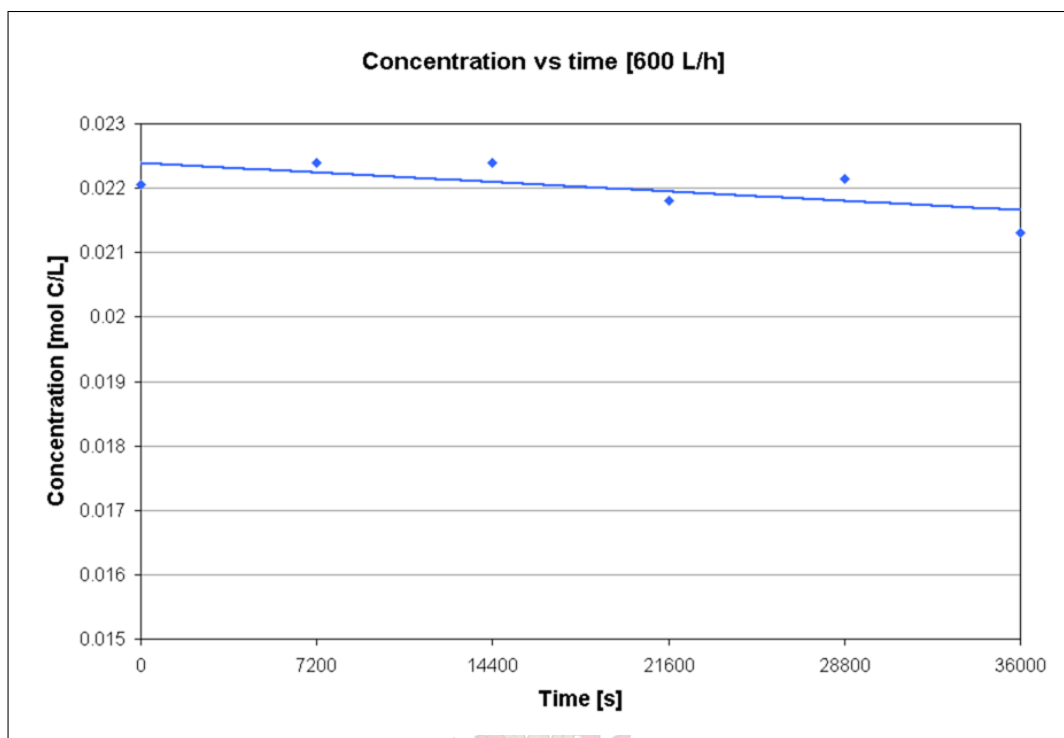


Figure 4.2: Breakdown curve for 600 L/h experiment

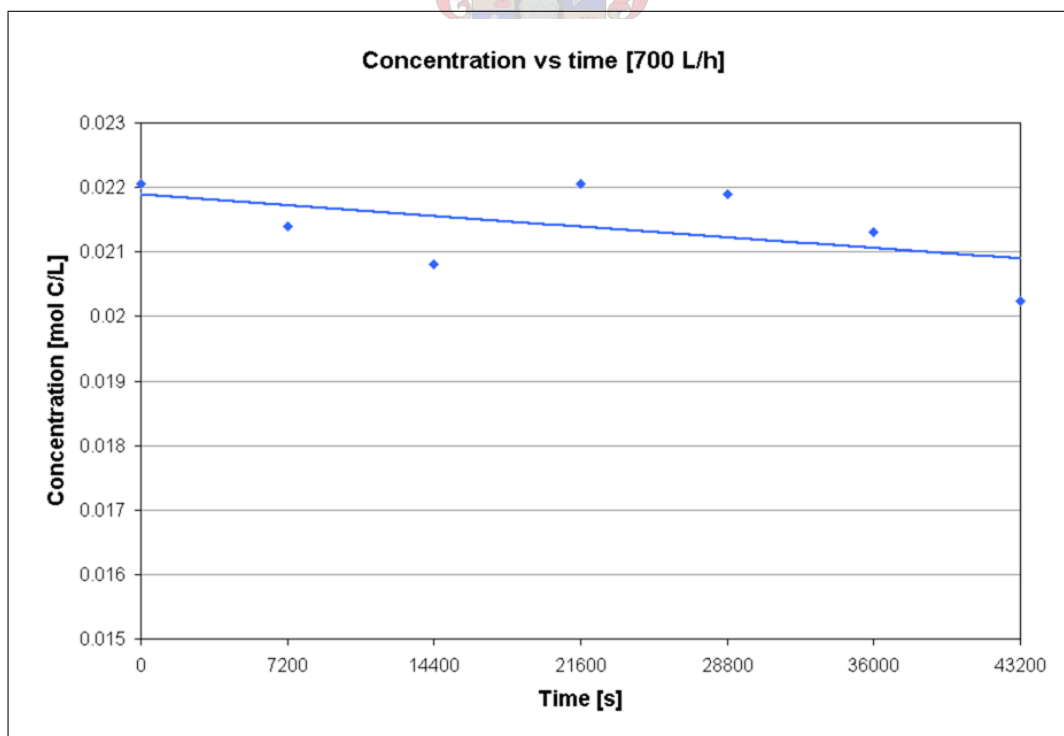


Figure 4.3: Breakdown curve for 700 L/h experiment

than in the laboratory experiments (4.4 vs 56.7 units). It is therefore possible that due to the passivation reaction, the electrode became completely deactivated before sufficient combustion could take place.

Theoretically, a charge 3.2 times greater than necessary to convert all of the phenol to carbon dioxide was supplied. As discussed in section 3.1.2, high current densities tend to damage and dehydrate the membrane and this could also account for the low conversions obtained. In such a case, the proton transfer in the membrane becomes the limiting step, with most of the electricity converted into heat energy due to resistance.

The calculated reaction rate constants are given in table 4.2 with the respective R^2 values and the 95% confidence interval values. Generally, if the coefficient determined by regression is much greater than the 95% confidence interval value, the proposed model or curve estimate the experimental values accurately. At least, the coefficient must be greater than the confidence interval value.

Table 4.2: Rate constants for initial experiments

Flow rate [L/h]	β [s ⁻¹]	k [m/s]	R^2	95% confidence interval
500	1.63×10^{-7}	8.27×10^{-8}	0.013	1.61×10^{-6}
600	9.24×10^{-7}	4.68×10^{-7}	0.032	1.45×10^{-6}
700	1.08×10^{-6}	5.46×10^{-7}	0.266	2.06×10^{-6}

Results of the experiments showed very poor fits of the exponential curve to the experimental data. In all cases the 95% confidence interval was greater than the absolute value of the coefficient β , indicating a poor fit. Also, the R^2 values were very close to zero, thus showing a significant deviation between the experimental values and the exponential fit.

If the values for the kinetic constants could be taken as is, one would assume that the process is under mass-transfer-limited control due to the increase in the constant with an increase in flow rate. Unfortunately, due to the variation in the

results leading to inaccurate constants, one cannot validate this assumption.

4.2 Laboratory Experiments – Galvanostatic

During the course of the project it was observed that the final reactor could only be used for the treatment of water with relatively low organic content wastes. The main reason for this was that the ratio of electrode area to organic compound mass must be less than a certain level or the electrode becomes overloaded and, moreover, unable to combust all of the organic material. Therefore, it was decided to reduce the initial concentration of the phenol from 250 ppm to 50 ppm. All further experiments (with the exception of those done to determine the effect of concentration) were therefore carried out using an initial phenol concentration of 50 ppm.

The most logical choices for the experimental parameters were current and flow rate. Current density was chosen because of the relationship described by Faraday's law (equation 2.2). On the other hand, if the process was in the mass-transfer-limited regime, flow rate would influence the reaction rate. Flow rate was therefore the second choice.

Several other parameters or factors expected to play a role on the observed reaction rates are:

1. phenol concentration,
2. assembly compression factor, and
3. separation of the catholyte and anolyte.

Concentration was considered to be a set variable in the final design. In some experiments however, concentration was used to determine the order of the reaction (see section 4.4.1). The compression of the MEA determines the quality of the contact between the electrodes and the membrane, so determining the local current densities, and would therefore directly influence the reaction rates. The results obtained for the MEA compression factor experiments are given in section 4.2.3. Finally, due to the reversible reaction between hydroquinone and *p*-benzoquinone, as well as

catechol and *o*-benzoquinone, as described in equation 2.71, the effect of separating the catholyte and anolyte was investigated. These results are summarised in section 4.2.4.

The values chosen for the individual experimental parameters for each set of experiments are given in table 4.3.

Table 4.3: Summary of experimental parameters for galvanostatic experiments

Flow rate [Re]	Current [mA]	Separated electrolytes	Torque [lb-in]	$C_{\text{Ph},0}$ [ppm Ph]	Section
650	20	No	15	50	
650	35	No	15	50	4.2.1
650	50	No	15	50	
650	50	Yes	15	50	4.2.2
1516	50	Yes	15	50	
650	50	No	25	50	4.2.3
650	50	No	15	150	4.4.1

4.2.1 Effect of Current Density

The choice of current densities to be tested depended on the power supply used. Due to the high overpotential at the electrode, only relatively low current densities could be maintained without pushing the operating potential above the maximum for the power supply. Therefore, currents of between 20 and 50 mA were selected. The exact parameters including the calculated current densities of the current experiments are given in table 4.4

The breakdown curves for the three currents are presented in figure 4.4. From the graph it can be seen that the intermediate current value results in the highest reaction rate compared to both the low and high current densities. The calculated reaction rate constants for the different currents are given in table 4.5. In all cases the experimental values were lower than the theoretical values. These theoretical values were obtained from the mass transfer correlation given by equation 2.47.

Table 4.4: Experimental parameters for current density experiments

Applied current		Flow Rate [L/h]	$C_{\text{Ph},0}$ [ppm Ph]	Volume [L]	Conversion []
I [mA]	i [$\frac{\text{A}}{\text{cm}^2}$]				
20	0.352	9.36	50	1.0	0.0623
35	0.617	9.36	50	1.0	0.100
50	0.881	9.36	50	1.0	0.0577

This correlation was set up for solid duct walls while the electrode is porous in the experiments. The correlation was therefore only an estimation of the external mass transfer to the surface of the electrode. It still however provided a measure against which the experimental values could be compared.

One of the side effects of the phenol oxidation reaction is oxygen evolution, whether by water electrolysis or by the reaction as shown in equation 2.67. This means that if the process is externally mass-transfer limited, higher experimental rate constants than the theoretical values shown in table 4.5 would be observed (as explained in section 2.1.4). Therefore, based on these results, one would assume that the process could not be externally mass-transfer limited. More information is required to make a better judgement of the exact limiting conditions prevalent in the reactor. Therefore, the next section will discuss the results of both the current and flow rate experiments.

Also note that, because of gas formation increasing the mass transfer, the Reynolds number as calculated is only a quantification of the flow and not necessarily a good characterisation of the flow.

The intermediate current value of 35 mA gives the highest reaction rate constant. The reaction rate should be proportional to the applied current and therefore it would be expected that the highest reaction rate constant would be associated with the highest current (50 mA). Some other effect must then account for the difference observed.

This could partly be explained by the covering effect, caused by the formation

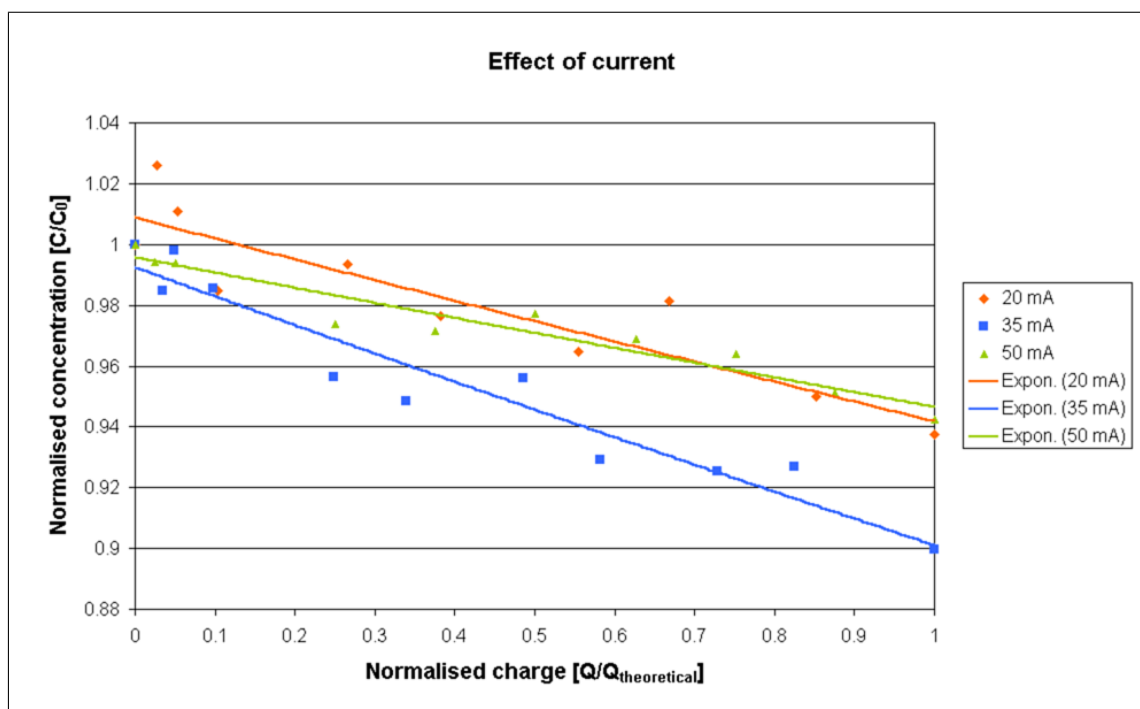


Figure 4.4: Effect of current density

of gas bubbles on the surface and in the pores of the catalyst. This phenomenon effectively reduces the fraction of the electrode surface available for reaction. Low current densities may force the selectivity of the reaction to be closer to the oxidation reaction due to lower applied potentials, but also causes the reaction to take place more slowly due to a lower current density.

Table 4.5: Reaction rate constants for current experiments

Current [mA]	β [s ⁻¹]	$k_{m,\text{experimental}}$ [m/s]	$k_{m,\text{theoretical}}$ [m/s]	R ² %	95% conf. interval
20	1.07×10^{-6}	4.86×10^{-7}	5.92×10^{-6}	82.5	4.00×10^{-7}
35	2.27×10^{-6}	1.04×10^{-6}	5.92×10^{-6}	93.1	4.64×10^{-7}
50	1.82×10^{-6}	8.30×10^{-7}	5.92×10^{-6}	92.4	4.26×10^{-7}

The high current density on the other hand speeds up the oxidation reaction, but also causes a larger fraction of the electrode surface to be covered, resulting in a lower overall oxidation rate. Some intermediate value of the current therefore maximises

the oxidation rate whilst minimising the formation of gas bubbles, resulting in a high overall reaction rate.

4.2.2 Effect of Flow Rate

Experiments to determine the effect of mass transfer were conducted at two different flow rates, both being in the laminar region of flow due to the limitations of the pumps available. The pressure drop in the reactor was very high because of the small equivalent diameter ($d_e = 4\text{mm}$), thus limiting the maximum flow rate. The values for the experimental parameters are given in table 4.6. The normalised concentration-charge data are presented in figure 4.5.

Table 4.6: Experimental parameters for flow rate experiments

Flow rate		Applied current I [mA]	$C_{\text{Ph},0}$ [ppm Ph]	Volume [L]	Conversion
[L/h]	[Re]				
9.36	650	50	50	1.0	0.101
21.8	1516	50	50	1.0	0.140

The reaction rate constants were calculated for both of the flow rates and are given in the table below:

Table 4.7: Reaction rate constants for flow rate experiments

Re	β [s ⁻¹]	$k_{m,\text{experimental}}$ [m/s]	$k_{m,\text{theoretical}}$ [m/s]	R ² %	95% conf. interval
650	3.64×10^{-6}	1.66×10^{-6}	5.92×10^{-6}	96.3	5.37×10^{-7}
1516	5.41×10^{-6}	2.47×10^{-6}	7.85×10^{-6}	98.6	4.79×10^{-7}

In both cases the experimental rate constants were lower than the theoretical rate constant. However, it must be noted that the ratio between the values for the high and low flow rate are almost the same (1.32 for the theoretical and 1.49 for the experimental values). The same applies in these experiments as for the current

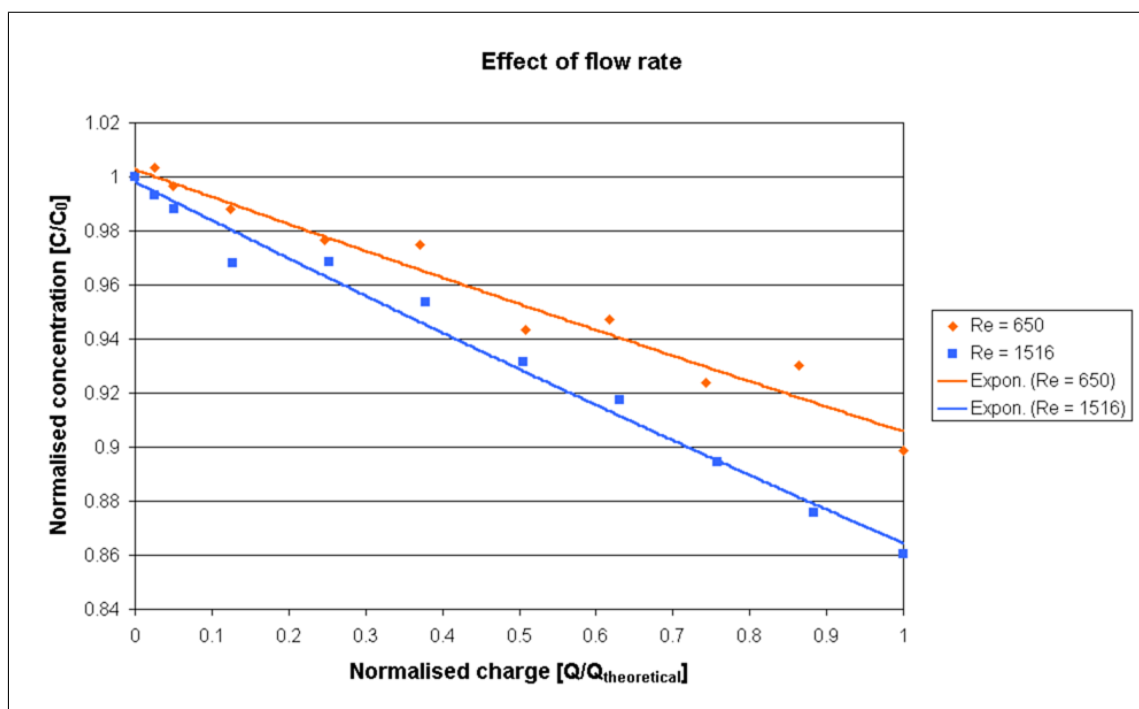


Figure 4.5: Effect of flow rate on reaction rate

experiments. The gas evolution would cause the mass transfer to be higher than theoretically predicted if external mass-transfer conditions limited the reaction.

It is realistic to assume that an increase in flow rate will cause a decrease in covering effect due to an increase in the bubble removal rate. From the experimental results presented in this section and the previous section, due to the dependency of the reaction rate on both the current density and the flow rate it seems that the reaction is in some intermediate limiting regime. This is entirely possible for electrochemical reactions and can be accounted for in the Butler-Volmer equation according to Wendt and Kreysa [22] (p. 56).

This of course complicates the extraction of the experimental parameters significantly, especially since very little information is available on the exact current density-potential relationships. In this case, the best approach would probably be to assume that the kinetics are similar to those encountered in chemical kinetics, assume a reaction order and obtain at least a reasonable estimation to the reaction order and reaction rate constants, as discussed in section 2.1.5.

4.2.3 Effect of the MEA Compression Factor

Due to the design of the reactor, the quality of the electrode-membrane contact plays an important role in the current distribution. If the reactor is not fastened tightly enough, high local current densities can exist, thereby changing the overpotential and thus the reaction. Therefore two different stack pressures were tested to observe the effect of this parameter. The values for the experimental parameters are given in table 4.8 and the breakdown curves for the two experiments are given in figure 4.6.

Table 4.8: Experimental parameters for MEA compression experiments

Torque [lb·in]	Flow rate [Re]	Applied current I [mA]	$C_{Ph,0}$ [ppm Ph]	Volume [L]	Conversion
15	650	50	50	1.0	0.0577
25	650	50	50	1.0	0.0533

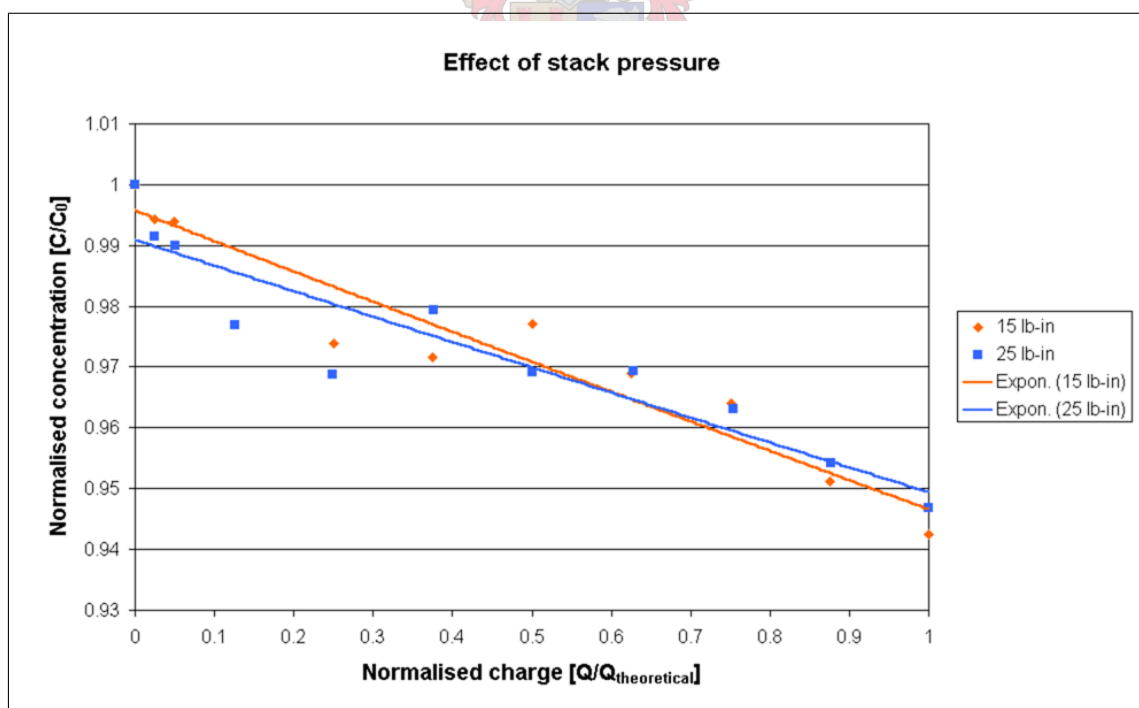


Figure 4.6: Effect of MEA compression on reaction rate

The reaction rate constants for the two stack pressures are given below. They are

given in terms of torque applied to the nuts used to fasten the frame of the reactor. The constants obtained for the two experiments are similar, differing by 15%, but

Table 4.9: Reaction rate constants for stack pressure experiments

Torque [lb-in]	β [s ⁻¹]	$k_{m,\text{experimental}}$ [m/s]	R ² %	95% conf. interval
15	1.82×10^{-6}	8.30×10^{-7}	92.4	4.26×10^{-7}
25	1.57×10^{-6}	7.16×10^{-7}	86.2	4.74×10^{-7}

with the lower rate constant associated with the higher stack pressure. This was unexpected, but the R² value of the second exponential fit was only 86% and may cause the constant to be slightly inaccurate. It was observed in the experimental work that for higher compression factors, lower potentials were obtained. This would imply a better distribution of current across the electrode. Since no real conclusive information could be extracted from this experiment, it was decided to at least keep the stack pressure constant for all the other experiments in order to eliminate any additional effects.



4.2.4 Anolyte-Catholyte Separation

One of the intermediate steps in the oxidation of phenol is the reversible reaction between *o*- and *p*-benzoquinone and their respective dihydroxybenzene structures. Therefore, the following can be expected: if the reverse reaction is somehow suppressed, an increase in the reaction rate should be observed. For the reverse reaction to take place, benzoquinone must be reduced, a reaction that takes place at the cathode. Thus, the easiest way of doing this is by the separation of the catholyte and the anolyte.

In the case of these experiments, peristaltic pumps were still used to pump the phenol solution through the reactor. An identical peristaltic pump was obtained and used to pump distilled water through the cathodic side of the reactor. As a result, the phenol solution was only pumped through the anodic side of the reactor.

The results obtained for this are presented in figure 4.7 in normalised form and the calculated rate constants are given in table 4.10.

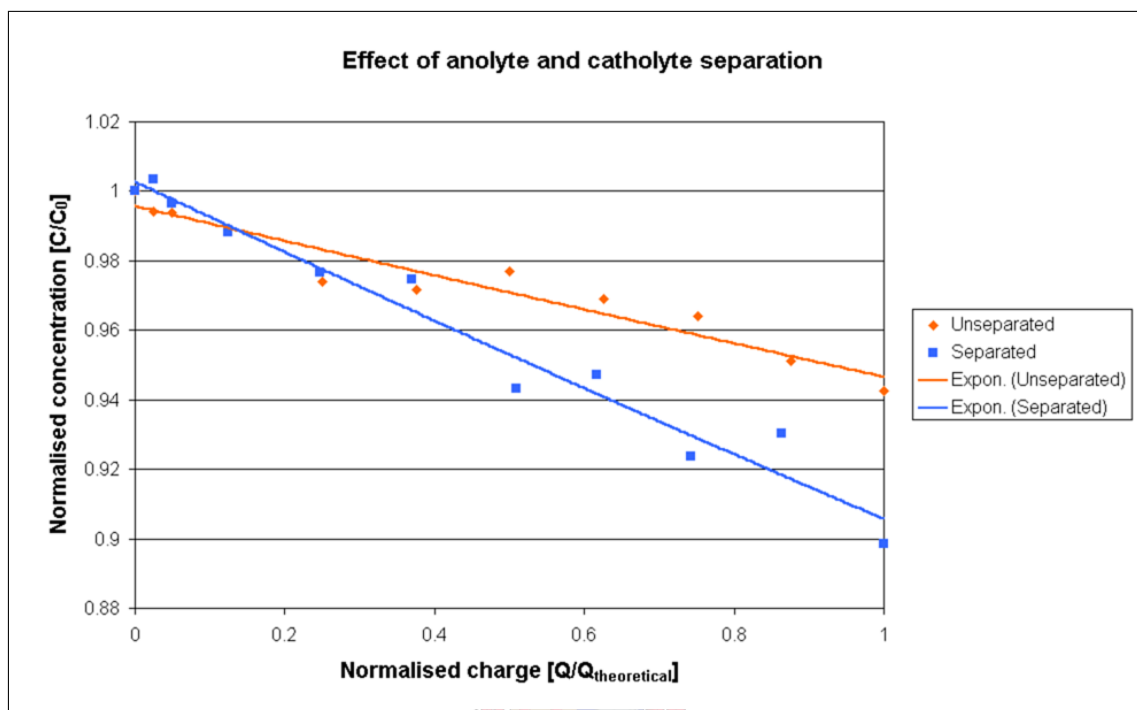


Figure 4.7: Effect of electrolyte separation on reaction rate

Table 4.10: Reaction rate constants for separated electrolytes

	β [s ⁻¹]	$k_{m,\text{experimental}}$ [m/s]	R ² %	95% conf. interval
Unseparated	1.82×10^{-6}	8.30×10^{-7}	92.4	4.26×10^{-7}
Separated	3.64×10^{-6}	1.66×10^{-6}	96.3	5.37×10^{-7}

It can be seen that the rate constant for the case where the electrolytes were separated is two times greater than that for the unseparated case. This will have a marked influence in the final design of the reactor. The cost of having an additional system responsible for pumping the catholyte must therefore be weighed off against the improvement in reaction rate. The remainder of the experiments, especially those done in the reactor by using titanium current collectors, were done unseparated (no

additional pumps were available). The effect of separating the catholyte and anolyte is compared economically in chapter 6.

4.2.5 Summary

To conclude, the current efficiencies obtained in the various experiments are summarised and compared. Since only some of the intermediates have been identified to date, some assumptions have to be made when calculating the current efficiencies. The current efficiencies can be calculated for two limiting conditions:

1. Assume all of the phenol removed is completely converted to carbon dioxide (28 electrons), or
2. Assume the converted phenol is only oxidised, in one step, to hydroquinone or catechol (2 electrons).

Both calculations are performed for the sake of comparison. The calculated values are given in table 4.11 The maximum value for the current efficiency in this case is

Table 4.11: Reaction rate constants for separated electrolytes

Current [mA]	Re	Stack pressure [lb-in]	Separated	Concentration [ppm Ph]	ϵ [%]
20	650	15	No	50	0.44-6.23
35	650	15	No	50	0.72-10.0
50	650	15	No	50	0.41-5.77
50	650	15	Yes	50	0.72-10.1
50	1516	15	Yes	50	1.00-14.0
50	650	25	No	50	0.38-5.33
50	650	15	No	150	0.31-4.32

the same as the maximum conversion of the reaction. The lowest conversion obtained was 4.32% and the maximum 14%. This is relatively low and is mainly caused by the large applied potentials of the experiment. This causes a large fraction of the current to be wasted on the evolution of oxygen. The reversible reactions between *o*-

and *p*-benzoquinone and between (1,2)- and (1,4)-dihydroxybenzene are responsible for additional inefficiencies.

For the 14% conversion experiment (the highest conversion) one can see that the anolyte and catholyte have been separated. From this it would appear that the best configuration for the reactor would be high flow rates, while keeping the anolyte and catholyte separate. So far, intermediate current values have resulted in the best reaction rate constants.

4.3 Laboratory Experiments – Potentiostatic Operation

Due to the low conversions obtained in the galvanostatic experiments, it was decided to perform experiments in which the potential is kept at a constant value below that required for the side reaction, but above the potential required for the oxidation of the phenol. The theoretical potential that corresponds with this value is about 1.4 V, whereas the ohmic losses due to the membrane and current collectors must still be accounted for. The phenol oxidation potential and the water hydrolysis reaction differ by 0.3 V (water hydrolysis being 1.7 V) and therefore a fixed potential value of 2.0 V was chosen. The potential for the hydrogen evolution reaction is between -0.2 to -0.4 V. Thus, the chosen potential, including the potential drop across the membrane, will be sufficient for the phenol oxidation but still under the oxygen evolution potential.

The graph in figure 4.8 shows the concentration versus time profiles of phenol, and some of the identified breakdown products. The phenol concentration is read off the left-hand axis and the concentrations of the breakdown products are read off the right-hand axis. Figure 4.9 shows the same concentration profiles, but uses normalised charge as the x-axis. This was done to show the theoretical extent of the reaction at the different sampling points. Note that after 55 hours of reaction, almost 80% of the theoretical charge has been supplied to the system, with only 23% conversion of the phenol.

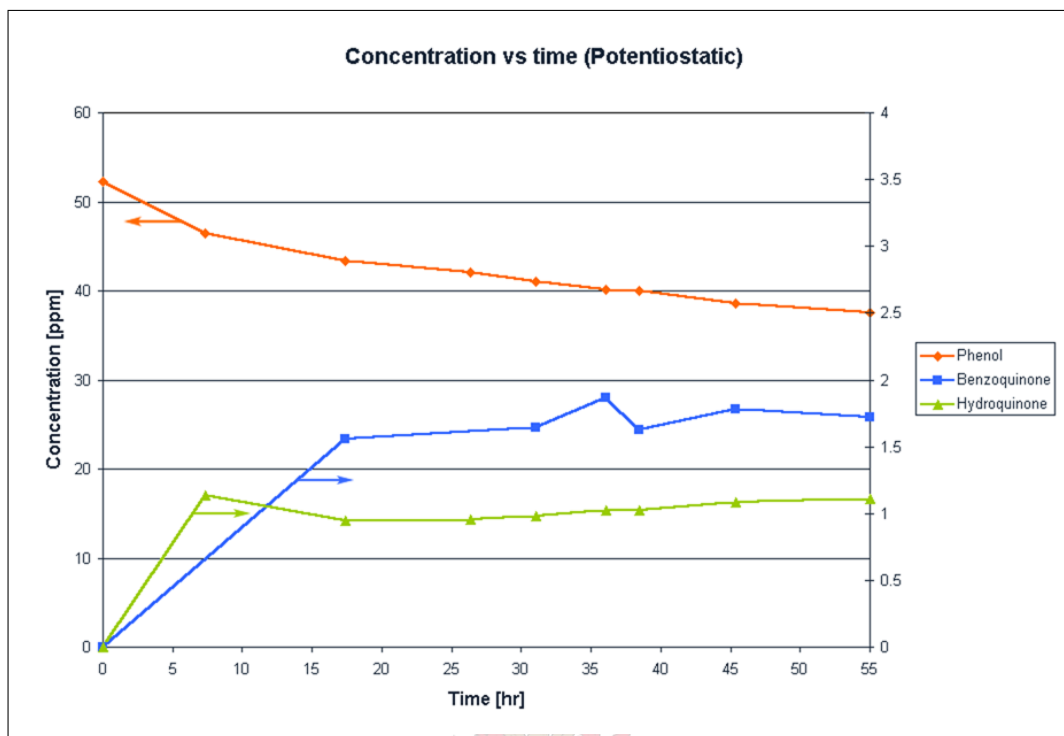


Figure 4.8: Results of potentiostatic experiments

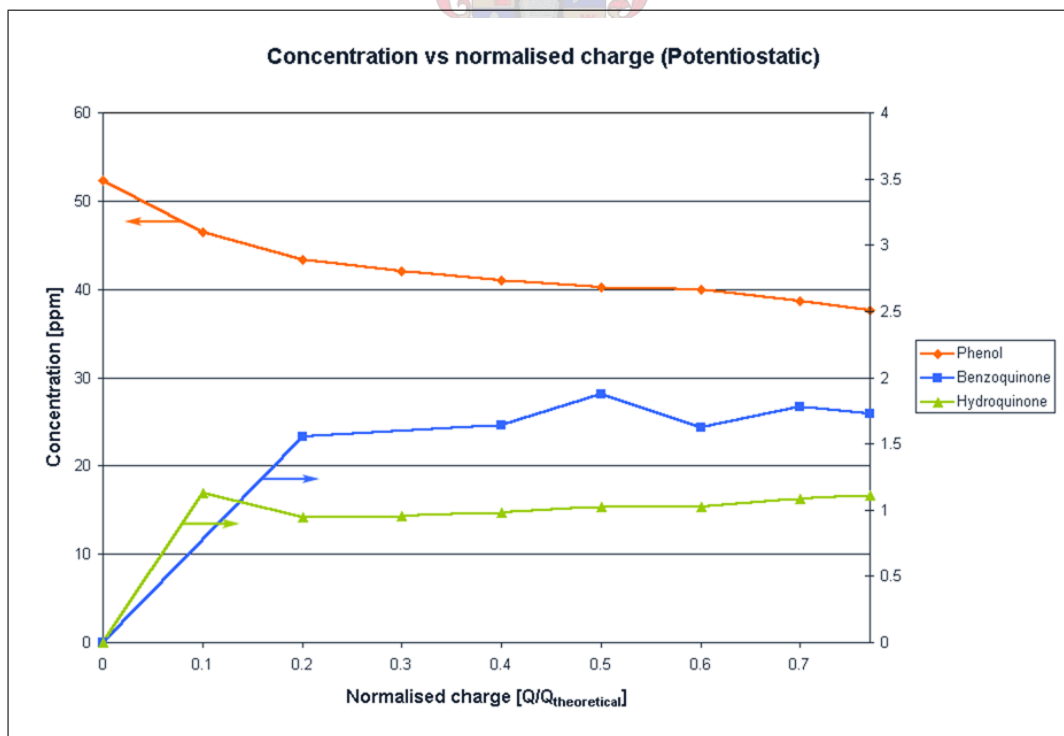


Figure 4.9: Normalised potentiostatic experimental results

The breakdown products that were analysed were *p*-benzoquinone and hydroquinone. These breakdown products form quickly (before the first sample point) and then seem to reach an equilibrium concentration. The concentrations are still very low and in some instances the analytical method used is not sensitive enough to discern between the corresponding peak and the baseline, especially in the case of *p*-benzoquinone. Typical concentrations obtained were below 1.8 ppm. Since none of the acid intermediates were detected (section 3.4), it was assumed that they were either broken down preferentially or not even formed.

The obtained conversions were compared to the theoretical conversions as calculated with Faraday's law. The total organic carbon was calculated based on the concentrations of the compounds in the samples and compared to the theoretical conversion (figure 4.10). Notice that after approximately 30% of the required charge was supplied to the system, the conversion slowed down significantly.

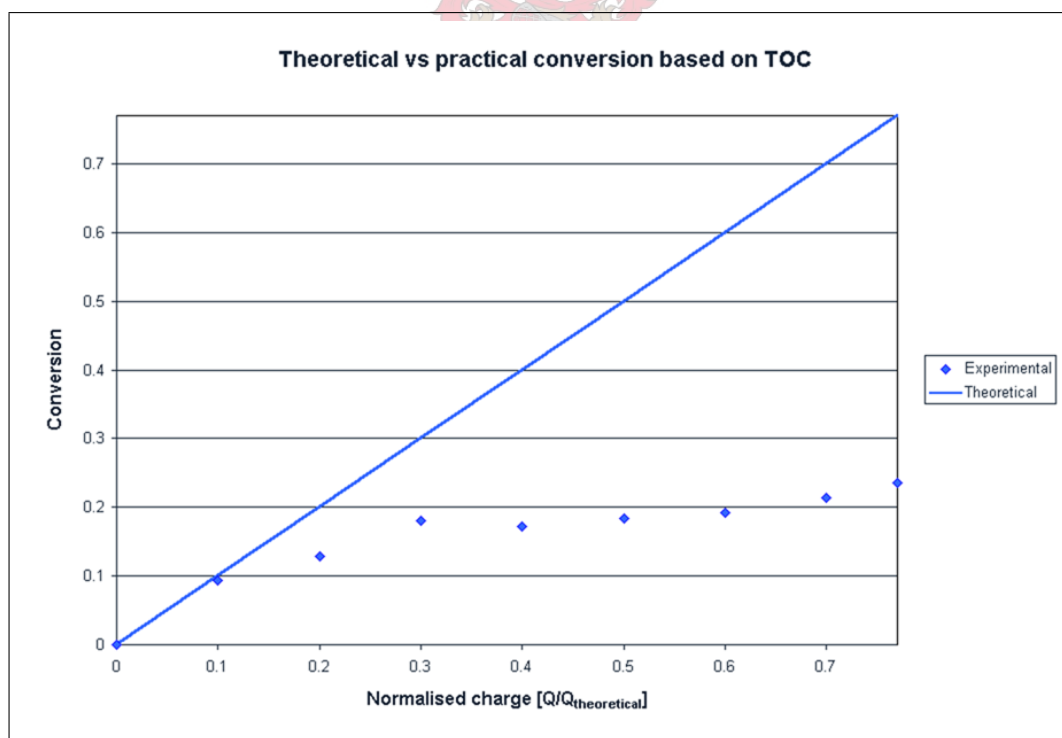


Figure 4.10: Theoretical vs practical conversion

Due to a suspicion that a polymeric film of polyphenol might be forming, an

experiment was carried out in which both the anode and the cathode were a titanium electrode coated with the $\text{SnO}_2/\text{ZrO}_2$ catalyst. The experiment was run for a set period of time (8 hours) after which the polarity was changed. This was done in an attempt to remove the polymeric film, a process that could take place in a couple of ways:

1. by reversing the polymeric reaction, or
2. by regenerating the catalyst surface by breaking up the film due to hydrogen evolution.

Because no analytical methods for determining the presence of a polymeric film were available, at this time it could not be said which one of these two phenomena were responsible for film removal, or even whether the film was removed. The concentration-time profiles for these experiments are given in figure 4.11. The normalised graph is given in figure 4.12.

Despite an experiment duration of 60 hours, only 33% of the theoretical charge was supplied, with a conversion of 21% with respect to phenol. This is only 1% more than the experiments without the polarity change — except that here the current, and hence the charge transfer, is considerably lower. Therefore, these experiments need to be repeated for a longer period of time to be able to see if the same trend is followed, as is the case of the experiments without the polarity changes. If, even with the lower rate of charge transfer, some regeneration of the surface takes place, this mode of operation can be used in a practical reactor to eliminate the need for electrode maintenance.

From the graphs it can be seen that the concentration of the breakdown products remains below 2 ppm. It can also be seen that certain cyclic intermediates react more favourably than others, i.e. catechol (1,2-dihydroxy-benzene) reaches its apparent maximum concentration much earlier than hydroquinone (1,4-dihydroxy-benzene) does. The benzoquinone concentration seemed to reach a constant value at 1.1 ppm. This could be explained by examining the reactions in figure 2.6. The first reaction was the formation of the dihydroxy compounds, followed by a reversible

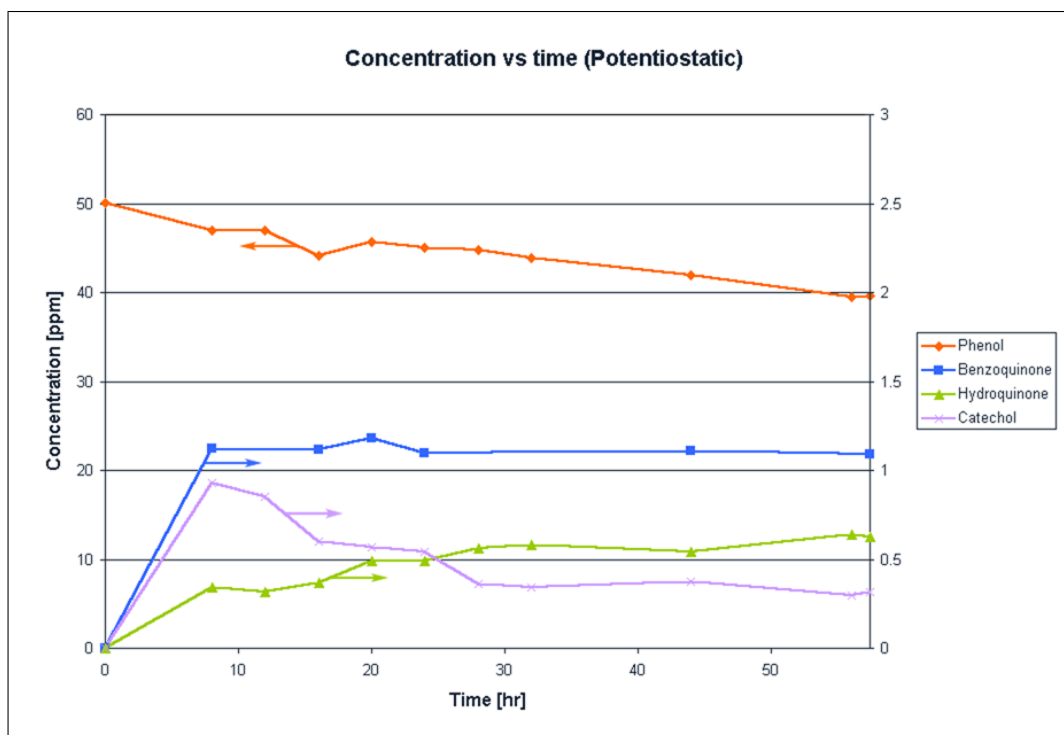


Figure 4.11: Potentiostatic breakdown curve (polarity changed)

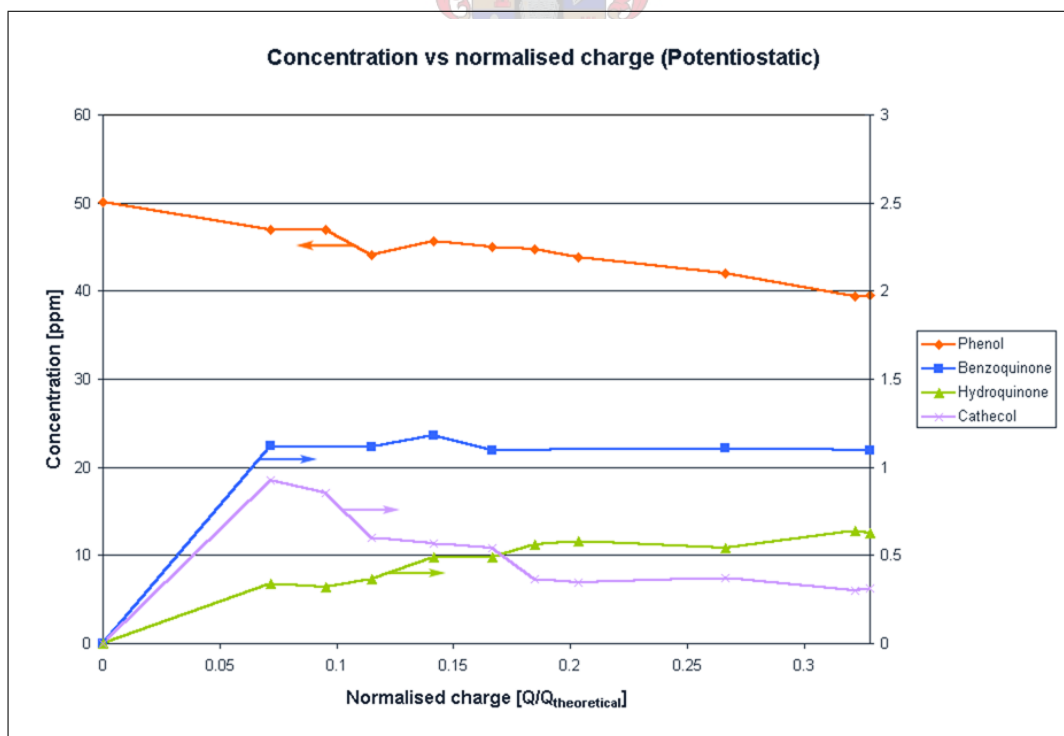


Figure 4.12: Normalised potentiostatic breakdown curve (polarity changed)

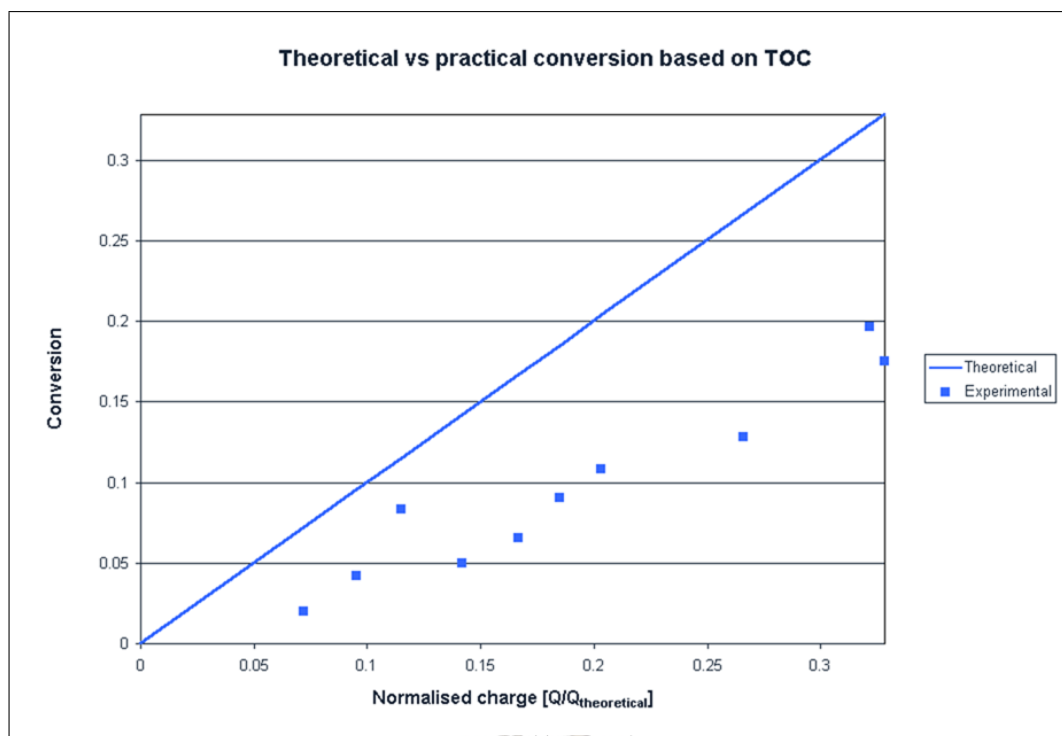


Figure 4.13: Theoretical vs practical conversion (polarity change)

reaction in which these dihydroxy compounds switch between their hydrogenated and non-hydrogenated forms. Therefore, the benzoquinone reached some equilibrium concentration. In the experiments where the polarity was changed, the benzoquinone only reached a maximum of 1.1 ppm compared to 1.8 ppm in the first experiment. This could simply mean that the catalyst as cathode has a higher potential for the reverse reaction.

The total organic carbon values for phenol and the individual breakdown products were calculated and the conversion based on this was plotted versus time (see figure 4.13). From this graph, the overall current efficiency was calculated to be just below 55%. This is a great improvement on the current efficiencies observed in the galvanostatic experiments — which averaged between 6 and 14%.

Whereas the experiments conducted under galvanostatic operation normally ranged from about 8 hours (50 mA) to 20 hours (20 mA) for 100% theoretical charge applied, these experiments take place at a much slower rate (60 hours) — with anything

from 35 to 80% charge applied. This however, can be justified with the much higher current efficiencies obtained. A full analysis of the data should prove which mode of operation would be the best.

The reaction rate constants calculated for the two separate experiments are given in table 4.12.

Table 4.12: Reaction rate constants for potentiostatic experiments — with and without polarity change

	β [s ⁻¹]	k [m/s]	R ² %	95% conf. interval
No polarity change	1.53×10^{-6}	6.98×10^{-7}	92.4	3.91×10^{-7}
Polarity change	1.08×10^{-6}	4.93×10^{-7}	98.5	1.08×10^{-7}

As can be seen from the R² values, the experimental values are predicted reasonably well with the exponential curve. In both cases, the initial point deviates significantly from the exponential curve. This could again imply the rapid initial deactivation of the catalyst to some steady-state value.

4.4 Laboratory Experiments – Titanium Current Collectors

Despite the precautions taken, it was still found that some of the nickel leached into the solution, thereby altering the conductivity of the water and also the reaction rates. From the analysis of the results (see chapter 6), it was still determined that the phenol oxidation process would not be economically viable. Therefore, titanium current collectors were constructed to determine if current efficiency could be improved, since they would not corrode in the same way.

Three sets of experiments were conducted at different flow rates. Each set was carried out at four different current values of 20, 30, 40 and 50 mA. No real differences between the potential-current values for the nickel-plated and titanium current-collectors were observed. Although the potential was not constant during

an experimental run, values for both the nickel-plated and titanium current collectors are given in table If these potential values are broken down into the separate

Table 4.13: Typical potential values for different currents

Current [mA]	Potential (nickel) [V]	Potential (titanium) [V]
20	18	14
50	22	24

contributions, as shown in equation 2.34a, then it is seen that most of the potential is attributed to the overpotential and ohmic losses. As mentioned in section 4.3, the value of V_{\min} is approximately 1.7-1.9 V. If the potential drop in the current collectors and external circuit is assumed to be negligible, this means that most of the potential is required in the overpotential to drive the reaction.

This would suggest that the kinetics of the reaction must be hindered causing high overpotentials. Hindered kinetics such as these would mean that if the process was operated galvanostatically, a limited fraction of the applied current would be used in the oxidation reaction — with the rest of the current wasted on side reactions. One solution to this is having very high aspect ratio flow channels, thereby increasing the electrode area to flow rate ratio.

Each experiment conducted with the titanium current collectors was run for a total of four hours. This experimental time did not correspond with a 100% theoretical conversion time using Faraday’s law, but had to be chosen due to time constraints. For the current values of 20 and 50 mA, this corresponded with a theoretical conversion of 20.1 and 50.2% respectively. Samples were taken every 15 minutes to obtain accurate information closer to the start of the experiment when most of the deactivation was assumed to take place.

The breakdown curves for each set of experiments are given in figures 4.14 to 4.16. Only the phenol concentrations were measured, since it was found in the previous analysis (section 4.3) that the quinones and dihydroxy-benzenes gave very low

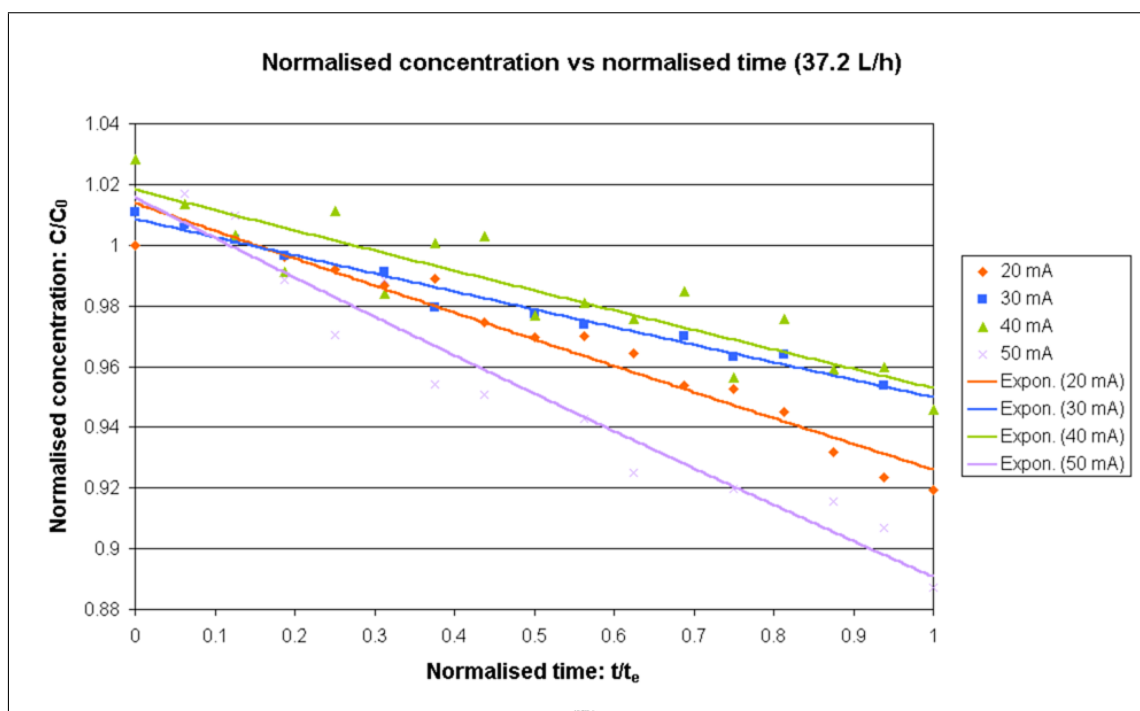


Figure 4.14: Concentration vs time curves for a flow rate of 37.2 L/h using titanium current collectors

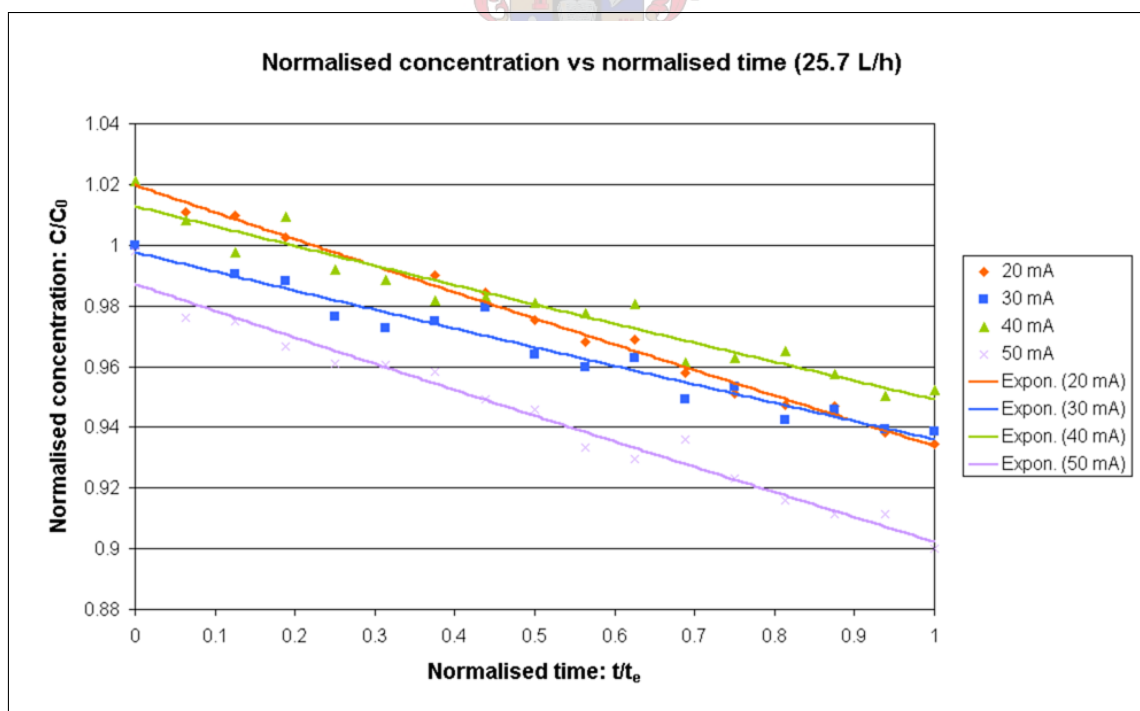


Figure 4.15: Concentration vs time curves for a flow rate of 25.7 L/h using titanium current collectors

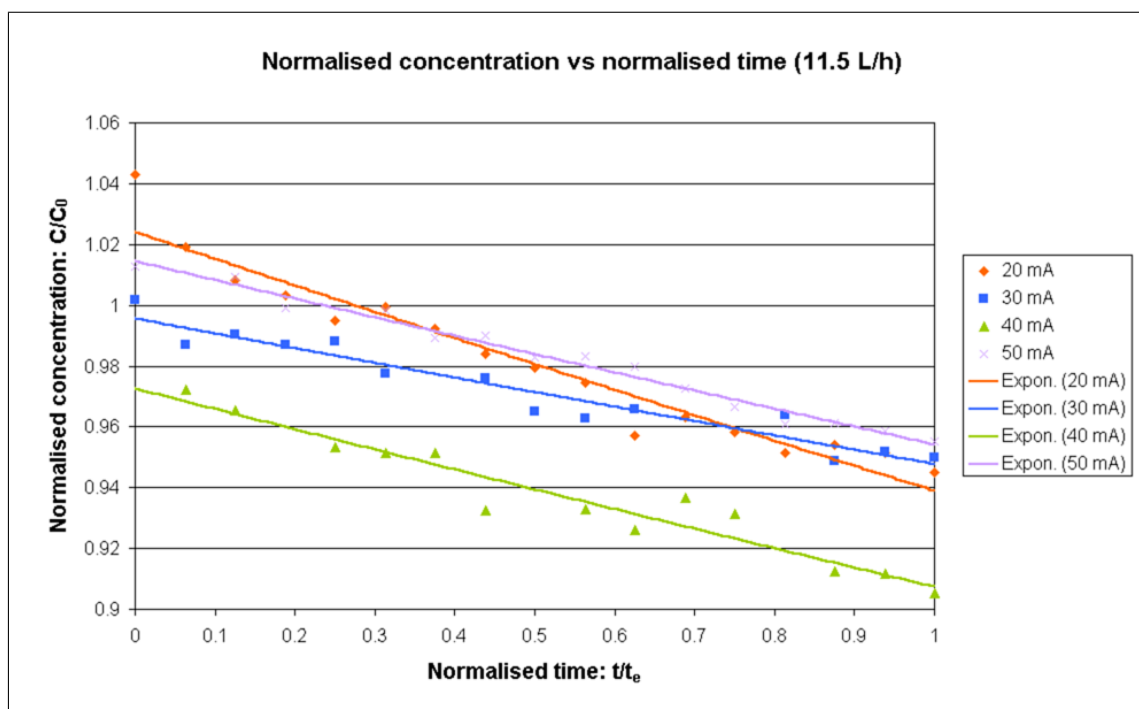


Figure 4.16: Concentration vs time curves for a flow rate of 11.5 L/h using titanium current collectors

concentrations. Also, the conversions in these experiments were much lower due to the short reaction times. As explained in section 3.4, for low very low concentrations of the intermediate products, especially benzoquinone, inaccurate values of the concentration were measured. Therefore, it was not deemed useful to analyse the intermediates, since the accuracy of the measured concentrations could not be accepted as meaningful.

For all of these curves the reaction model was fitted and the appropriate reaction rate constants extracted. Once this is done some empirical correlation for the value of the reaction rate constants can be obtained. This can then be used in design equations for larger scale reactors (chapter 6).

4.4.1 Reaction Order Experiments

Notwithstanding all of the experimental results obtained to date, very little is still known about what processes take place and their relative kinetics. Therefore more

information needs to be gathered to attempt to answer these questions. The reaction order can sometimes give a clear indication of the limiting step in the reaction. For instance, if a reaction order other than unity is obtained, one can normally assume that the reaction is not mass transfer limited.

The method of numerically differentiating the concentration versus time data is used for the extraction of the reaction orders of constant volume systems as explained in section 2.1.5. The system in this application is not exactly a batch reactor, but the conversion per pass is very low — one can assume that it is similarly to a batch reactor. The exact derivation of the method, using a numerical example, is given in Appendix B.

The experiments were conducted with initial concentrations of 40, 50 and 60 ppm phenol. The concentrations were kept relatively close together to prevent any passivation effects to alter the results. An applied current of 50 mA was chosen, because high conversions were expected with this current value, and thus an improvement in the accuracy of the results. Both a 2nd and 3rd-order polynomial was fitted to the concentration time data, differentiated, and evaluated according to the differential method in order to determine the reaction orders. The results obtained are summarised in table 4.14.

Table 4.14: Reaction orders determined from the differential method

Concentration [ppm]	Reaction order	
	2nd-order	3rd-order
40	15.4	11.2
50	7.27	5.05
60	2.92	4.22

The reaction orders obtained in this fashion varied widely, with no clear pattern to the data. Variation in the concentration-time data could be responsible for the wide range of observed values — although, taking deactivation into account, similar dependence of the reaction rate on the concentration could be observed. If deacti-

vation of the catalyst takes place rapidly, with the catalyst activity reaching some steady-state value, this would also correspond with a similar profile. This profile would exhibit a rapid decrease in concentration at the start of the experiment while the concentration of phenol is high. Once the steady-state value is attained, the reaction rate will decrease, becoming independent of the activity of the catalyst, and so reflecting a lower dependence of the reaction rate on the concentration.

Earlier in this chapter, the prevailing conditions were assumed to be in the mixed region of control. This implies that the effect of mass transfer on the reaction rate is comparable to the effect of charge transfer. External mass transfer effects always exhibit a first-order dependence of the reaction rate on concentration and therefore assuming a first-order dependence of the apparent reaction rate on concentration can be accurate. Regardless, the exponential curves that were fitted to the data present good statistical properties, with the calculated 95% confidence intervals being smaller than the coefficient in the exponent in all cases. Once again, the number of contributing factors complicates the accurate modelling of the system and, therefore, some simplifications, such as these, had to be made.

4.5 Conclusions

From the results obtained in the various experimental sections a number of conclusions can be drawn:

1. The reaction is in the mixed control regime.
2. The reaction is first-order with respect to phenol.
3. Passivation effects are negligible.

The results discussed in both section 4.2 and section 4.4 showed that the reaction rate is dependent on current density and flow rate. This implies that neither the mass transfer coefficient, k_m , nor the reaction rate coefficient, k is predominant. Reports in the literature indicate low reaction rate constants for the combustion of phenol [48, 8], and therefore, assuming that $k < k_m$ would not be unreasonable. The

apparent reaction rate constant that will be used in the model will therefore be equal to some value, such that $k < k_{\text{app}} < k_m$. This has been shown to be true in section 4.2 where the calculated k -values are compared to the predicted k -values. In all of the cases, the predicted values were slightly higher than the calculated ones.

The hypotheses that the reaction is first-order with respect to phenol, is derived from the statistical data of the various functions fitted against the data. Both the second and third-order polynomials gave 95% confidence intervals greater than the respective polynomial coefficients. This was not the case with the exponential fit, implying that the exponential curve resulted in a stable model of the data. This in turn, means that the coefficient would not change remarkably with the removal of one or two data points.

From these results it can also be said that the effect of passivation is negligible. The catalyst may undergo a brief period of catalytic deactivation until some steady-state level is reached, thereby accounting for the higher reaction rates at the start of the experiments. Often, the first two or three data points is found to be significantly higher than the exponential fit; a trend that supports this hypothesis.

A factor that must be taken into consideration, is that the surface where the oxidation is then taking place is not the metal oxide surface any more, but rather the polyphenol film, which would then act as the catalyst.

Chapter 5

Microbiological Experiments

As discussed in section 3.3, the response of the electrochemical combustion system towards three different species of pathogens was investigated. Two sets of experiments were conducted using different levels of contamination. The first experiment was done using very high concentrations of organisms. The results of these experiments are discussed in section 5.1. More realistic levels of contamination were also tested and the results of these experiments are presented in section 5.2

5.1 High-concentration Experiments

The results of the experiments conducted with a high concentration (20×10^6) of cells are given in figure 5.1. It can be seen that the reactor system effectively removes the micro-organisms from the test volume to a significantly lower concentration. The reactor rapidly removes the cells up to a certain concentration of about 1×10^6 cells and then steadily keeps decreasing the cells.

It was noted during the experimental runs that gas was being developed in the anodic compartment. This may have been carbon dioxide resulting from the high organic carbon content of the solution being combusted, or it could be the development of chlorine from dissolved NaCl. Thus the question arises as to whether it is the reactor in itself killing the organisms or the chlorine gas acting as disinfectant. It must also be noted that for these experiments 100% TSB solutions were used which contained high levels of chlorine ions. This was later adjusted to the level stated in

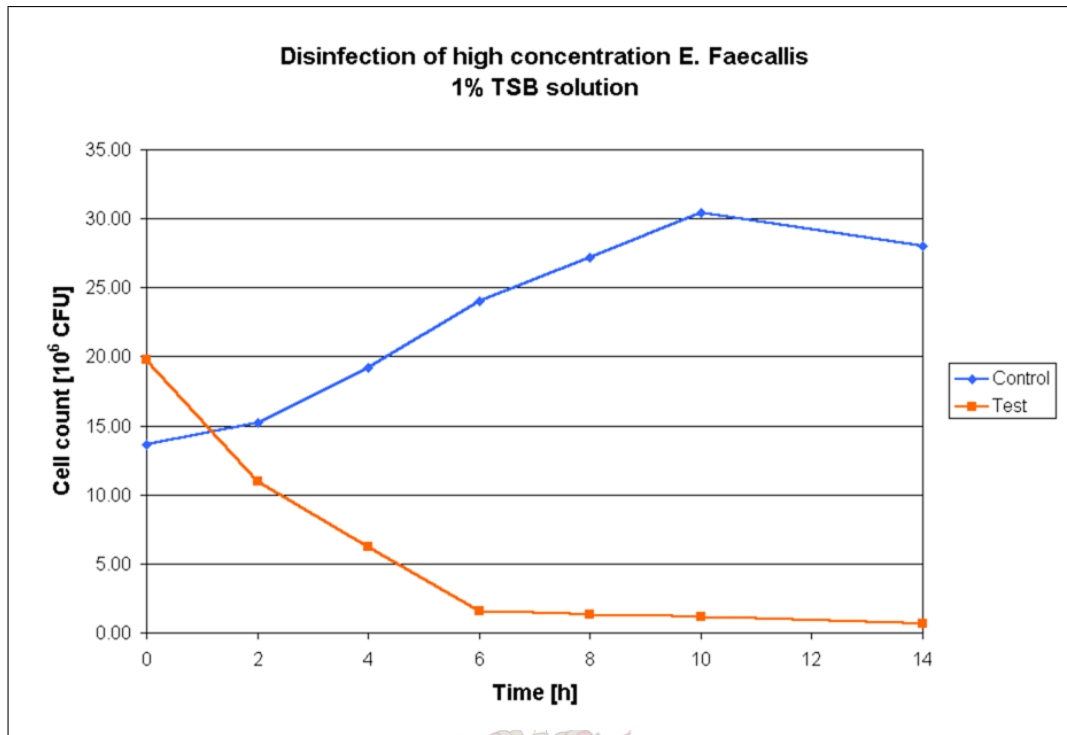


Figure 5.1: Disinfection of high concentration samples

the experimental method (section 3.3.3).

On completion of the experiment, the test volume was removed from the reactor system and left for a period of 24 hours, after which the cell count was observed. It was found that the cell count returned to its initial value. Thus, no residual effect was obtained from the reactor itself. It is therefore vital that the reactor system decreases the number of micro-organisms to a significant level, where no growth will be observed for a period of at least one week, to ensure that stored water remains uncontaminated.

5.2 Low-Concentration Experiments

Additional experiments with initial concentrations closer to realistic values (section 3.3.3) were conducted. Despite the precautions taken in the preparation of the inoculum, variations of up to two orders of magnitude in the initial concentration were still obtained. In all cases the initial concentration was higher than the

maximum observed contamination levels stated in the literature.

Despite these slightly higher concentrations, the reactor system still successfully removed all the micro-organisms. As discussed in section 3.3 the samples were left for an additional period of time, corresponding with the times of the individual micro-organisms exponential growth phase. After this period of time no living organisms were detected in the samples. The cell counts of these experiments are given in figure 5.2. Note that a period of only four hours is required for the elimination of all living cells.

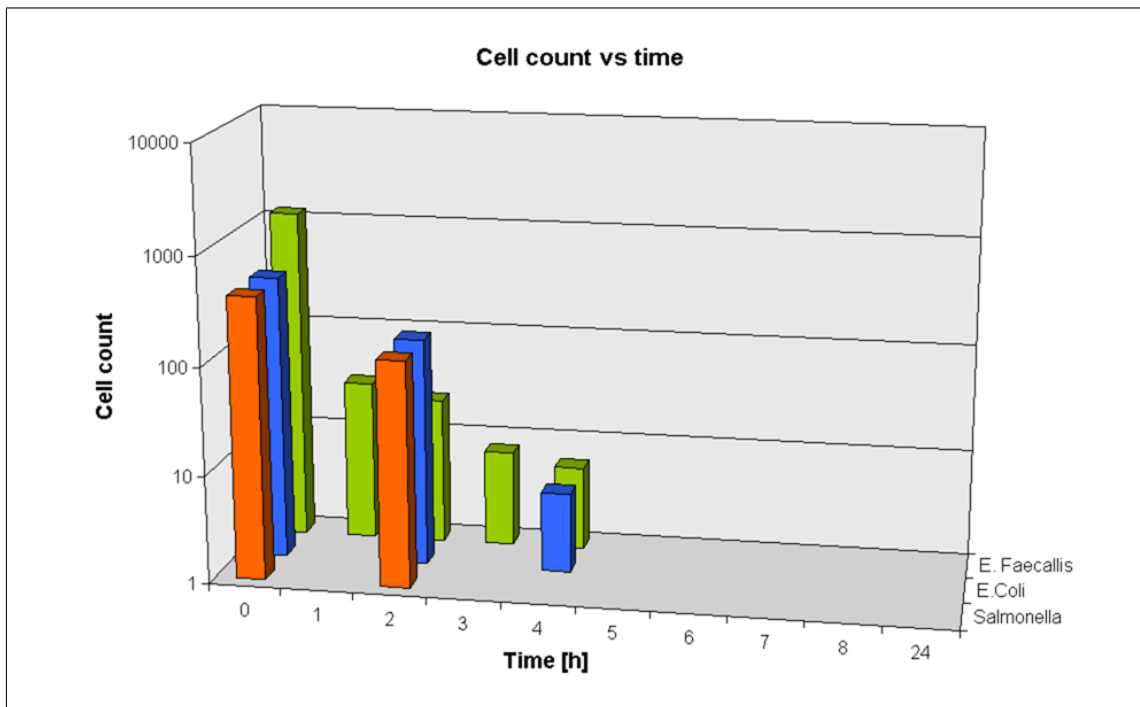


Figure 5.2: Disinfection of various micro-organisms

Additional experiments were carried out to assign a pseudo-rate constant to the disinfection of the samples. The same form of the equation as that used for phenol (equation 4.1) was used for the disinfection experiments. Unfortunately, the results obtained from the *E. Coli* experiments were contaminated and the results could not be used. The results for *Salmonella* and *Enterococcus Faecallis* are given in figures 5.3 and 5.4.

The individual values obtained for the coefficient in the exponential fit, together

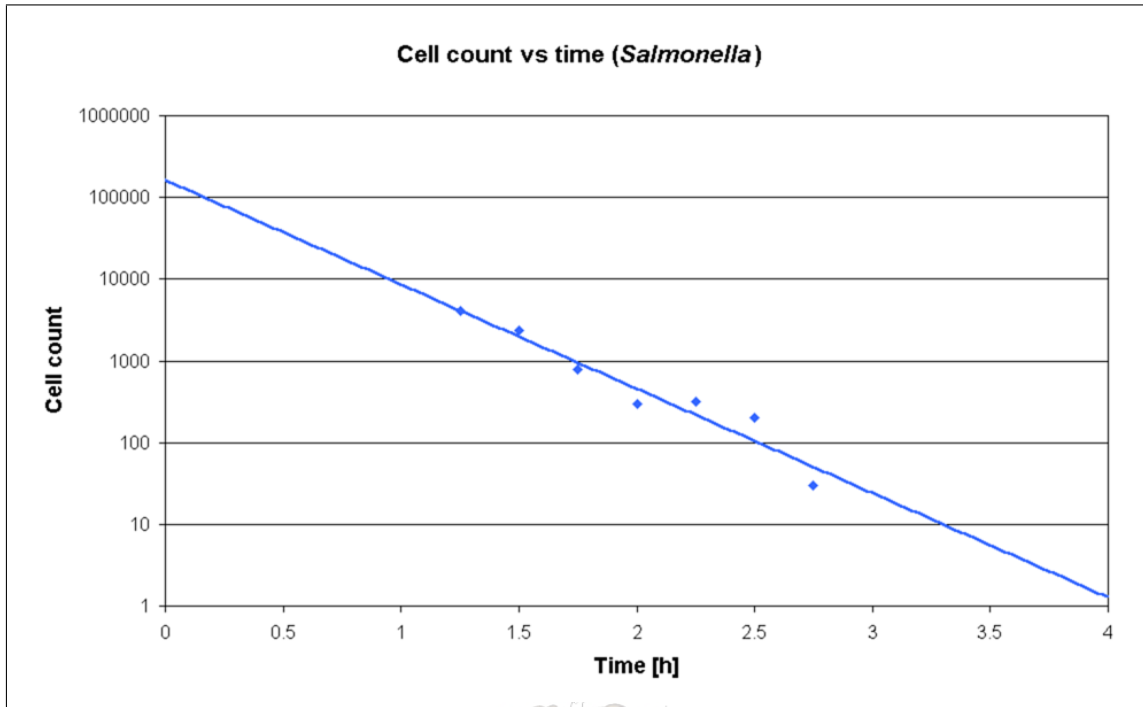


Figure 5.3: Disinfection of *Salmonella*

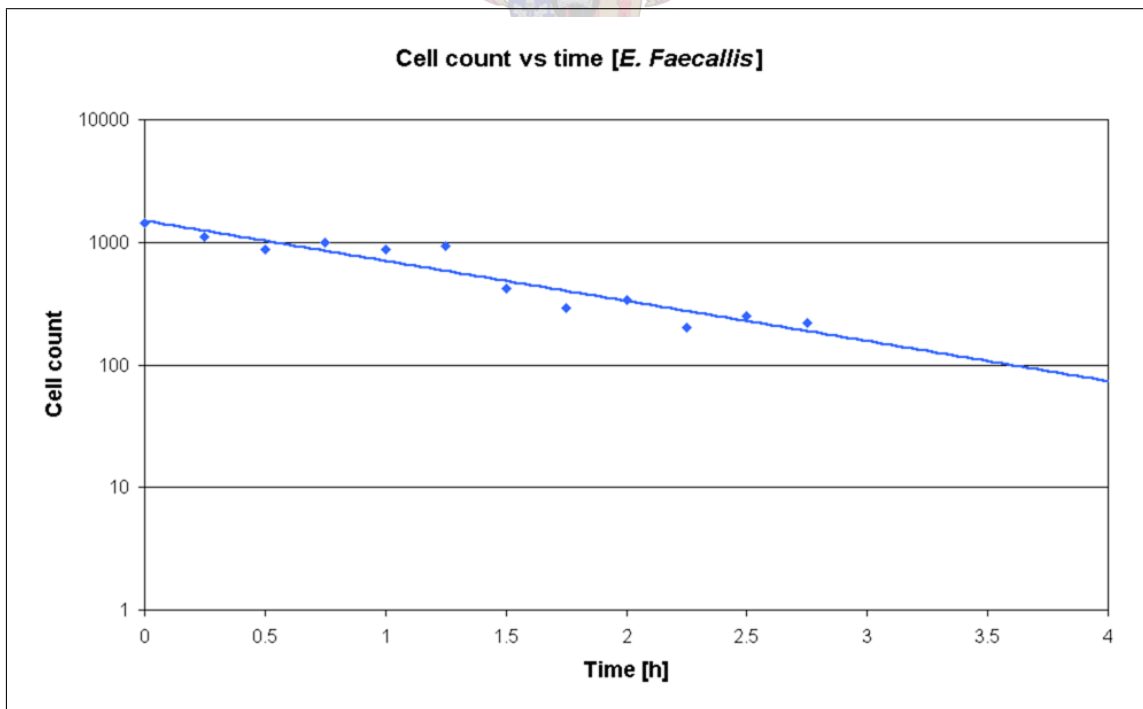


Figure 5.4: Disinfection of *E. Faecallis*

with the respective R^2 values and 95% confidence interval values, are given in table 5.1.

Table 5.1: Reaction rate constants for microbiological experiments

Species	β [s ⁻¹]	k [m/s]	R^2 %	95% conf. interval
<i>E. Faecallis</i>	-2.09×10^{-4}	9.65×10^{-5}	89.7	5.02×10^{-5}
<i>Salmonella</i>	-8.17×10^{-4}	3.88×10^{-4}	93.4	2.49×10^{-4}

The coefficients obtained for the disinfection of the above micro-organisms were on average two orders of magnitude greater than those obtained for the oxidation of phenol. These coefficients are used in chapter 6 as comparison when the lengths of the reactors are considered.

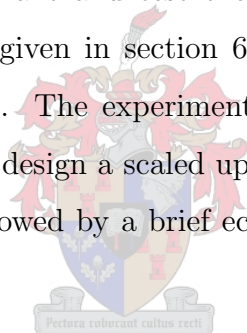
It was suspected that the formation of the hydroxyl radicals might not be directly involved in the destruction of the micro-organisms, and that the potential difference in the reactor might disrupt the functioning of the cell membranes, thereby killing the micro-organisms. To determine which of these two processes were responsible, inert electrodes (electrodes that do not produce hydroxyl radicals) were tested with *E. Coli*. The inert electrodes were graphite electrodes (see section 3.3.3).

Experimentation times and conditions were identical to those used in the previous experiments. Analysis of the samples showed that the concentrations of organisms in all of the samples exceeded the top limit of the resolution of the analysis method. This meant that during the entire experiment the cell count in the solution was higher than 300 000 cell per 100 mL. This is 30 times the acceptable limit. Therefore the disinfection could be directly attributed to the action of the catalyst.

Chapter 6

Application of Experimental Data

In this chapter the experimental data presented in the previous sections is used in the derivation of a simple model for the oxidation process. This model is then used to design a hypothetical pilot plant and test the viability of the reactor system. The derivation of the model is given in section 6.1, with the exact details of the derivation given in Appendix A. The experimental data are discussed in greater detail in section 6.2 and used to design a scaled up version of the reactor, described in section 6.3). This will be followed by a brief economic evaluation of the reactor system in section 6.4.



6.1 Reactor Model

As discussed in chapter 3, the reactor set-up in both the oxidation and disinfection experiments consisted of a reservoir that contained the source contaminant and the electrochemical cell. To obtain a model of the concentration-time effects a mass balance had to be performed on both units. Finally, an expression for the concentration in terms of the major parameters is obtained.

As discussed in section 4.4.1, due to the suspicion that fouling may still play a role in the performance of the electrode, provision will be made for the deactivation of the catalyst in the model.

6.1.1 Reservoir

The reservoir basically functions as a continuously stirred tank with the feed stream leaving the reservoir at the bottom and the recycle and reactor effluent entering at the top. Some basic assumptions are necessary to simplify the derivation of an expression for the reservoir. The assumptions were the following:

1. The effect of gas evolution in the reactor on the mass flow rate of the inlet and outlet is negligible.
2. The conversion per pass in the reactor is so low that it can be assumed that the physical properties (density) of the inlet and outlet are the same.
3. The content of the reservoir is assumed to be perfectly mixed, due to stirring.

It is to be noted that in this mass balance the subscript 'in' refers to the outlet of the reservoir and the inlet of the reactor. The same, but opposite, applies to the subscript 'out'. At this point the reader is referred to Appendix A for the detail derivation of the model. Only the most important expressions will be given here. Based on the above assumptions, an overall and component mass balance can be performed on the inlet and outlet of the reservoir to give the differential form of the mass balance. Selecting phenol as the compound with which to do a component mass balance on, we can write

$$\frac{dC_{\text{Ph,in}}}{dt} = \frac{(C_{\text{Ph,out}} - C_{\text{Ph,in}})}{\tau} \quad (6.1)$$

The right-hand side of equation 6.1 contains an expression for the difference between the inlet and the outlet concentration of the reactor at any time t . To solve this differential equation an expression for this term must be obtained. Once this has been done, the differential equation can be evaluated to obtain an expression for the concentration in terms of the time of the experiment.

6.1.2 Reactor

In order to obtain an expression for the right-hand side of equation 6.1 a component mass balance must be done on the reactor. The mass balance for the reactor, in

differential form, can be written as:

$$\frac{dC_{\text{Ph}}}{dz} = \frac{r_{\text{Ph}}^{\text{II}} a(t) W}{v_{\text{R}}} \quad (6.2)$$

where $a(t)$ is some expression in time for the activity of the catalyst. Since the reaction rate is normally dependent on the concentration of the reacting species, an appropriate form of the rate equation must be selected, either based on experimental data or assumption. In section 2.1 the dependence of the reaction rate on current density and its analogy to chemical kinetics were shown. If a similar form of the rate equation can be assumed here,

$$r_{\text{Ph}}^{\text{II}} = \frac{\varepsilon_{\text{Ph}} i}{\nu_e F} = -k C_{\text{Ph}}^n \quad (6.3)$$

then the general form of the mass balance in differential form can be written as

$$\frac{dC_{\text{Ph}}}{dz} = \frac{-k C_{\text{Ph}}^n a(t) W}{v_{\text{R}}} \quad (6.4)$$

In the case of a reaction such as described in equation 6.3 the units for k will be $\left[\frac{\text{m}^{3(n-1)+1}}{\text{kmol}^{n-1} \cdot \text{s}} \right]$. This equation can be integrated to obtain an expression for the outlet concentration in terms of the inlet concentration as follows:

$$C_{\text{Ph,out},t}^{1-n} - C_{\text{Ph,in},t}^{1-n} = -\frac{(1-n)ka(t)W}{v_{\text{R}}} L \quad (6.5)$$

This equation applies for all values of $n \neq 1$. For $n = 1$ one obtains the following form of the equation

$$C_{\text{Ph,out}} = C_{\text{Ph,in}} \exp \left\{ -\frac{ka(t)W}{v_{\text{R}}} L \right\} \quad (6.6)$$

Since the reaction order cannot be determined accurately, it will be taken as one. Thus, substituting equation 6.6 into equation 6.1 one obtains the differential equation in terms of the reactor inlet concentration $C_{\text{Ph,in}}$ and t .

$$\frac{dC_{\text{Ph,in}}}{dt} = \frac{C_{\text{Ph,in}}}{\tau} \left(\exp \left\{ -\frac{ka(t)W}{v_{\text{R}}} L \right\} - 1 \right) \quad (6.7)$$

Simultaneously, for catalyst deactivation by poisoning it has been found that the deactivation rate of the catalyst can be given by [25] (p. 296):

$$\frac{da}{dt} = -k'_d C_{\text{P}}^m a^q$$

where the subscript P denotes the poison. In this case, if the poison is the same as discussed in section 2.2.3, the concentration of the poison should be proportional to the phenol concentration, giving

$$\frac{da}{dt} = -k'_d C_{\text{Ph,in}}^m a^q \quad (6.8)$$

which, together with equation 6.7, gives two differential equations that must be solved simultaneously in order to obtain concentration-time and activity-time information.

Since it has been shown previously that the effect of passivation is negligible, it is assumed that the activity is unity throughout the entire experiment

$$a(t) = 1 \quad (6.9)$$

In such a case equation 6.7 can be solved analytically to give

$$C_{\text{Ph,in,t}} = C_{\text{Ph,in,0}} \exp \left(\frac{t}{\tau} \left\{ \exp \left(-\frac{kWL}{v_R} \right) - 1 \right\} \right) \quad (6.10)$$

This model can now be used in the estimation of real reactor lengths. This is done in the next section for the various types of experiments and current collectors used.

6.2 Discussion of Experimental Work

The analysis discussed in the previous section can thus be performed on the data obtained in the initial experiments. The rate constant was calculated by fitting an exponential curve to the concentration time data, thus

$$C_{\text{Ph}} = C_{\text{Ph,0}} e^{\beta t} \quad (6.11)$$

with β being

$$\beta = \frac{1}{\tau} \left(e^{-\frac{kWL}{v_R}} - 1 \right) \quad (6.12)$$

and solving for k :

$$k = -\frac{v_R}{WL} \ln(\beta\tau + 1) \quad (6.13)$$

The analysis method discussed in section 6.1 was performed on the results obtained, using the respective k -values calculated in chapter 4. The lowest and highest rate constants will be given here for comparison, followed by the implication of the results for the design in a pilot plant. The current efficiencies presented here are calculated with regards to the full combustion of phenol to carbon dioxide. The current efficiencies for the microbiological experiments are not given, since the equivalent number of electrons required to kill one cell are not known.

Table 6.1: Comparison of experimental reaction rate constants for different experiments

Experiment	k_m [m/s]		ε %	
Nickel-plated current collectors				
	Low		High	
Galvanostatic	7.16×10^{-7}	5.33	2.47×10^{-6}	14.0
Potentiostatic	4.93×10^{-7}	32.4	6.98×10^{-7}	54.3
Titanium current collectors				
	Low		High	
	1.56×10^{-6}	17.2	3.16×10^{-6}	30.1

From table 6.1 it can be seen that potentiostatic operation gives significantly higher current efficiencies — thus, on the surface, it would seem that the potentiostatic operation will prove to be the best mode of operation. The titanium current collectors were all operated galvanostatically and yielded significantly higher current efficiencies, the highest of which almost equals those obtained for potentiostatic operation.

Due to the complexity of the system and the many factors influencing the reaction rate constants, it would be the best course of action at this stage to find some empirical correlation between the reaction rate constant and the main parameters. Therefore, some relationship of the following form can be fitted to the data:

$$k^* = \text{fn}(i, v_R) \tag{6.14}$$

The reaction rate constants obtained from the experiments utilising titanium current collectors are shown in graphical format in figure 6.1. In the graph, the

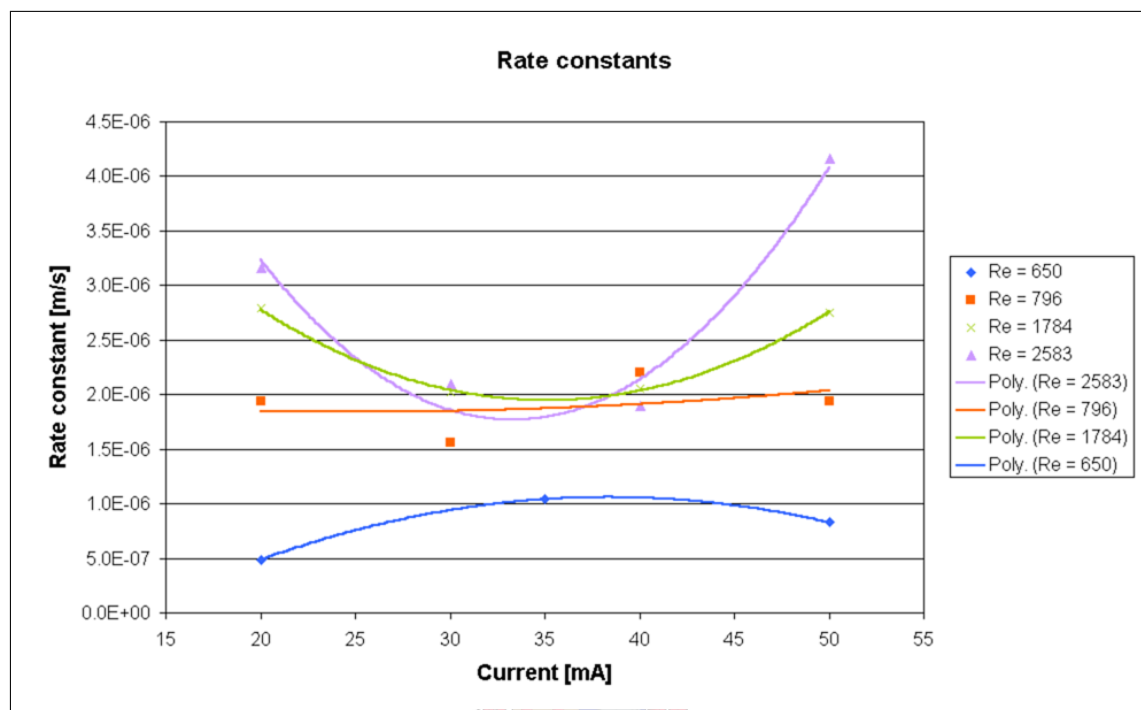


Figure 6.1: Reaction rate constants for titanium and nickel-plated current collectors

apparent reaction rate constants are plotted versus current for various values of the flow rate. The exception is the constants obtained for a Reynolds number of 650 that are slightly below the other curves. These constants were obtained using nickel-plated current collectors. Rate constants obtained with the nickel-plated current collectors were lower due to the nickel that was assumed to take part in a separate reaction, thereby lowering current efficiencies.

Nonetheless, a definite trend could be observed in the data. For the low and high current values, the reaction rate constant appeared to have a strong dependency on the flow rate, whereas for the intermediate values, almost no change was observed for the reaction rate. In the next section, these values will be used to perform rough scale-up calculations.

6.3 Scale-up Calculations

The scale-up calculations are done for a MEA and current collector set-up similar to that used in the experimental reactors. This will prevent any errors that may be introduced due to changes in the flow channel dimensions. The cross-sectional area available to flow will be changed, to accommodate larger flows.

In order to quantify this scale-up, practical sizes for the substrate were obtained. The largest porous titanium sheets obtained, were from Mott Corporation in America. The maximum dimensions of these porous titanium sheets were 0.5 m by 0.25 m. As seen from the derivation of the model in section 6.1, the length of the reactor directly influences the conversion obtained in the reactor, and is therefore more important than the width of the electrode. Due to this, the channels in one section of the pilot reactor will be 0.5 m long. As mentioned, the flow channels in the reactor will have the same dimensions as those in the experimental reactors, and thus a total of 30 flow channels can be fitted onto one electrode. This value will be used consistently throughout the rest of the scale-up calculations.

To determine the length of the reactor required to obtain a certain conversion X , the same mass balance as that done in section 6.1.2 can be used. The only difference is that L in this case is the unknown, and k is known or can be calculated. The expression for L then becomes

$$L = -\frac{v}{Wk} \ln(1 - X) \quad (6.15)$$

The predicted reactor lengths were calculated for all of the experimental values, and are given in tables 6.2 (nickel-plated current collectors) and 6.3 (titanium current collectors) for the highest and lowest conversions. In comparison, reactor lengths for the potentiostatic and microbiological experiments are given in table 6.4.

The values given in the table are calculated using the flow rate at which the experiments are conducted, since no expression has yet been obtained to express the reaction rate constant in terms of the flow rate. Also note that the flow rate as calculated here is 30 times that of the experiments. This factor of 30 is introduced

because of the number of flow channels that the larger reactor has. The Reynolds number in the individual flow channels is still the same as in the experiments.

Table 6.2: Calculated reactor lengths – nickel-plated current collectors

Re []	I [mA]	Separated electrolyte	$L_{X=0.99}$	$L_{X=0.5}$ [m]
650	20	No	6159	927.0
650	35	No	2878	433.2
650	50	No	3606	542.8
650	50	Yes	1803	271.4
1516	50	Yes	3011	453.2

Table 6.3: Calculated reactor lengths – titanium current collectors

Re []	I [mA]	$L_{X=0.99}$	$L_{X=0.5}$ [m]
796	20	6124	921.8
796	30	7623	1147
796	40	5406	813.7
796	50	6130	922.7
1784	20	2945	443.2
1784	30	4067	612.2
1784	40	3994	601.2
1784	50	2987	449.7
2583	20	1160	174.5
2583	30	1929	290.3
2583	40	1745	262.7

The reactor lengths calculated for the potentiostatic experiments, compared to those for the galvanostatic experiments, showed that the mode of operation for the pilot reactor would be galvanostatic. Despite the lower current efficiencies observed for galvanostatic operation, the lengths were more than an order of a magnitude less compared to the lengths obtained for potentiostatic operation.

Table 6.4: Calculated reactor lengths – potentiostatic and microbiological experiments

Potentiostatic experiments		
	$L_{X=0.99}$ [m]	$L_{X=0.5}$ [m]
No polarity change	17044	2565
Polarity changed	24131	3632
Microbiological experiments		
	$L_{X=0.99}$ [m]	$L_{X=0.5}$ [m]
<i>Salmonella</i>	123.3	18.6
<i>E. Faecallis</i>	30.7	4.6

It can be seen that the reactor lengths for the oxidation of phenol are unrealistic, especially if a large volumetric flow rate of waste needs to be treated in a single-pass reactor system. Therefore, introducing a recycle stream that returns a fraction of the effluent to the inlet could reduce the required length of the reactor. The proposed flow diagram for the pilot plant reactor is given in figure 6.2.

An overall and component mass balance can be performed, on various parts of the reactor system, to obtain an expression for the overall conversion in the reactor. If one defines the recycle ratio as

$$\text{Recycle ratio} = Y \equiv \frac{v_r}{v_p} \quad (6.16)$$

an expression can be obtained for the conversion in terms of reactor length and recycle ratio. The full derivation of this expression is given in Appendix A. The expression reads as follows:

$$\frac{C_{\text{Ph,out}}}{C_{\text{Ph,in}}} = 1 - X = \frac{\exp\left(-\frac{kWL}{v_p(Y+1)}\right)}{Y + 1 - Y \exp\left(-\frac{kWL}{v_p(Y+1)}\right)} \quad (6.17)$$

Notice that the only independent variables in the expression are L and Y . v_p is a set variable, and will be determined by the specific application of the reactor system. The applied current does not feature as a variable in the expression, but determines the rate constant, k , that will be used.

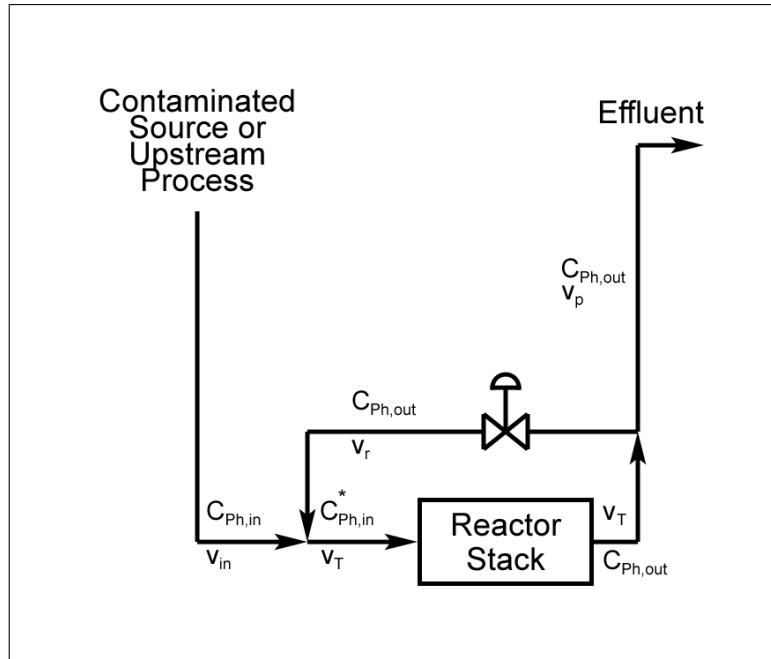


Figure 6.2: Proposed flow diagram for pilot plant

In order to demonstrate the steps involved in the optimisation based on economic considerations of the reactor system, a simple expression for the rate constant will be derived for a fixed current value of 50 mA. This current value corresponds with the highest reaction rate constants for all of the flow rates except one ($Re = 650$). As an approximation, a straight line is fitted through the rate constant versus Reynolds number data to yield:

$$k = 1.4621 \times 10^{-9} Re + 3.9402 \times 10^{-8} \quad (6.18)$$

The Reynolds number in equation 6.18 can be converted to a product flow rate. Equation 6.18 will then have the following form:

$$\begin{aligned} k &= 1.4621 \times 10^{-9} \cdot 8.33 \times 10^6 (Y + 1) v_p + 3.9402 \times 10^{-8} \\ k &= 0.01218 \cdot (Y + 1) v_p + 3.9402 \times 10^{-8} \end{aligned} \quad (6.19)$$

Equation 6.19 can then be substituted into equation 6.17, in order to obtain an expression in which conversion is only dependant on reactor length, recycle ratio and product flow rate. The conversion was calculated for various values of the recycle ratio and plotted versus reactor length. The graph hereof is presented in figure 6.3.

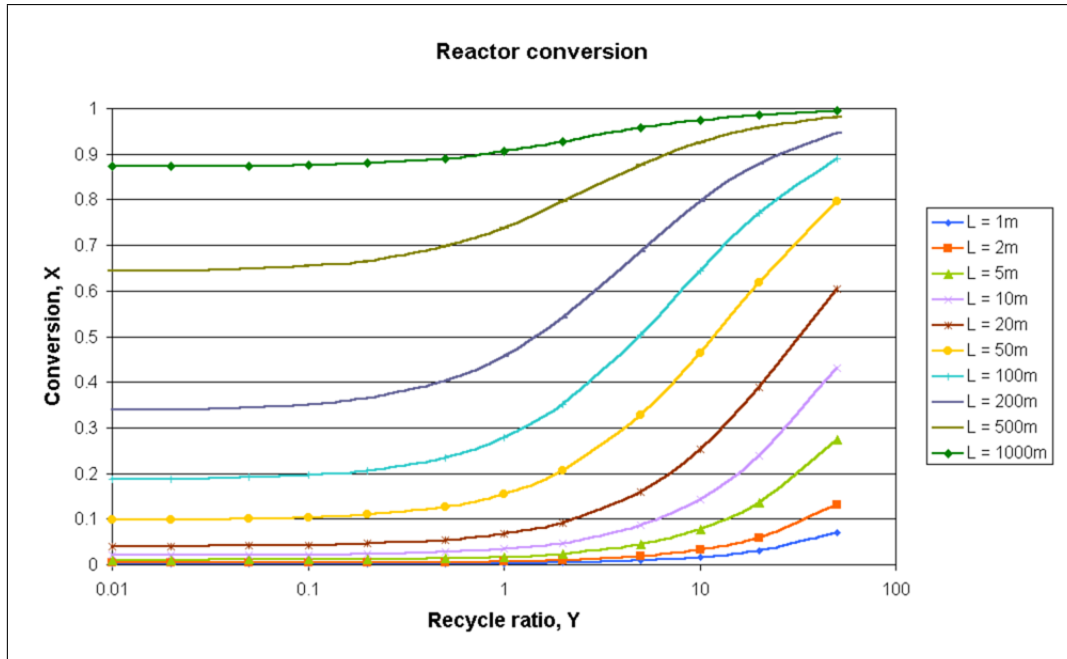
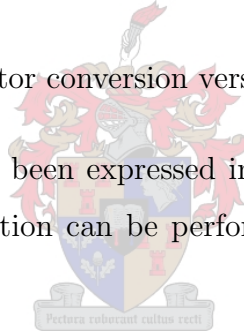


Figure 6.3: Reactor conversion versus reactor length

Now that the conversion has been expressed in terms of the major variables of the reactor, an economic evaluation can be performed to find optimum values for these variables.



6.4 Economic Evaluation

For a practical reactor, the most important factors that contribute to the overall cost involved in building and operating the reactor are the following:

1. **Capital cost** – the price of the materials, cost of construction and installation.
2. **Operating cost** – the cost involved in keeping the reactor running. This includes electricity costs, and any chemicals required on a continuous basis.
3. **Maintenance cost** – the cost involved in maintaining the final reactor. This includes cost of training personnel, paying salaries, general maintenance, etc.

The maintenance cost will not be evaluated at this stage since it requires more information on the practical lifetimes of the membrane and catalyst. No long-term

experiments have yet been done to determine the long-term response of the catalyst and membrane under electrolysis conditions.

The major contributing factors to the capital cost are the porous titanium support, titanium current collectors and membrane. To determine the cost of a typical small pilot scale reactor, quotes were obtained in June 2003. It was found that a reactor consisting of 20 units in series would require porous titanium substrates that would amount to approximately R80 000.

The cost of such a reactor was evaluated per meter length of reactor. Pressure drop through the reactor was an important consideration due to the small flow channels in the current collectors. The pressure drop in the reactor will determine the pump size required, and therefore influence the pumping costs involved and also the initial capital cost. Also, since the fraction of the flow being recycled is also a factor in the design of the reactor system, a trade-off between pump size and reactor length will determine the optimum values for the recycle ratio, Y , and the reactor length, L .

The capital cost of the reactor based on a meter length is shown in table 6.5. of the reactor. The expressions for the capital cost of the reactor, in terms of the

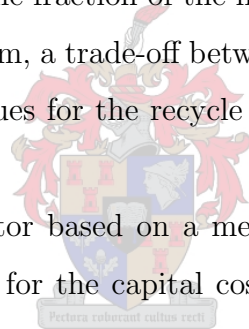


Table 6.5: Estimated capital costs of reactor (June 2003)

Part	Cost [R/m]
Electrode	5 860
Membrane	930
Materials	1 650
Total	8 440

reflux ratio and reactor length, can be derived considering the following simplifying assumptions:

1. Only the pressure drop due to friction in the flow channels will be considered. This assumes that the friction losses due to pipe fittings are negligible, relative to the reactor.

2. Only phenol will be considered as compound taking part in the reaction. This assumes that the phenol is directly converted to carbon dioxide. This is not unreasonable considering the low concentrations observed for the intermediate organics.

The expression relating conversion to reactor length, recycle ratio and product flow rate was derived in the previous section. In order to obtain optimum values for the recycle ratio and reactor length, economic values must be assigned. The prices calculated in this section relate only to the reactor and do not reflect installed prices of such a unit.

All of the major costs involved are linked to both variables (reactor length and recycle ratio). This will become clear as the cost of each major part of the reactor is evaluated. The total cost can therefore be subdivided into the following elements:

$$C_{\text{total}} = C_{\text{reactor}} + C_{\text{pump}} + C_{\text{reactor,running}} \quad (6.20)$$

Each term in equation 6.20 will now be discussed and expanded upon. The first element of the total cost is the capital cost of the reactor itself. This can be expressed as:

$$C_{\text{reactor}} = (C_{\text{substrate}} + C_{\text{membrane}} + C_{\text{materials}})L \quad (6.21)$$

The values supplied in 6.5 can be used directly in the above equation. The equation merely states that the capital cost is the cost (per meter) of the titanium substrate, membrane and construction materials, multiplied by the length of the reactor.

Next, the cost of the reactor pump must be evaluated. Based on the assumption that the major pressure drop in the system is due to the reactor, the energy balance can be simplified to express the pump's power requirement in terms of the friction losses:

$$P_{\text{pump}} = v_T \rho_T \left(\frac{2f u_T^2 L}{d_e} \right) \quad (6.22)$$

The friction losses were calculated using [53] (p. 199):

$$fRe = 24 [1 - 1.3553\gamma + 1.9467\gamma^2 - 1.7012\gamma^3 + 0.9564\gamma^4 - 0.2537\gamma^5] \quad (6.23)$$

From this the electricity cost of the pump can be calculated:

$$C_{\text{pump,running}} = \frac{P_{\text{pump}} \cdot t_{\text{life}} \cdot C_{\text{electricity}}}{1000\eta_{\text{pump}}} \quad (6.24)$$

The factor 1000 in the denominator was introduced to convert the pump power to kW. If the lifetime of the reactor is measured in hours, an expression for the required power in terms of kWh is obtained. $C_{\text{electricity}}$ is the unit price for electricity. Equation 6.24 only accounts for the running cost of the pump — the actual capital cost of the pump can also be significant relative to the other costs.

The capital cost of the pump was calculated using the Marshall and Swift index as published in *Chemical Engineering* [55]. The pump cost was calculated using an exponential method [54] (p. 9–67) and a Marshall and Swift index of 1000. Thus, the cost of the pump was calculated by

$$C_{\text{pump,capital}} = C_{\text{pump,capital}}^* \left(\frac{q_2}{q_1} \right)^n \quad (6.25)$$

where $C_{\text{pump,capital}}^*$ is the published cost for a pump of capacity q_1 . q_2 is the desired capacity of the pump. n is the exponent used to determine the new cost. The calculated value was then adjusted using the Marshall and Swift index published in [55]:

$$\text{Cost in year A} = \text{Cost in year B} \frac{\text{Index in year A}}{\text{Index in year B}} \quad (6.26)$$

Since the values calculated by equation 6.25 were based on an index of 1000, and the most recent index was 1089.0 in 2000, the capital cost could be calculated. The total pump cost is the sum of the pump capital and running cost.

$$C_{\text{pump}} = C_{\text{pump,capital}} + C_{\text{pump,running}} \quad (6.27)$$

The running cost of the reactor itself can be calculated based on the applied current density.

$$C_{\text{reactor,running}} = \frac{iWLVt_{\text{life}}C_{\text{electricity}}}{1000} \quad (6.28)$$

From the various equations contributing to the total cost, it can be seen that the cost is dependent on the applied current, the total flow through the reactor (and therefore the recycle ratio) and the length of the reactor.

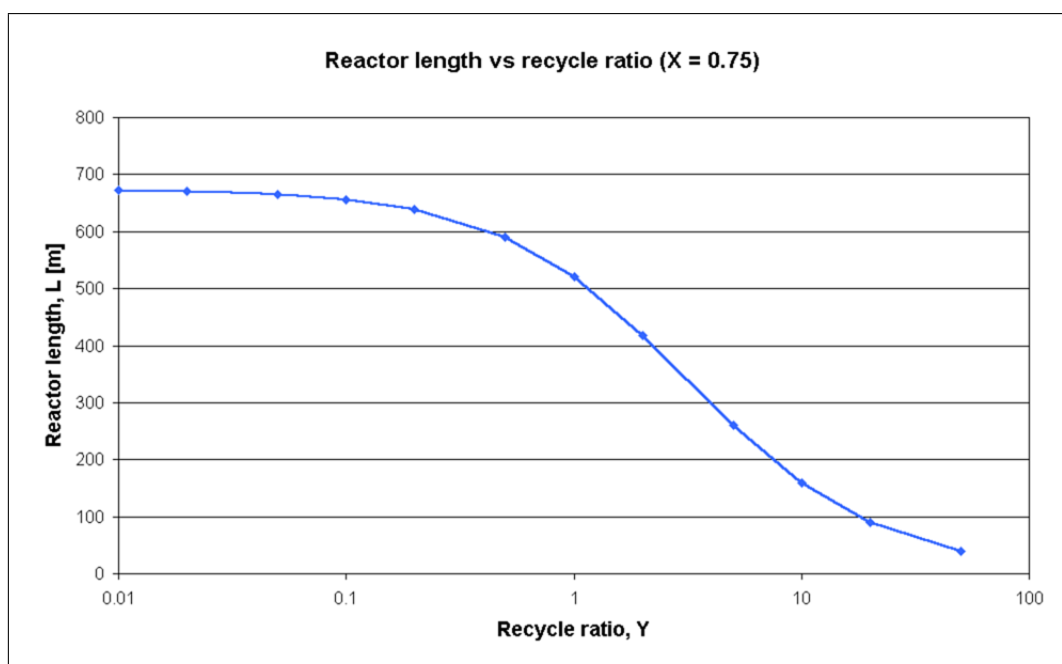


Figure 6.4: Reactor length versus recycle ratio for $X = 0.75$

If for an arbitrary conversion, and various values of the recycle ratio, the required reactor lengths are calculated using equation 6.17; a plot of reactor length versus recycle ratio for a fixed conversion can be obtained such as the one presented in figure 6.4. Here a conversion of 75% was chosen.

The various costs can now be calculated for the two values of Y and L and plotted. This has been done for typical values, with the exception of the pump costs, since no information was available regarding this aspect of the cost at the time of the evaluation. The graph of cost versus recycle ratio is presented in figure 6.5. It can be seen that for the current costs of the reactor parts, the running cost and capital cost of the reactor overshadow the pumping costs. Therefore, at the moment it is more cost effective to have a very large pumping system and a short reactor.

In future, as more research is done on materials, and the price of the construction materials are reduced, the cost of those two elements will become comparable to that of the pumping cost. The minimum cost would then shift to lower recycle ratios, and some intermediate recycle ratio will give the minimum cost for the reactor system.

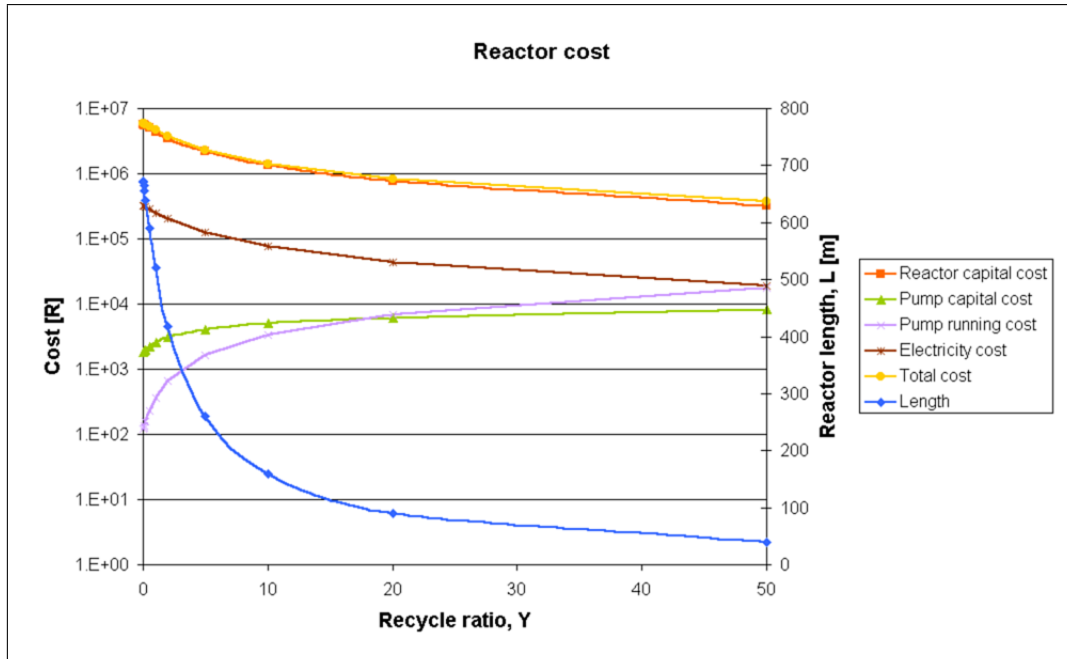


Figure 6.5: Cost of various parts of a typical reactor (June 2003)

This analysis was performed for a flow rate of 186 L/h. Although this may be enough to supply a small rural community with water, it must be remembered that this was done for a conversion of 0.75 and therefore not all of the harmful chemicals will be destroyed. Fortunately, the system is very efficient in the destruction of the micro-organisms, and therefore no pathogens will be present in a reactor of that length.

Increasing the conversion to 99% would increase the length of the reactor significantly, and thus increase both the capital cost and running cost of the reactor significantly. Therefore, it can be said that the reactor system using the current technologies available for this kind of water treatment is not economically viable. There exist other water treatment methods that are currently more efficient at disinfecting and purifying water (such as UV treatment and the use of ozone).

Chapter 7

Conclusions and Recommendations

The following conclusions can be drawn from this study:

- The HPLC method that was developed can be accurately used in the quantitative detection of phenol and its breakdown products.
- The SPE reactor system is only partially successful in removing organic content from waste water. It does however, completely destroy all living organisms present in the samples.
- The range of experimental parameters that was investigated showed that the process is under mixed control, i.e. the effects of mass transfer and charge transfer on the reaction rate are in the same order of magnitude.
- Despite the higher current efficiencies observed under potentiostatic control, it was found that galvanostatic control, due to the much higher rate of charge transfer, is the better choice for the mode of operation of the reactor. Reductions in the length of the reactor of up to an order of magnitude can be obtained.
- The reactor system, using the current catalyst and reactor set-up, is not economically viable for treating contaminated water due to high costs involved in materials and operation.
- The required length for the reactor can be reduced by up to an order of a magnitude when treating waste streams that are contaminated with micro-

organisms. Therefore, in such a case the cost of the reactor may be comparable to that of current technologies. The analysis could not be performed though, because insufficient data is available for determining k -values at different flow rates.

The following recommendations can be made for future work in this field of research:

- The $\text{SnO}_2/\text{ZrO}_2$ catalyst was chosen based on results obtained by the Department of Chemistry at the University of Stellenbosch. Only the removal of phenol was analysed, for and it was only for this purpose that the zirconium dopant was found to be superior. This does not necessarily mean that the catalyst is good in a practical sense. Further testing needs to be done on a range of these catalysts to determine the selectivity that each has towards the combustion versus the conversion reaction (see section 2.2).
- High overpotentials are observed for the electrode reactions. One of the main reasons causing the high overpotential, can be the contacting provided between the electrode and the membrane. If the catalyst and membrane can be combined into one part, two contacting surfaces would be removed.
- Although most of the important parameters were investigated in this project, further improvements may be achieved by changes to the following aspects of the reactor:
 1. Substrate properties, such as specific surface area, mean pore size, thickness, etc.
 2. Flow channel design
 3. Cheaper alternative materials of construction
- It is not possible to identify and quantitatively analyse all of the intermediates. Accurate measurement of the oxygen generated in the reaction will however give an indication of the extent of the reaction. Measurement of carbon dioxide will

indicate the extent of the full reaction. If reliable methods can be obtained to measure the concentrations of these gases, more accurate assumptions can be made about the mechanisms involved.

- Due to the complex interaction of the different parameters in the system, it may be beneficial to use advanced computational techniques to solve the process.



References

- [1] Goto, S. Levec, J. and Smith J.M. Trickle-bed oxidation reactors. *Catal. Rev. Sci. Eng.*, **15**:187–247, 1977.
- [2] Levec, J. Catalytic oxidation of toxic organics in aqueous solution. *Applied Catalysis A: General*, **63**:L1–L5, 1990.
- [3] Pintar, A. and Levec, J. Catalytic oxidation of organics in aqueous solutions i: Kinetics of phenol oxidation. *Journal of Catalysis*, **135**:345–357, 1992.
- [4] Gonze, E. Gonthier, Y. Boldo, P. and Bernis, A. Etude de l'oxydation du pentachlorophénol dans différentes géométries de réacteurs à ultrasons de haute fréquence. *Canadian Journal of Chemical Engineering*, **75**:245–255, 1997.
- [5] Duprez, D. Delanoë, F. Barbier Jr, B. Isnard, P. and Blanchard, G. Catalytic oxidation of organic compounds in aqueous media. *Catalysis Today*, **29**:317–322, 1996.
- [6] Inazu, K. Nagata, Y. and Maeda, Y. Decomposition of chlorinated hydrocarbons in aqueous solutions by ultrasonic irradiation. *Chemistry Letters*, **1**:57–60, 1993.
- [7] Comninellis, Ch. and Pulgarin, C. Electrochemical oxidation of phenol for wastewater treatment using SnO₂ anodes. *J. Appl. Electrochem.*, **23**:108–112, 1993.
- [8] Petrov, K.M. Kaba, L.M. Srinivasan, S. and Appleby, A.J. Water post-treatment without expendables — proton exchange membrane based electrolysis system. *J. Hydrogen Energy*, **18**:377–382, 1993.

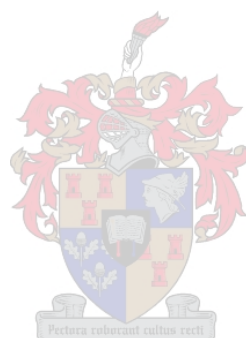
- [9] Comninellis, Ch. Electrochemical oxidation of organic pollutants for wastewater treatment. In C.A.C. Sequeira, editor, *Environmental oriented electrochemistry*, Amsterdam, Elsevier, 1994.
- [10] Polcaro, A.M. Palmas, S. Renoldi, F. and Mascia, M. On the performance of Ti/SnO₂ and Ti/PbO₂ anodes in electrochemical degradation of 2-chlorophenol for wastewater treatment. *J. Appl. Electrochem.*, **29**:147–151, 1999.
- [11] Kötzt, R. Stucki, S. and Carcer, B. Electrochemical waste water treatment using high overvoltage anodes. Part I: Physical and electrochemical properties of SnO₂ anodes. *J. Appl. Electrochem.*, **21**:14–20, 1991.
- [12] Kirk, D.W. Sharifian, H. and Foulkes, F.R. Anodic oxidation of aniline for waste water treatment. *J. Appl. Electrochem.*, **15**:285–292, 1985.
- [13] Sharifian, H. and Kirk, D.W. Electrochemical oxidation of phenol. *J. Electrochem. Soc.*, **133**:921–924, 1986.
- [14] Tahar, N.B. and Savall, A. Mechanistic aspects of phenol electrochemical degradation by oxidation on a Ta/PbO₂ anode. *J. Electrochem. Soc.*, **145**:3427–3434, 1998.
- [15] Grimm, J. *Electrochemical purification of hazardous organic compounds from wastewater by means of novel electrode materials and a solid-polymer-electrolyte-reactor system*. PhD thesis, University of Stellenbosch, South Africa, 1999.
- [16] Fang, G. Liu, Z. Zhang, Z. Hu, Y. Ashur, I.A. and Yao, K.L. Preparation of SnO₂-cuo nanocrystalline powders in two different ways by the sol-gel method. *Phys. Stat. Sol. A*, **156**:15–22, 1996.
- [17] Casey, V. and Stephenson, M.I. A study of undoped and molybdenum doped, polycrystalline, tin oxide thin films produced by a simple reactive evaporation technique. *J. Phys. D: Appl. Phys.*, **23**:1212–1215, 1990.

- [18] Gouvea, D. Varela, J.-A. Longo, E. Smith, A. and Bonnet, J.-P. Chemical synthesis of homogenous SnO₂ powders doped with manganese. *Eur. J. Solid State Inorg. Chem.*, **30**:915–927, 1993.
- [19] Correa-Lozano, B. Comninellis, Ch. and De Battisti, A. Physicochemical properties of Ti/SnO₂-Sb₂O₅ films prepared by the spray pyrolysis technique. *J. Electrochem. Soc.*, **143**:203–209, 1996.
- [20] Baker, P.G.L. *Sol-gel preparation, characterisation and electrochemistry of mixed metal tin oxide electrodes*. PhD thesis, University of Stellenbosch, South Africa, to be submitted, 2004.
- [21] Pickett, D.J. *Electrochemical reactor design*. Elsevier Scientific Publishing Company, Amsterdam, 2nd edition, 1979.
- [22] Wendt, H. and Kreysa, G. *Electrochemical engineering – science and technology in chemical and other industries*. Springer-Verlag, Berlin, Heidelberg, 1999.
- [23] Kortüm, G. *Treatise on Electrochemistry*. Elsevier, Amsterdam, 2nd edition, 1965.
- [24] Fahidy, T.Z. *Principles of Electrochemical Reactor Analysis*. Elsevier, 1985.
- [25] Fogler, H.S. *Elements of chemical reaction engineering*. Prentice-Hall, 2nd edition, 1992.
- [26] Comninellis, Ch. Electrocatalysis in the conversion/combustion of organic pollutants for waste water treatment. *Electrochim. Acta*, **39**:1857–1862, 1994.
- [27] Comninellis, Ch. and De Battisti, A. Electrocatalysis in anodic oxidation of organics with simultaneous oxygen evolution. *J. Chim. Phys.*, **93**:673–679, 1996.
- [28] Gattrell, M. and Kirk, D.W. A fourier transform infrared spectroscopy study of the passice film produced during aqueous acidic phenol electro-oxidation. *J. Electrochem. Soc.*, **139**:2736–2744, 1992.

- [29] Gattrell, M. and Kirk, D.W. A study of the oxidation of phenol at platinum and preoxidized platinum surfaces. *J. Electrochem. Soc.*, **140**:903–911, 1993.
- [30] Valendo, A. Ya Norikov, Yu. D. and Blyumberg, E.A. No title. *Neftekhimiya*, **9**:866–?, 1969.
- [31] Gattrell, M. and Kirk, D.W. A study of the oxidation of phenol at platinum and preoxidized platinum surfaces. *J. Electrochem. Soc.*, **140**:1534–1540, 1993.
- [32] Koile, R.C. and Johnson, D.C. *Anal. Chem.*, **51**:741, 1979.
- [33] Vicent, F. Morallón, E. Quijada, C. Vázquez, J.L. and Aldaz, A. Characterization and stability of doped SnO₂ anodes. *J. Appl. Electrochem.*, **28**:607–612, 1998.
- [34] Correa-Lozano, B. Comninellis, Ch. and De Battisti, A. Preparation of SnO₂-Sb₂O₅ films by the spray pyrolysis technique. *J. Appl. Electrochem.*, **26**:83–89, 1996.
- [35] Correa-Lozano, B. Comninellis, Ch. and De Battisti, A. Electrochemical properties of Ti/SnO₂-Sb₂O₅ electrodes prepared by the spray pyrolysis technique. *J. Appl. Electrochem.*, **26**:683–688, 1996.
- [36] Burke, L.D. and Murphy, O.J. Surface area – voltammetric charge correlation for RuO₂/TiO₂-based anodes. *J. Electroanal. Chem.*, **112**:39–50, 1980.
- [37] Comninellis, Ch. and Vercesi, G.P. Problems in DSA coating deposition by thermal decomposition. *J. Appl. Electrochem.*, **21**:136–142, 1991.
- [38] Park, S. and Mackenzie, J.D. Sol-gel-derived tin oxide thin films. *Thin Solid Films*, **258**:268–273, 1995.
- [39] Hench, L.L. and West, J.K. The sol-gel process. *Chem. Rev.*, **90**:33–72, 1990.
- [40] Lu, F. Chen, S. and Peng S. Ultrafine SnO₂ prepared by supercritical fluid drying technique (SCFDT) for gas sensors. *Catalysis Today*, **30**:183–188, 1996.

- [41] Ward, D.A. and Ko, E.I. Preparing catalytic materials by the sol-gel method. *Ind. Eng. Chem. Res.*, **34**:421–433, 1995.
- [42] Maddalena, A. Dal Maschio, R. Diré, S. and Raccanelli, A. Electrical conductivity of tin oxide films prepared by the sol-gel method. *J. Non-Cryst. Solids*, **121**:365–369, 1990.
- [43] Chatelon, J.P. Terrier, C. Bernstein, E. Berjoan, R. and Roger, J.A. Morphology of SnO₂ thin films obtained by the sol-gel technique. *Thin Solid Films*, **247**:162–168, 1994.
- [44] Terrier, C. Chatelon, J.P. Berjoan, R. and Roger, J.A. Sb-doped SnO₂ transparent conducting oxide from the sol-gel dip-coating technique. *Thin Solid Films*, **263**:37–41, 1995.
- [45] Grimm, J. Bessarabov, D. Maier, W. Storck, S. and Sanderson, R.D. Sol-gel film-preparation of novel electrodes for the electrocatalytic oxidation of organic pollutants in water. *Desalination*, **115**:295–302, 1998.
- [46] Stucki, S. Kötz, R. Carcer, B. and Suter, W. Electrochemical waste water treatment using high overvoltage anodes: Part II Anode performance and applications. *J. Appl. Electrochem.*, **21**:99–104, 1991.
- [47] Comninellis, Ch. Electrochemical treatment of wastewater containing organic pollutants. In E.E. Eckenfelder, A.R. Bowers, and J.A. Roth, editors, *Proceedings of the 3rd International Symposium on Chemical Oxidation, Chemical Oxidation: Technology for the Nineties*. Technomic Publishing, 1994.
- [48] Murphy, O.J. Hitchens, G.D. Kaba, L. and Verostko, C.E. Direct electrochemical oxidation of organics for wastewater treatment. *Wat. Res.*, **26**:443–451, 1992.
- [49] Comninellis, Ch. and Nerini, A. Anodic oxidation of phenol in the presence of NaCl for wastewater treatment. *J. Appl. Electrochem.*, **25**:23–28, 1995.
- [50] <http://www.obf.on.ca/watertest2002.htm>.

- [51] <http://www.nature.ca/rideau/c/c2.e.htm>.
- [52] Water quality — Determination of phenol index — 4-Aminoantipyrine spectrometric methods after distillation, SABS SM 211:1992. (equivalent to ISO 6439:1990).
- [53] Shah, R.K. and London, A.L. *Laminar flow forced convection in ducts*. Academic Press, 1978.
- [54] Perry, R.H. and Green, D.W. *Perry's chemical engineers' handbook*. McGraw-Hill, 7th edition, 1997.
- [55] Economic indicators. *Chemical Engineering*, **109**:122, 2002.



Appendix A

Model derivations

A.1 Reactor model

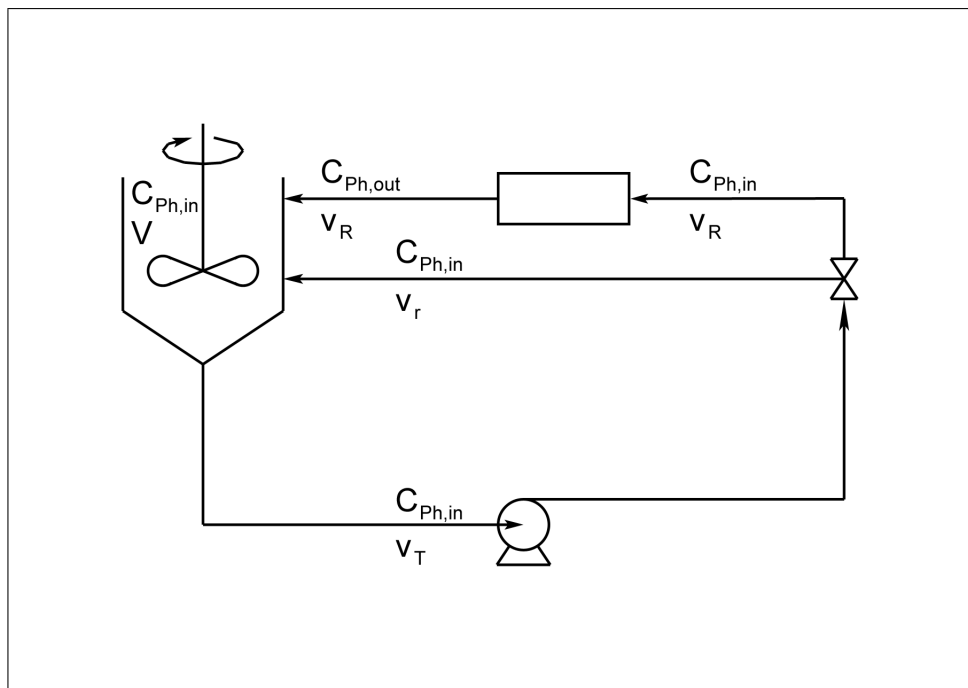


Figure A.1: Nomenclature used in model derivation

As mentioned in section 6.1, an overall mass balance can be performed on the

reservoir as shown in figure A.1.

$$\begin{aligned}
 \text{IN:} & \quad \rho_{\text{out}}v_{\text{R}} + \rho_{\text{in}}v_{\text{r}} \\
 \text{OUT:} & \quad - \rho_{\text{in}}v_{\text{T}} \\
 \text{GENERATION:} & \quad + 0 \\
 \text{ACCUMULATION:} & \quad = 0
 \end{aligned} \tag{A.1}$$

From the assumption that the physical properties of the inlet and outlet are the same, i.e. $\rho_{\text{in}} = \rho_{\text{out}}$, the following relationship is obtained

$$v_{\text{T}} = v_{\text{R}} + v_{\text{r}} \tag{A.2}$$

Performing a component mass balance on the reservoir using phenol as compound, one obtains

$$\begin{aligned}
 \text{IN:} & \quad (C_{\text{Ph,out}}v_{\text{R}} + C_{\text{Ph,in}}v_{\text{r}}) M_{\text{R,Ph}}\Delta t \\
 \text{OUT:} & \quad - C_{\text{Ph,in}}v_{\text{T}}M_{\text{R,Ph}}\Delta t \\
 \text{GENERATION:} & \quad + 0 \\
 \text{ACCUMULATION:} & \quad = M_{\text{R,Ph}}V (C_{\text{Ph,in}}|_{t+\Delta t} - C_{\text{Ph,in}}|_t)
 \end{aligned} \tag{A.3}$$

Dividing equation A.3 by $M_{\text{R,Ph}}\Delta t$ and letting $\Delta t \rightarrow 0$ one obtains the differential form of the defining equation for the reservoir:

$$V \frac{dC_{\text{Ph,in}}}{dt} = v (C_{\text{Ph,out}} - C_{\text{Ph,in}}) \tag{A.4}$$

Replacing $\frac{V}{v}$ with τ , the residence time, the final form of the differential equation can be obtained as shown in equation 6.1.

$$\frac{dC_{\text{Ph,in}}}{dt} = \frac{(C_{\text{Ph,out}} - C_{\text{Ph,in}})}{\tau} \tag{6.1}$$

The same mass balances can be done for an infinitesimally small length element

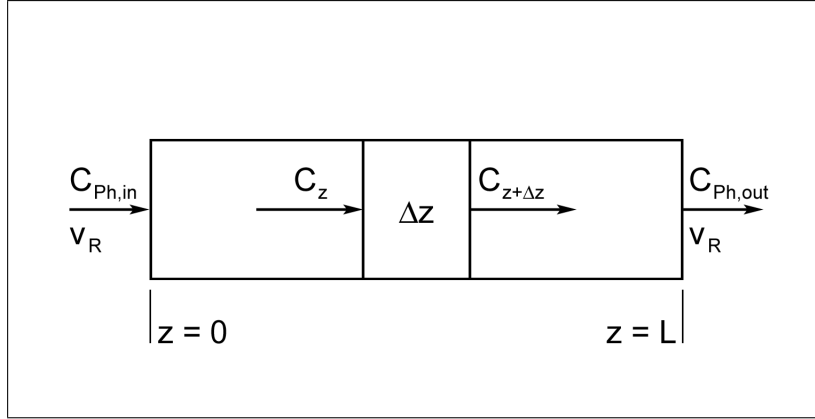


Figure A.2: Nomenclature used for reactor

in the reactor. The component mass balance based on phenol gives:

$$\begin{aligned}
 \text{IN:} & \quad C_{\text{Ph}}|_z M_{R,\text{Ph}} v_R \\
 \text{OUT:} & \quad - C_{\text{Ph}}|_{z+\Delta z} M_{R,\text{Ph}} v_R \\
 \text{GENERATION:} & \quad + r_{\text{Ph}}'' a(t) M_{R,\text{Ph}} W \Delta z \\
 \text{ACCUMULATION:} & \quad = 0
 \end{aligned} \tag{A.5}$$

Dividing by $\Delta z M_{R,\text{Ph}}$ and letting $\Delta z \rightarrow 0$ gives the differential form of the mass balance for the reactor:

$$\frac{dC_{\text{Ph}}}{dz} = \frac{r_{\text{Ph}}'' a(t) W}{v_R} \tag{6.2}$$

Replacing r_{Ph}'' with the appropriate form as given in equation 6.3 one obtains the general form of the mass balance in differential form can be written as

$$\frac{dC_{\text{Ph}}}{dz} = \frac{-k C_{\text{Ph}}^n a(t) W}{v_R} \tag{6.4}$$

This can then be integrated for two different cases of n . For $n \neq 1$:

$$\begin{aligned}
 \int_{C_{\text{Ph},\text{in}}|_t}^{C_{\text{Ph},\text{out}}|_t} \frac{dC_{\text{Ph}}}{C_{\text{Ph}}^n} &= -\frac{ka(t)W}{v} \int_0^L dz \\
 \frac{1}{1-n} C_{\text{Ph}}^{1-n} \Big|_{C_{\text{Ph},\text{in}}|_t}^{C_{\text{Ph},\text{out}}|_t} &= -\frac{ka(t)W}{v} L
 \end{aligned}$$

giving

$$C_{\text{Ph,out},t}^{1-n} - C_{\text{Ph,in},t}^{1-n} = -\frac{(1-n)ka(t)W}{v_R}L \quad (6.5)$$

$$C_{\text{Ph,out},t} = \left\{ C_{\text{Ph,in},t}^{1-n} - \frac{(1-n)ka(t)W}{v_R}L \right\}^{\frac{1}{1-n}} \quad (A.6)$$

and for $n = 1$:

$$\int_{C_{\text{Ph,in},t}}^{C_{\text{Ph,out},t}} \frac{dC_{\text{Ph}}}{C_{\text{Ph}}} = -\frac{ka(t)W}{v} \int_0^L dz$$

$$\ln C_{\text{Ph}} \Big|_{C_{\text{Ph,in},t}}^{C_{\text{Ph,out},t}} = -\frac{ka(t)W}{v}L$$

giving

$$C_{\text{Ph,out},t} = C_{\text{Ph,in},t} \exp \left\{ -\frac{ka(t)W}{v_R}L \right\} \quad (6.6)$$

A.2 Scale-up Calculation

Performing an overall mass balance on the system, assuming that the difference between the physical properties of the inlet and outlet is negligible, one obtains:

$$v_{\text{in}} = v_{\text{p}} \quad (A.7)$$

Performing the same mass balance on the T-junction just before the inlet of the reactor where the recycle and inlet streams meet, an expression for the total flow rate through the reactor is found

$$v_{\text{T}} = v_{\text{r}} + v_{\text{p}} \quad (A.8)$$

An expression can be obtained for the concentration of the stream entering the reactor. This can be done by performing a component mass balance at the same junction:

$$C_{\text{Ph,in}}v_{\text{in}} + C_{\text{Ph,out}}v_{\text{r}} = v_{\text{T}}C_{\text{Ph,in}}^* \quad (A.9)$$

$$C_{\text{Ph,in}}^* = \frac{C_{\text{Ph,in}}v_{\text{in}} + C_{\text{Ph,out}}v_{\text{r}}}{v_{\text{T}}} \quad (A.10)$$

Performing a component mass balance on the reactor, assuming first order reaction kinetics, the expression for the outlet concentration can be obtained in terms of the inlet concentration:

$$v_T C_{\text{Ph},z} - v_T C_{\text{Ph},z+\Delta z} + r_{\text{Ph}} W \Delta z = 0 \quad (\text{A.11})$$

$$-v_T \frac{dC_{\text{Ph},z}}{dz} = k C_{\text{Ph},z} W \quad (\text{A.12})$$

$$\frac{dC_{\text{Ph},z}}{C_{\text{Ph},z}} = -\frac{kW dz}{v_T} \quad (\text{A.13})$$

$$C_{\text{Ph},\text{out}} = C_{\text{Ph},\text{in}}^* \exp\left(-\frac{kWL}{v_T}\right) \quad (\text{A.14})$$

Substituting equation A.10 into equation A.14, the final form of the expression giving $C_{\text{Ph},\text{out}}$ in terms of $C_{\text{Ph},\text{in}}$ is obtained:

$$C_{\text{Ph},\text{out}} = \frac{C_{\text{Ph},\text{in}} v_{\text{in}} + C_{\text{Ph},\text{out}} v_r}{v_T} \exp\left(-\frac{kWL}{v_T}\right) \quad (\text{A.15})$$

$$C_{\text{Ph},\text{out}} \left[1 - \frac{v_r}{v_T} \exp\left(-\frac{kWL}{v_T}\right)\right] = C_{\text{Ph},\text{in}} \frac{v_{\text{in}}}{v_T} \exp\left(-\frac{kWL}{v_T}\right) \quad (\text{A.16})$$

If Y is defined as $\frac{v_r}{v_p}$

$$C_{\text{Ph},\text{out}} \left[Y + 1 - Y \exp\left(-\frac{kWL}{v_T}\right)\right] = C_{\text{Ph},\text{in}} \exp\left(-\frac{kWL}{v_T}\right) \quad (\text{A.17})$$

and v_T is written as $v_p(Y + 1)$,

$$\frac{C_{\text{Ph},\text{out}}}{C_{\text{Ph},\text{in}}} = 1 - X = \frac{\exp\left(-\frac{kWL}{v_p(Y+1)}\right)}{Y + 1 - Y \exp\left(-\frac{kWL}{v_p(Y+1)}\right)} \quad (6.17)$$

Appendix B

Miscellaneous Calculations

B.1 Reaction Rate Constants

Equation 6.13 will be used in the calculation of the reaction rate constants. As an example, the constant will be calculated for one of the experiments conducted with the nickel-plated current collectors (50 mA, Re = 650, 15 lb-in, not separated). In this case, the flow rate is $2.6 \times 10^{-6} \left[\frac{\text{m}^3}{\text{s}} \right]$. Thus,

$$\tau = \frac{V}{v} = \frac{0.001}{2.6 \times 10^{-6}} = 384.6\text{s} \quad (\text{B.1})$$

The constant obtained in the exponential fit for the specific experiment was -1.82×10^{-6} . Substituting the appropriate values into equation 6.13:

$$k = -\frac{2.6 \times 10^{-6}}{0.004 \cdot 0.548} \ln(-1.82 \times 10^{-6} \cdot 384.6 + 1) = 8.30 \times 10^{-7} \quad (\text{B.2})$$

B.2 Differential Method of Rate Analysis

As an example of this method, the determination of the reaction order for the 60 ppm phenol experiment will be shown here using the technique described in section 2.1.5. The first step is the fitting of the polynomial to the experimental data. The data points are shown in table B.1. Both a 2nd and 3rd order polynomial was fitted to the data.

The coefficients obtained for the polynomials, together with the appropriate statistical data, are given in table B.2 Note that in all cases (except a_0) the 95% confidence interval is greater than the corresponding coefficient, indicating an unstable

Table B.1: Data for the derivation of reaction orders (60 ppm)

t [s]	C_{Ph} [mM]	$\left(\frac{dC_{Ph}}{dt}\right)_2$ [$\frac{mmol}{dm^3 \cdot s}$]	$\left(\frac{dC_{Ph}}{dt}\right)_3$ [$\frac{mmol}{dm^3 \cdot s}$]	$\ln(C_{Ph})$	$\ln\left(-\frac{dC_{Ph}}{dt}\right)$ 2nd-order	$\ln\left(\frac{dC_{Ph}}{dt}\right)$ 3rd-order
0	0.6189	-4.38×10^{-6}	-2.50×10^{-6}	-0.4797	-12.34	-12.90
900	0.6309	-4.29×10^{-6}	-2.98×10^{-6}	-0.4606	-12.36	-12.72
1800	0.6305	-4.21×10^{-6}	-3.39×10^{-6}	-0.4612	-12.38	-12.59
2700	0.6223	-4.12×10^{-6}	-3.72×10^{-6}	-0.4743	-12.40	-12.50
3600	0.6128	-4.04×10^{-6}	-3.98×10^{-6}	-0.4898	-12.42	-12.43
4500	0.6321	-3.95×10^{-6}	-4.15×10^{-6}	-0.4587	-12.44	-12.39
5400	0.5963	-3.87×10^{-6}	-4.26×10^{-6}	-0.5170	-12.46	-12.37
6300	0.5812	-3.78×10^{-6}	-4.29×10^{-6}	-0.5427	-12.49	-12.36
7200	0.6049	-3.70×10^{-6}	-4.24×10^{-6}	-0.5027	-12.51	-12.37
8100	0.6038	-3.61×10^{-6}	-4.12×10^{-6}	-0.5045	-12.53	-12.40
9000	0.5846	-3.53×10^{-6}	-3.92×10^{-6}	-0.5368	-12.56	-12.45
9900	0.5924	-3.44×10^{-6}	-3.65×10^{-6}	-0.5236	-12.58	-12.52
10800	0.6065	-3.36×10^{-6}	-3.30×10^{-6}	-0.5001	-12.60	-12.62
11700	0.5850	-3.27×10^{-6}	-2.87×10^{-6}	-0.5361	-12.63	-12.76
12600	0.5786	-3.19×10^{-6}	-2.37×10^{-6}	-0.5471	-12.66	-12.95
13500	0.5702	-3.10×10^{-6}	-1.80×10^{-6}	-0.5619	-12.68	-13.23
14400	0.5827	-3.02×10^{-6}	-1.14×10^{-6}	-0.5401	-12.71	-13.68

fit to the data. This means that the removal or addition of a point can cause large changes in these coefficients.

The logarithmic plots of the rate of change in concentration vs the concentration are given in figure B.1.

B.3 Reactor Cost

The economic evaluation was based on a conversion of 75%. An example of the reactor cost calculation will be shown for a recycle ratio of 1. The first step is to determine the reactor length that, together with a recycle ratio of 1, will result in a conversion of 0.75. This can be done by solving equation 6.17; yielding a value of

Table B.2: Statistical data for polynomial fits

	2nd-order		3rd-order	
	Coefficient	95% c.i.	Coefficient	95% c.i.
a_0	0.6301	0.01645	0.6282	0.02081
a_1	-4.38×10^{-6}	5.30×10^{-6}	-2.50×10^{-6}	1.29×10^{-5}
a_2	4.72×10^{-11}	3.55×10^{-10}	-2.89×10^{-10}	2.12×10^{-9}
a_3	-	-	1.55×10^{-14}	9.67×10^{-14}
R^2	69.9%		70.2%	

520.7 for the reactor length. The capital cost of the reactor is only dependant on the length, and can therefore be calculated using R 8440 as the cost per unit length:

$$C_{\text{reactor}} = 8440 \cdot 520.7 = \text{R } 4\,394\,591 \quad (\text{B.3})$$

To determine the pressure drop required for the pump, the linear velocity of the water needs to be determined. A product flow rate of 5.17×10^{-5} was chosen, since this would ensure that the estimation of the k values are relatively accurate. Thus, the total flow rate can be calculated using the recycle ratio:

$$v_{\text{T}} = (Y + 1)v_{\text{p}} = 2v_{\text{p}} = 1.03 \times 10^{-4} \left[\frac{\text{m}^3}{\text{s}} \right] \quad (\text{B.4})$$

Taking into consideration that there are 30 flow channels in the current collectors, the linear velocity can be calculated:

$$u_{\text{T}} = \frac{v_{\text{T}}}{A_{\text{c}}} = \frac{1.03 \times 10^{-4}}{30 \cdot 0.004 \cdot 0.004} = 0.215 \left[\frac{\text{m}}{\text{s}} \right] \quad (\text{B.5})$$

corresponding to a Reynolds number of

$$\text{Re}_{\text{T}} = \frac{1000 \cdot 0.004 \cdot 0.215}{0.001} = 861.1 \quad (\text{B.6})$$

Using equation 6.23, and an aspect ratio of one, the friction factor can be determined as 0.0165. This can then be substituted into equation 6.22 to obtain the power requirement of the pump (assuming a pump efficiency of 50%).

$$P_{\text{pump}} = 1.03 \times 10^{-4} \cdot 1000 \left(\frac{2 \cdot 0.0165 \cdot 0.215^2 \cdot 520.7}{0.004} \right) = 41.2\text{W} \quad (\text{B.7})$$

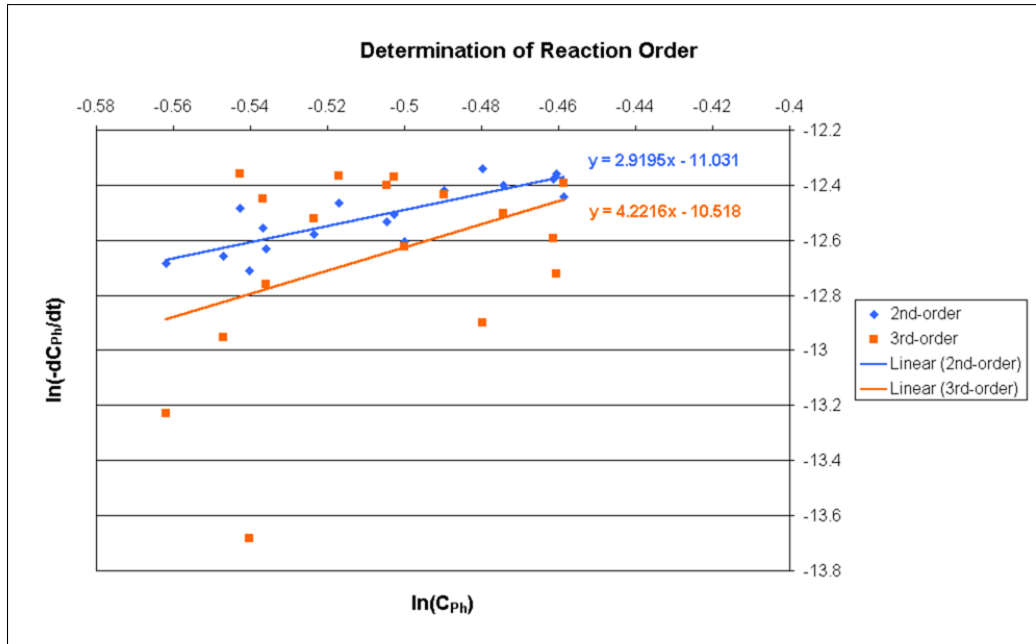


Figure B.1: Determination of reaction order – example

This can be used to calculate the capital cost of the pump. The prices listed in [54] were for North America, but a reasonable estimate of the contribution of the pump to the cost can be obtained in this way. Assuming an exchange rate of R 7.00 to the dollar, the capital cost can be calculated as

$$C_{\text{pump, capital}} = 1600 \left(\frac{41.2}{7500} \right)^{0.3} = \text{R } 2350 \quad (\text{B.8})$$

Taking into account the Marshall and Swift index, the total cost amounts to

$$C_{\text{pump, capital}} = 2350 \frac{1089}{1000} = \text{R } 2560 \quad (\text{B.9})$$

To determine the running cost of the reactor, a lifetime needs to be determined for the reactor system. Since no experiments were done involving catalyst and membrane lifetime, no information is available regarding the lifetime. Thus, a lifetime of 5 years was chosen for the reactor. The pump running cost can therefore be calculated using equation 6.24. The electricity cost was approximately R 0.20 per kWh.

$$C_{\text{pump, running}} = \frac{41.2 \cdot 43800 \cdot 0.20}{1000} = \text{R } 361 \quad (\text{B.10})$$

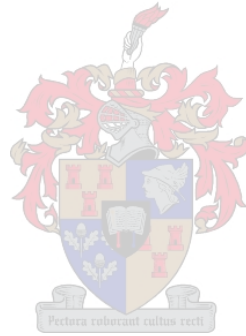
APPENDIX B. MISCELLANEOUS CALCULATIONS

Equation 6.28 can be used to calculate the electricity cost of the power source. The width used in this case, must be the width of the reactor, which is 0.25 m. A current density of $0.88 \left[\frac{\text{A}}{\text{cm}^2} \right]$ was selected.

$$C_{\text{reactor,running}} = \frac{8.811 \cdot 0.25 \cdot 520.7 \cdot 25 \cdot 43800 \cdot 0.20}{1000} = \text{R } 251\,180. \quad (\text{B.11})$$

All of the individual elements of the cost can now be added up:

$$C_{\text{total}} = 4394591 + 2560 + 361 + 251180 = \text{R } 4\,648\,692 \quad (\text{B.12})$$



Appendix C

Growth Curves

The growth curves for the individual pathogens are given in this Appendix. The growth curves were set up by allowing an inoculated vessel containing various concentrations of TSB to grow for a period of 24 hours. At selected times, samples were taken and the absorbance were measured using a photospectrometer. The absorbance is normally directly proportional to the number of cells in the solution at any time. To prove this, cell counts were obtained for *Enterococcus Faecallis* and compared to the absorbance. This is done in figure C.1. Notice the excellent correlation between the absorbance and cell count. The growth curves for *E. Faecallis*, *Salmonella* and *E.Coli* are given in figures C.2, C.3 and C.4 respectively.

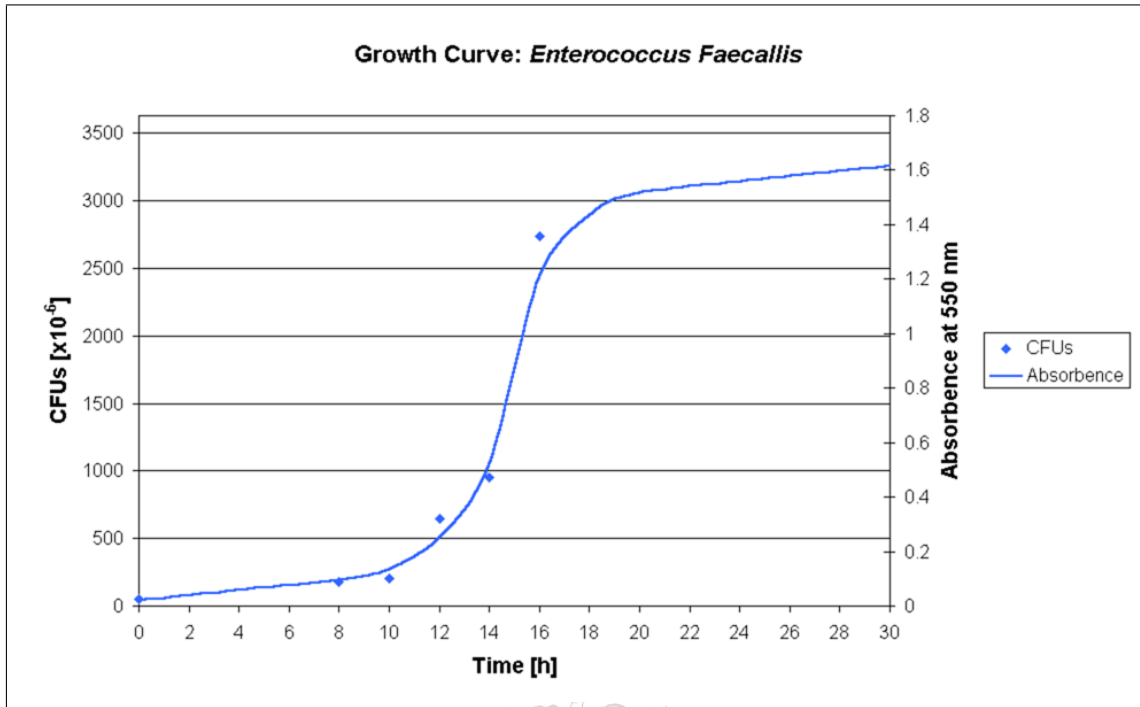


Figure C.1: Growth curve for *E. Faecallis*: Absorbance and cell count

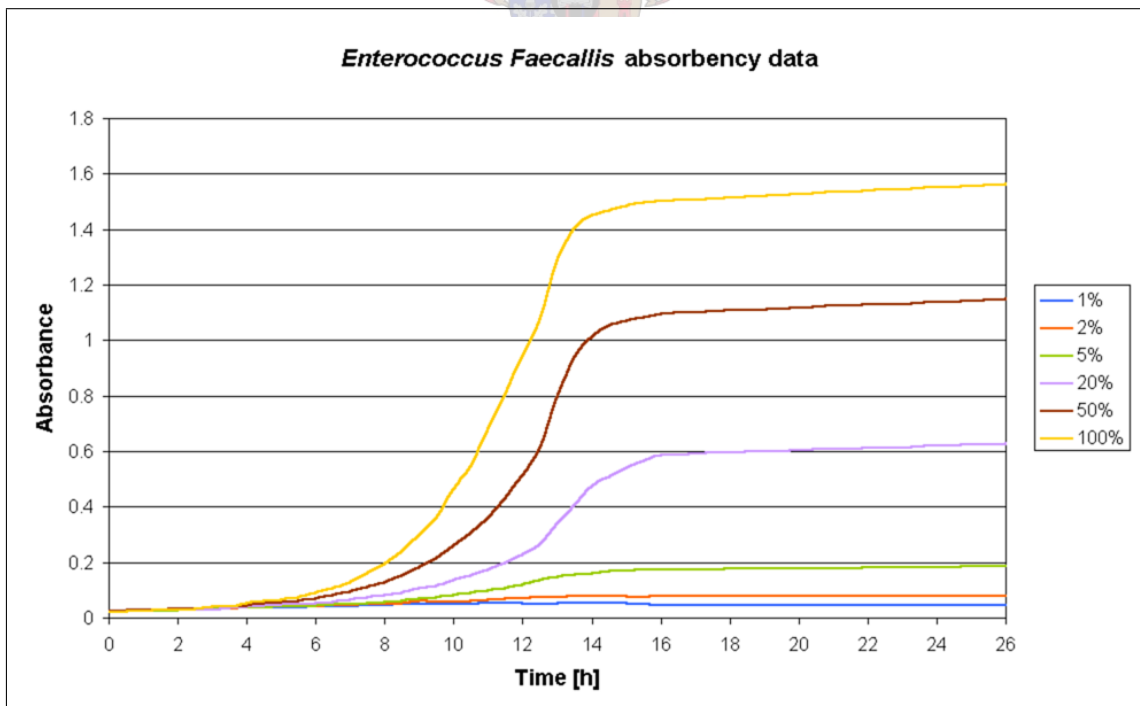


Figure C.2: Growth curve for *E. Faecallis* at various TSB concentrations

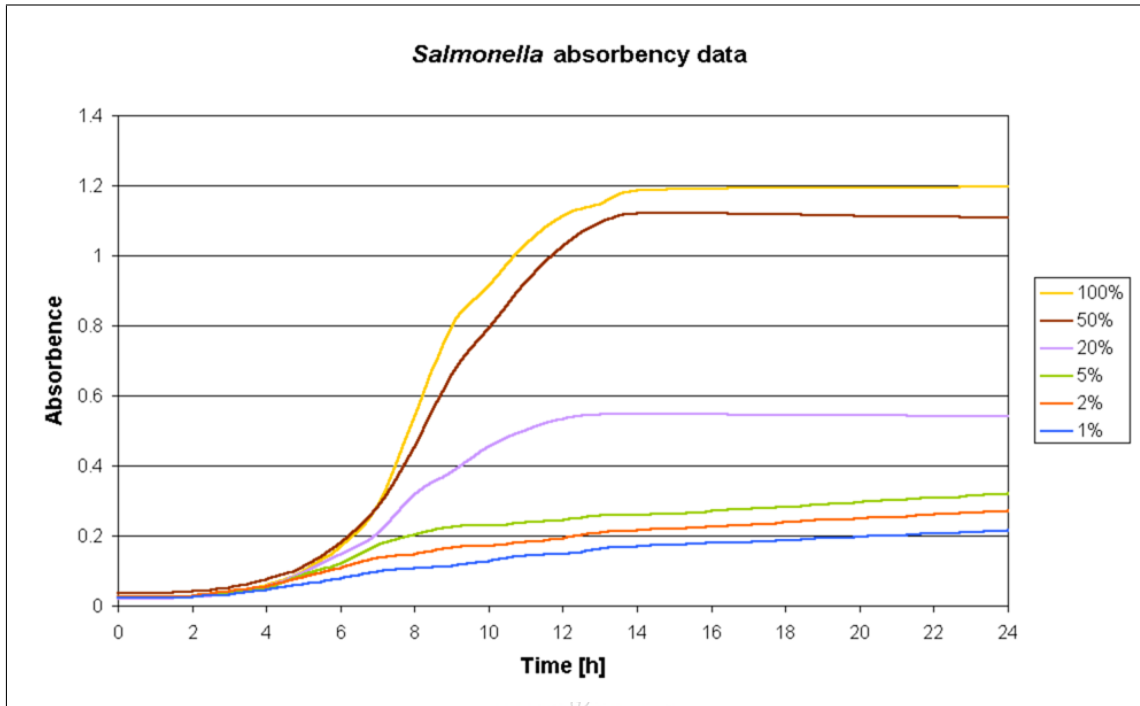


Figure C.3: Growth curve for *Salmonella* at various TSB concentrations

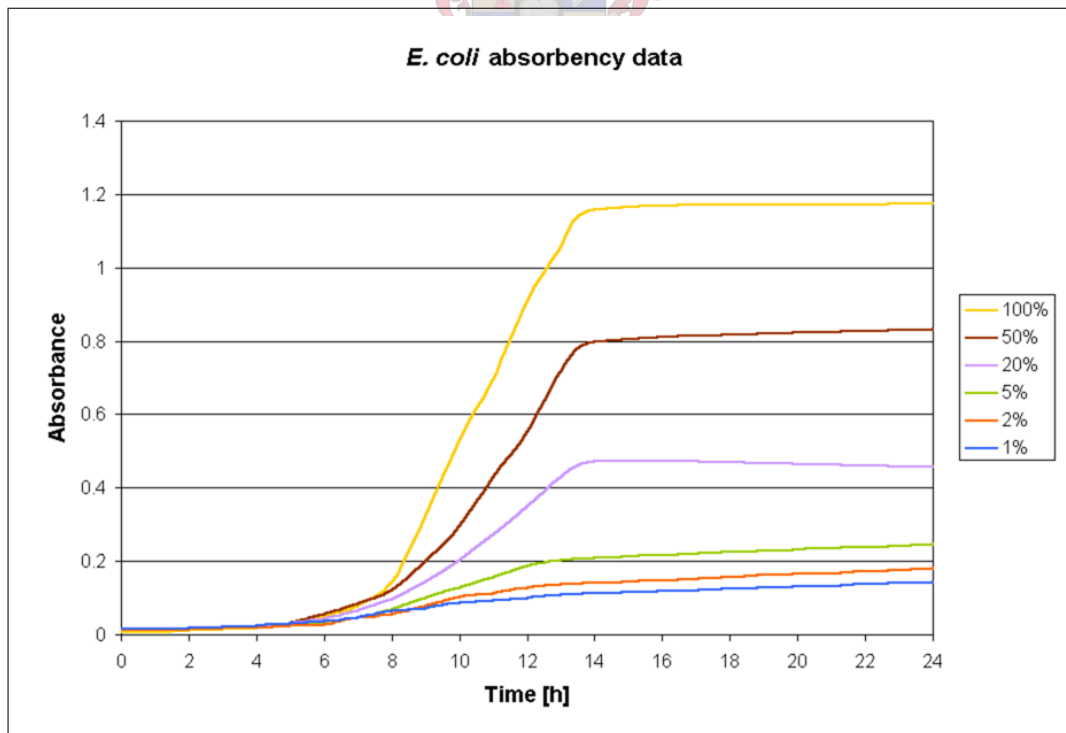
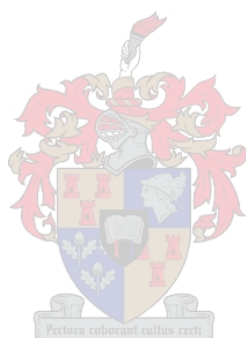


Figure C.4: Growth curve for *E. Coli* at various TSB concentrations

Appendix D

Technical Drawings

Drawings of the initial reactor are given in figures D.1 to D.3. The schematic drawings of the laboratory-scale reactor are given in figures D.4 to D.6.



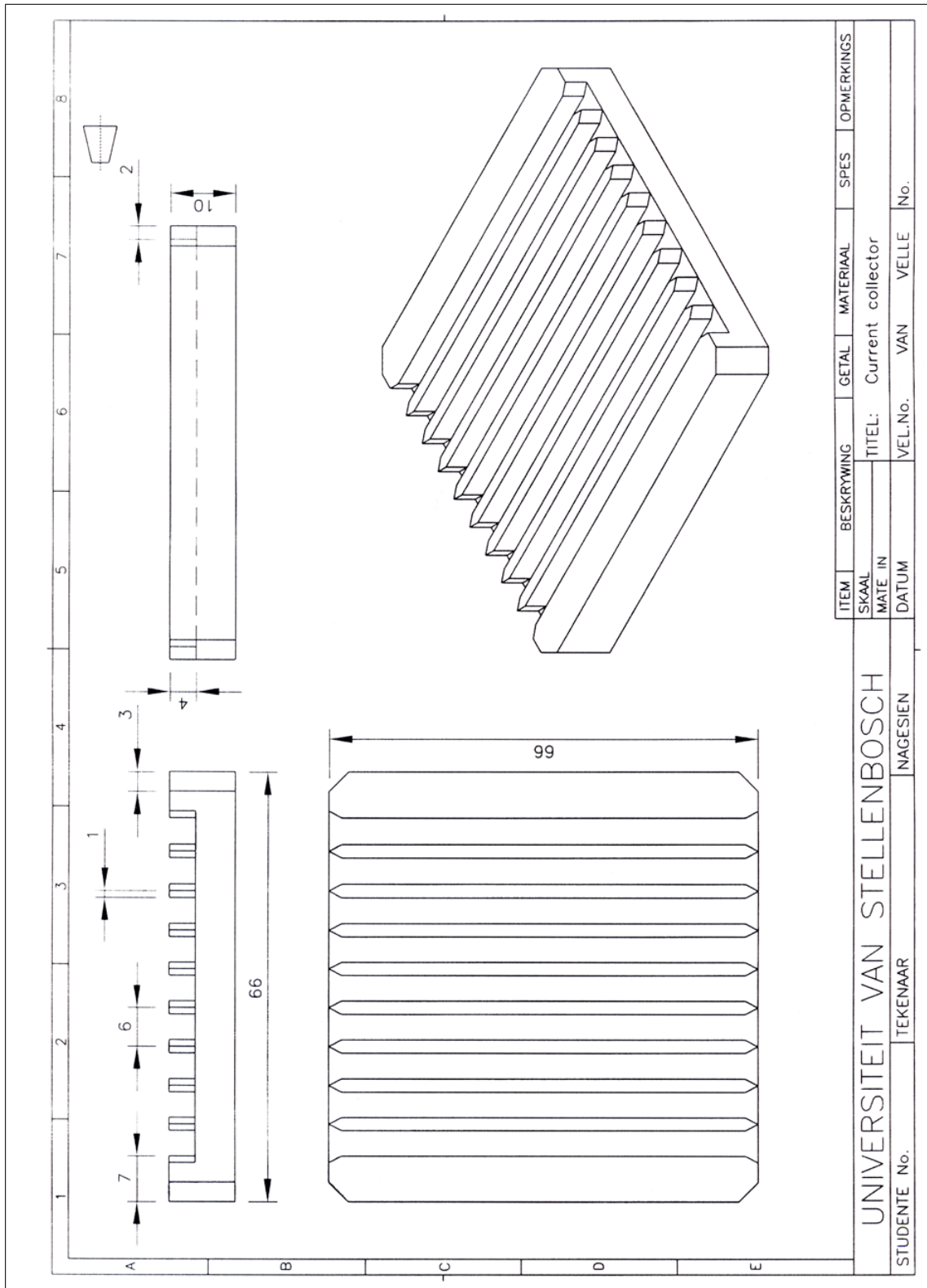


Figure D.1: Technical drawing showing initial reactor current collector

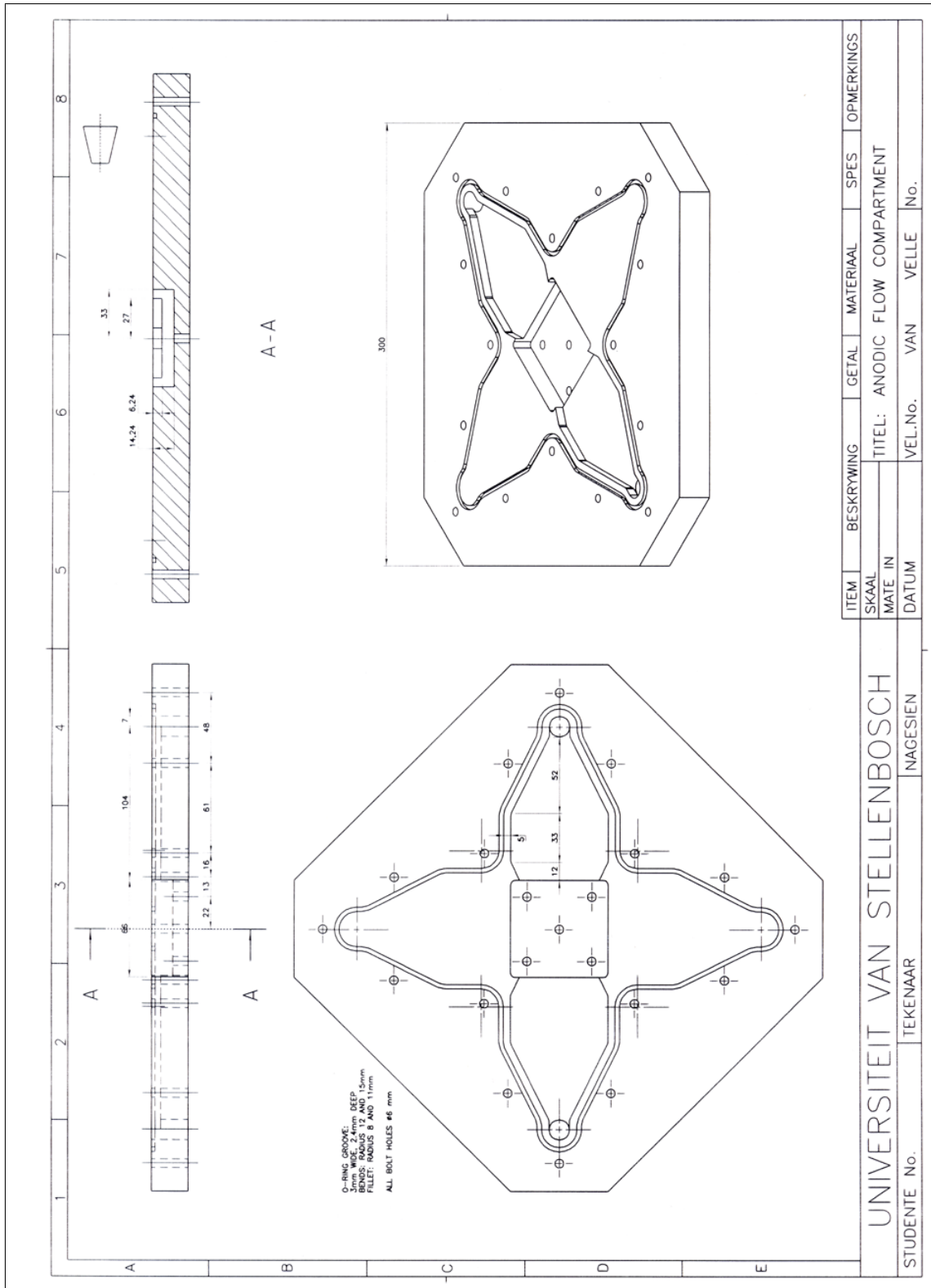


Figure D.2: Technical drawing of initial reactor anodic frame

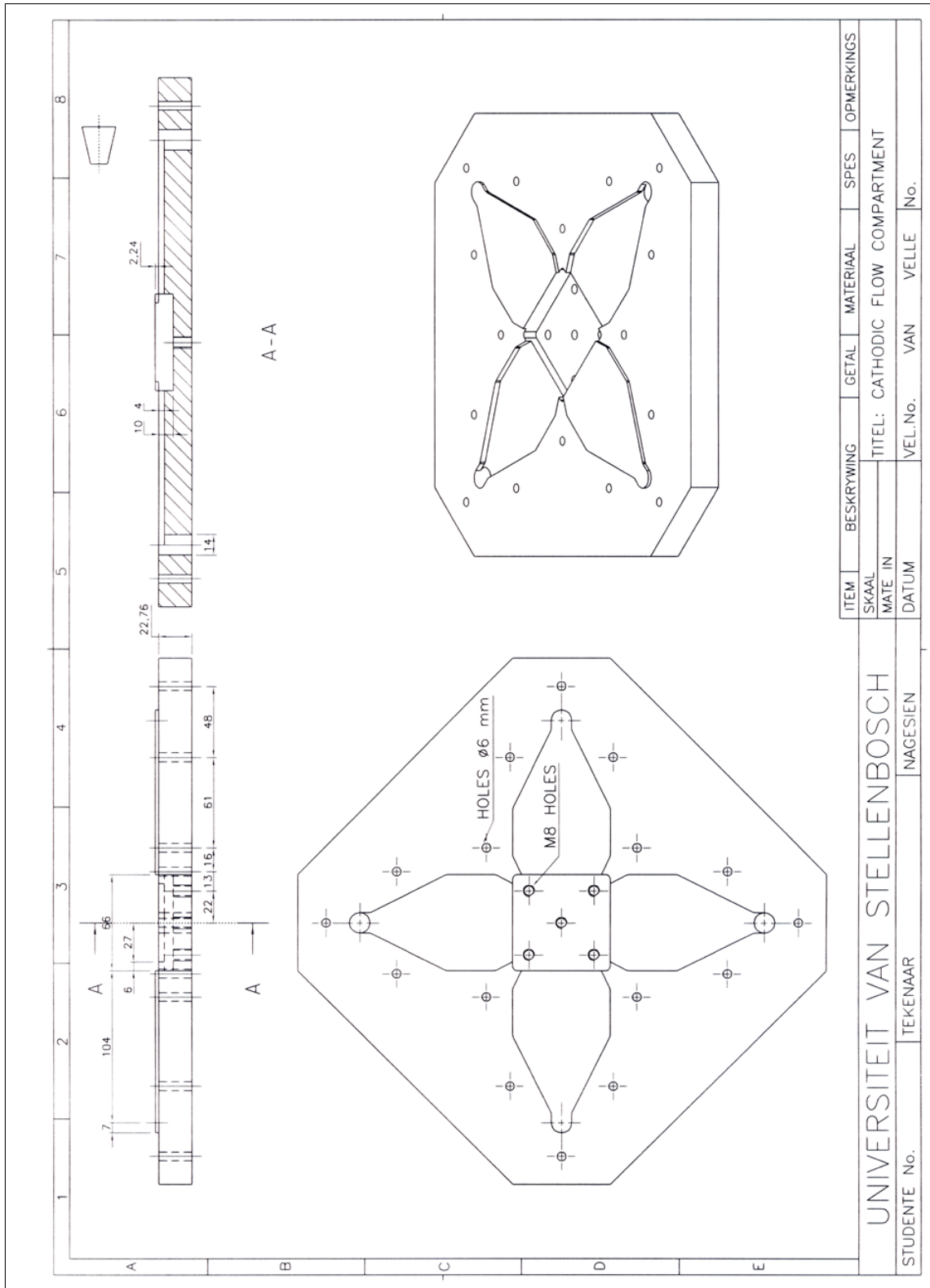


Figure D.3: Technical drawing of initial reactor cathodic frame

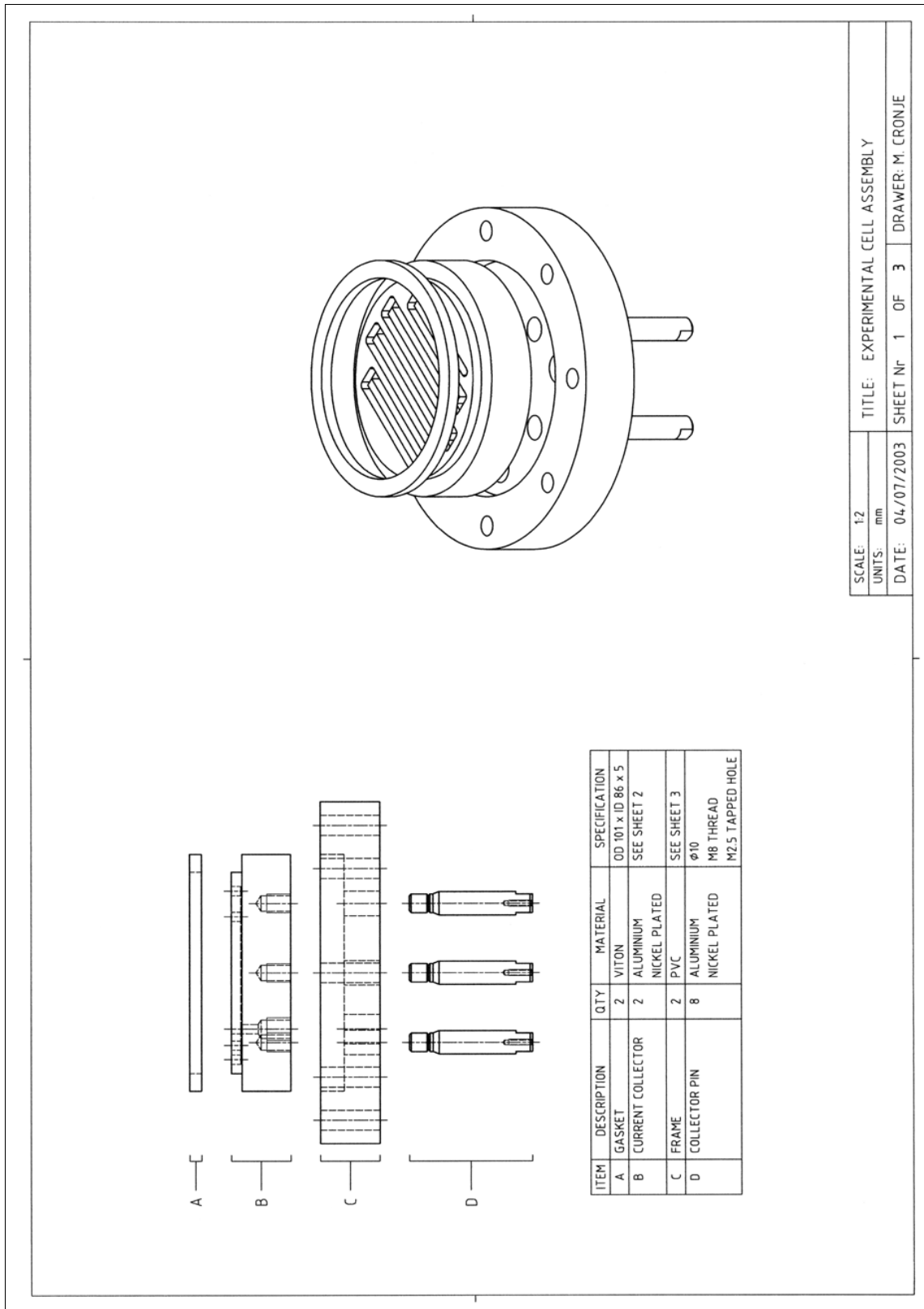


Figure D.4: Technical drawing showing all parts of the laboratory reactor

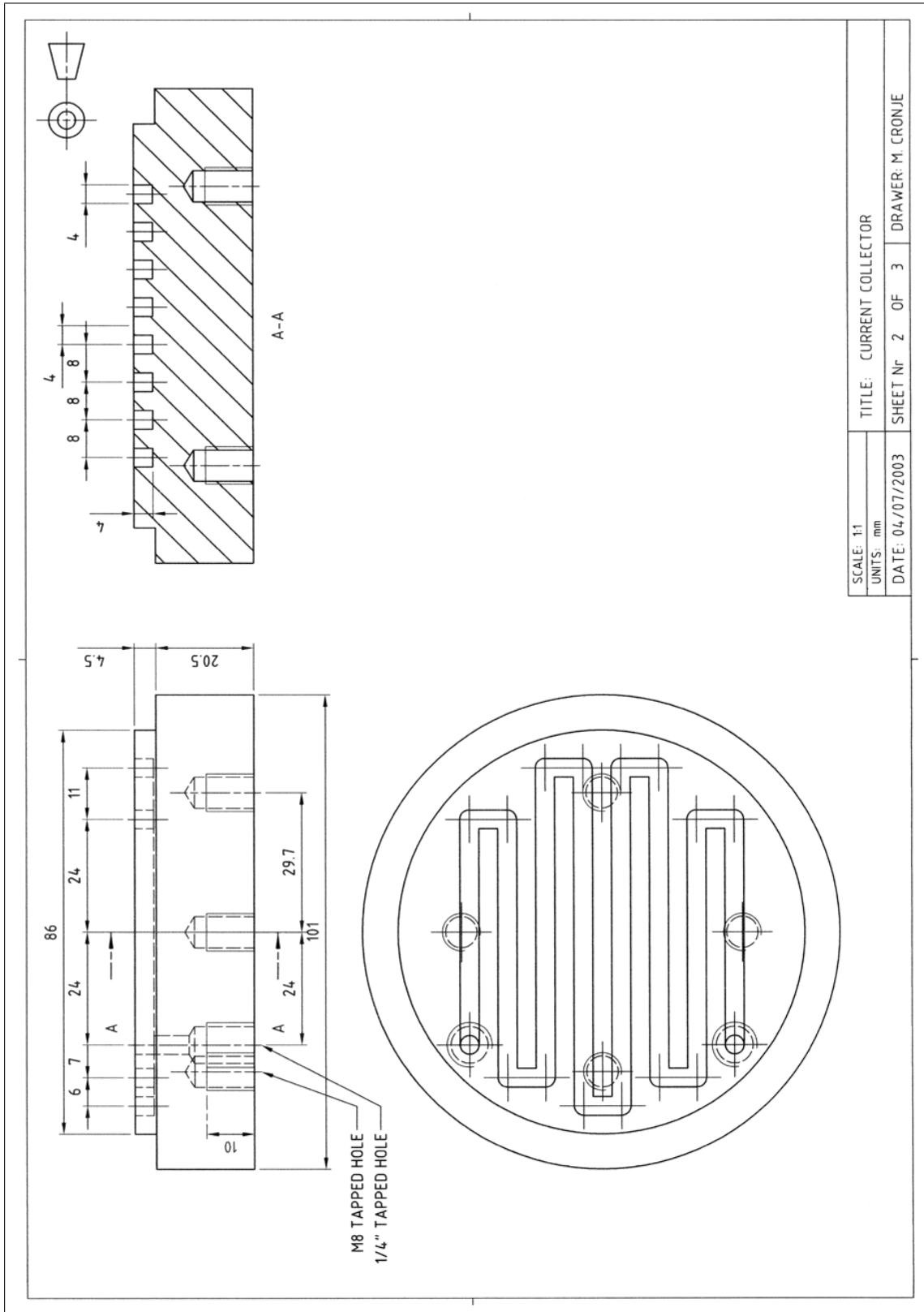


Figure D.5: Technical drawing of laboratory reactor current collector

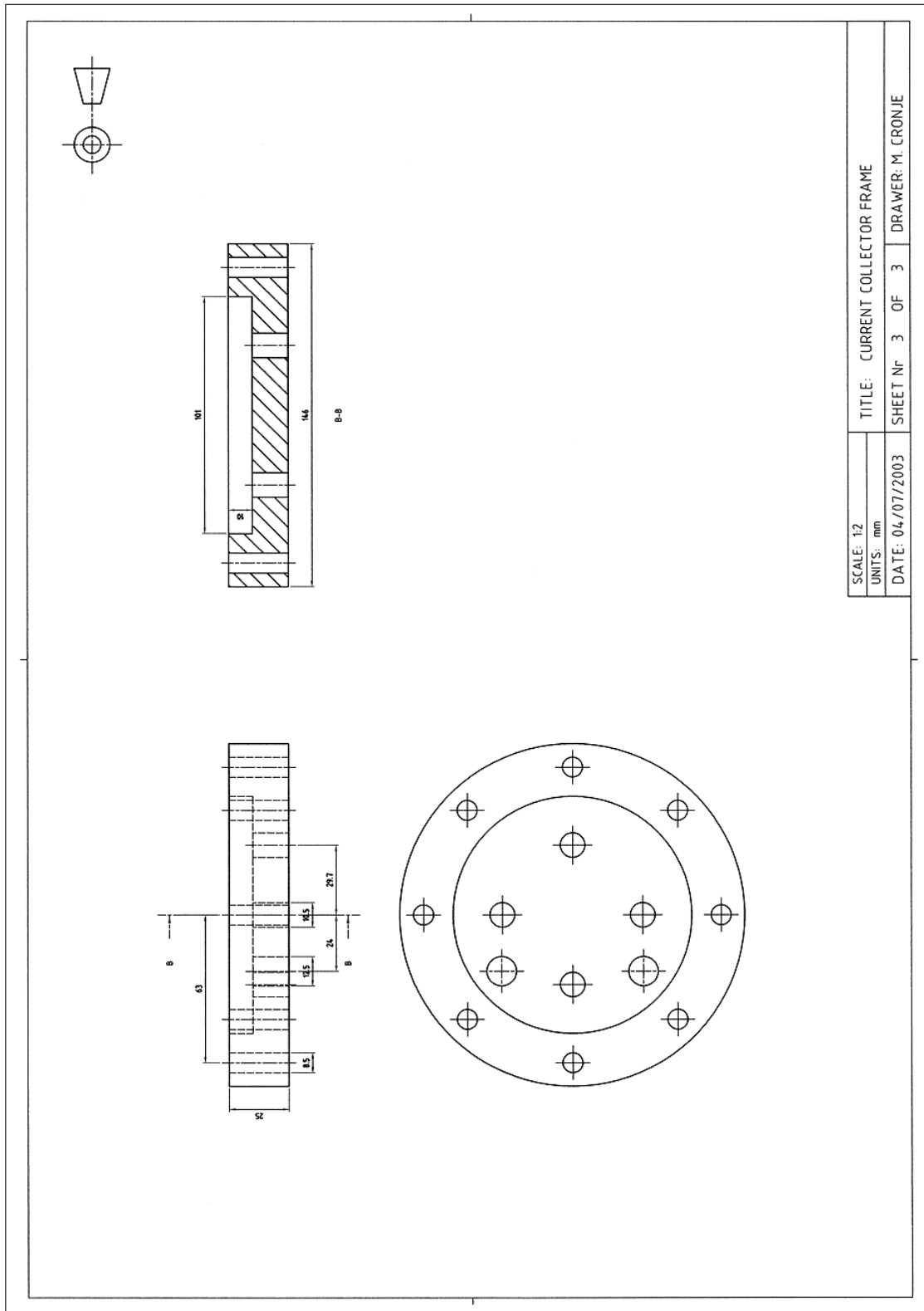


Figure D.6: Technical drawing of laboratory reactor current collector frame

Appendix E

Experimental Measurements

All of the experimental measurements taken during the experiments are presented here in tabular form. The initial experimental measurements are given in section E.1. The laboratory-scale measurements are subdivided into those taken with the nickel-plated current collectors (section E.2), and those taken with the titanium current collectors (section E.3).

E.1 Initial Work

The total organic carbon readings that were taken in the initial experiments are summarised in the table below

Table E.1: Initial experiments – total organic carbon values

Time [h]	TOC (500 L/h) [ppm C]	TOC (600 L/h) [ppm C]	TOC (700 L/h) [ppm C]
0	250	265	265
2	247	269	257
4	251	269	250
6	237	262	265
8	249	266	263
10	253	256	256
12	244	-	243

E.2 Laboratory-Scale Experiments – Nickel

Table E.2: Experimental readings (Re = 650, 20 mA, 15 lb-in, unseparated)

Time [s]	Current [mA]	Potential [V]	Concentration [ppm Ph]
0	22.7	-	50.300
60	22.3	8.14	-
120	22.1	9.42	-
180	21.9	10.28	-
240	21.9	11.18	-
300	21.8	12.81	-
600	20.3	15.29	-
900	20.7	16.90	-
1200	20.9	17.65	-
1500	21.2	18.11	-
1800	20.7	18.18	51.600
2700	20.7	18.56	-
3600	20.4	18.84	50.850
7200	19.5	18.52	49.525
18000	23.2	19.55	49.964
25200	22.5	18.83	49.113
36000	22.8	18.28	48.519
43200	21.9	17.77	49.371
55200	21.5	16.89	47.778
64878	21.8	17.08	47.165

Table E.3: Experimental readings (Re = 650, 35 mA, 15 lb-in, unseparated)

Time [s]	Current [mA]	Potential [V]	Concentration [ppm Ph]
0	36.2	-	50.900
60	35.8	14.12	-
1440	34.4	17.26	50.118

Table E.3: (continued)

2040	34.4	17.34	50.801
4140	34.6	17.21	50.173
10560	33.8	16.19	48.681
14400	35.1	15.97	48.279
20580	34.3	15.19	48.669
24660	34.3	14.98	47.300
30840	34.8	14.59	47.097
34980	33.8	14.18	47.187
41700	34.1	14.11	-
42000	34.3	14.12	-
42300	34.9	14.15	-
42503	34.8	14.14	45.791

Table E.4: Experimental readings (Re = 650, 50 mA, 15 lb-in, unseparated)

Time [s]	Current [mA]	Potential [V]	Concentration [ppm Ph]
0	50.7	-	50.1
60	48.9	17.13	-
120	52.0	19.93	-
240	51.3	20.9	-
300	51.1	21.1	-
600	51.3	21.8	-
692	-	-	49.813
900	51.4	22.1	-
1200	51.5	22.3	-
1393	-	-	49.799
1500	51.2	22.4	-
1800	51.2	22.5	-
2160	51.2	22.5	-
2520	50.5	22.5	-
2880	51.3	22.6	-
3240	51.5	22.6	-

Table E.4: (continued)

3506	-	-	47.992
3600	51.6	22.7	-
4200	51.7	22.7	-
4800	51.6	22.7	-
5400	51.3	22.7	-
6000	51.6	22.6	-
6600	51.3	22.6	-
6999	-	-	48.789
7200	51.8	22.6	-
9060	51.7	22.5	-
9900	50.9	22.4	-
10488	-	-	48.678
10800	51.6	22.4	-
12600	51.6	22.3	-
13500	51.4	22.2	-
13984	-	-	48.950
14400	51.4	22.1	-
16200	51.3	22.0	-
17486	-	-	48.545
18000	52.0	21.9	-
19920	51.8	21.8	-
20400	51.8	21.7	-
20957	-	-	48.301
21600	52.0	21.7	-
23400	50.8	21.3	-
24446	-	-	47.657
27000	50.7	21.1	-
27300	50.8	21.2	-
27600	50.9	21.1	-
27973	50.8	21.1	47.217

Table E.5: Experimental readings (Re = 650, 50 mA, 15 lb-in, separated)

Time [s]	Current [mA]	Potential [V]	Concentration [ppm Ph]
0	50.1	-	50.800
120	49.2	23.8	-
300	48.2	28.4	-
600	52.4	31.8	-
725	-	-	50.980
900	52.7	31.0	-
1200	52.9	32.1	-
1407	-	-	50.630
1500	53.2	32.1	-
1800	52.6	31.8	-
2700	52.2	32.0	-
3462	-	-	50.200
3600	52.6	31.9	-
5400	52.2	30.2	-
6897	-	-	49.617
7200	52.4	29.6	-
9000	52.7	28.6	-
10328	-	-	49.516
10800	51.9	28.1	-
14220	-	-	47.915
14400	51.9	26.5	-
17100	52.2	26.4	-
17252	-	-	48.116
17400	52.0	26.5	-
20762	-	-	49.932
20820	52.3	26.4	-
24154	-	-	47.257
24600	52.5	26.3	-
27937	52.3	25.3	45.652

Table E.6: Experimental readings (Re = 1516, 50 mA, 15 lb-in, separated)

Time [s]	Current [mA]	Potential [V]	Concentration [ppm Ph]
0	51.4	-	49.7
60	50.5	13.53	-
120	49.9	18.04	-
300	49.1	21.3	-
600	53.6	23.9	-
711	-	-	49.369
900	54.1	24.0	-
1260	54.1	24	-
1374	-	-	49.101
1800	53.7	23.7	-
2700	53.8	23.5	-
3387	-	-	48.109
3600	53.8	23.1	-
5400	54.1	22.6	-
6726	-	-	48.141
7200	53.5	22.2	-
9000	53.7	21.6	-
10076	-	-	47.391
10800	53.9	21	-
12900	53.3	19.8	-
13437	-	-	45.593
13500	53.8	19.69	-
16800	53.3	18.83	-
19560	54.0	17.4	-
20100	54.0	17.26	-
20144	-	-	44.455
23400	53.1	16.22	-
23502	-	-	43.529
26520	53.3	15.4	-
26636	53.3	15.4	42.758

Table E.7: Experimental readings (Re = 1516, 50 mA, 25 lb-in, unseparated)

Time [s]	Current [mA]	Potential [V]	Concentration [ppm Ph]
0	56.1	-	50.0
60	55.4	10.6	-
120	54.7	12.5	-
180	54.9	13.3	-
240	54.7	13.6	-
300	54.1	14.4	-
600	53.9	15.6	-
655	-	-	49.576
1200	54.1	16.7	-
1327	-	-	49.497
1800	53.6	17.0	-
3000	53.4	17.3	-
3342	-	-	48.848
3420	53.1	17.2	-
6540	52.9	17.2	-
6693	-	-	48.434
6780	53.0	17.2	-
9900	52.8	17.0	-
10142	-	-	48.967
10200	52.5	17.0	-
13528	-	-	48.458
13560	52.6	16.8	-
16800	52.7	16.7	-
16988	-	-	48.670
17100	52.8	16.7	-
20420	-	-	48.153
20460	52.8	16.5	-
23580	52.4	16.3	-
23758	-	-	47.711
23820	52.6	16.3	-
26700	52.8	16.2	-

Table E.7: (continued)

26940	52.2	16.2	-
27056	52.3	16.2	-
27107	52.1	16.2	47.337

Table E.8: Experimental readings (Re = 1516, 50 mA, 25 lb-in, unseparated)

Time [s]	Current [mA]	Potential [V]	Concentration [ppm Ph]
0	57.3	-	150.200
60	57.0	10.6	-
120	56.6	12.5	-
180	56.8	13.3	-
240	56.2	13.6	-
300	56.0	14.4	-
600	54.7	15.6	-
900	55.3	16.7	-
2040	-	-	153.277
2100	54.0	17.2	-
2880	54.2	17.2	-
3300	53.7	17.0	-
3600	53.6	17.0	-
3955	-	-	152.973
4020	53.7	16.8	-
9000	53.4	16.7	-
9600	53.3	16.7	-
9900	53.5	16.5	-
10014	-	-	151.353
10200	54.0	16.3	-
19320	54.1	16.3	-
19800	53.3	16.2	-
20029	-	-	149.626
20100	52.9	16.2	-
29756	52.0	16.2	-

Table E.8: (continued)

30047	52.9	16.2	-
30265	-	-	148.317
30347	53.0	16.2	-
39647	52.8	16.2	-
39947	52.7	16.2	-
40172	-	-	147.094
40247	52.8	16.2	-
50267	53.0	16.2	-
50447	53.0	16.2	-
50684	-	-	146.864
50747	52.7	16.2	-
60047	53.1	16.2	-
60120	-	-	145.233
60227	53.0	16.2	-
71098	-	-	144.351
71207	53.6	16.2	-
80447	53.4	16.2	-
80747	53.6	16.2	-
80962	53.3	16.2	143.709

E.3 Laboratory-Scale Experiments – Titanium

Table E.9: Experimental readings (37.2 L/h ,20 mA)

Time [h]	Concentration [ppm]	Current [mA]	Potential [V]	pH	Conductivity [μ S]	Temperature [$^{\circ}$ C]
0.0	51.418	40.9	6.09	4.91	2.9	17.5
0.25	50.683	39.6	29.4	4.34	4	17.9
0.5	50.163	39.5	27.5	4.41	5	18.9
0.75	49.562	39.6	26.5	4.38	5	19.4
1.0	50.562	39.6	25.7	4.49	5	20.3
1.25	49.196	39.7	25.3	4.43	6	20.4
1.5	50.032	40.2	24.8	4.46	7	20.8
1.75	50.147	39.7	24.9	4.49	7	22.5

Table E.9: (continued)

2.0	48.835	39.7	24.9	4.49	8	23.0
2.25	49.049	40.3	24.2	4.51	8	22.4
2.5	48.787	39.0	23.7	4.46	8	22.2
2.75	49.245	39.3	24.2	4.49	9	22.2
3.0	47.819	39.6	24.7	4.59	9	22.4
3.25	48.783	40.1	23.6	4.50	10	23.5
3.5	47.951	39.1	23.9	4.51	9	23.0
3.75	48.000	40.0	24.1	4.63	9	23.0
4.0	47.295	39.2	23.6	4.60	10	23.2

Table E.10: Experimental readings (37.2 L/h, 30 mA)

Time [h]	Concentration [ppm]	Current [mA]	Potential [V]	pH	Conductivity [μ S]	Temperature [$^{\circ}$ C]
0.0	50.544	30.6	9.83	5.12	2	19.5
0.25	50.327	30.0	23.2	4.72	4	19.2
0.5	50.092	30.0	24.6	4.72	5	20.3
0.75	49.834	29.9	24.1	4.69	6	20.8
1.0		29.8	23.8	4.72	6	21.4
1.25	49.551	29.8	23.5	4.75	7	21.7
1.5	48.979	30.7	23.6	4.78	7	22.2
1.75		30.7	23.5	4.68	8	22.9
2.0	48.867	30.0	23.3	4.76	8	22.7
2.25	48.689	30.5	23.2	4.67	8	22.8
2.5		30.1	23.1	4.69	9	22.9
2.75	48.508	30.6	23.1	4.80	9	22.8
3.0	48.162	29.9	23.2	4.71	9	20.8
3.25	48.200	30.2	23.1	-	10	-
3.5		30.3	23.2	4.63	10	20.1
3.75	47.683	30.0	22.9	4.66	9	19.7
4.0		30.7	23.0	4.66	10	19.8

Table E.11: Experimental readings (37.2 L/h, 40 mA)

Time [h]	Concentration [ppm]	Current [mA]	Potential [V]	pH	Conductivity [μ S]	Temperature [$^{\circ}$ C]
0.0	51.418	40.9	6.09	4.91	2.9	17.5
0.25	50.683	39.6	29.4	4.34	4	17.9
0.5	50.163	39.5	27.5	4.41	5	18.9
0.75	49.562	39.6	26.5	4.38	5	19.4
1.0	50.562	39.6	25.7	4.49	5	20.3
1.25	49.196	39.7	25.3	4.43	6	20.4
1.5	50.032	40.2	24.8	4.46	7	20.8
1.75	50.147	39.7	24.9	4.49	7	22.5
2.0	48.835	39.7	24.4	4.48	8	23.0
2.25	49.049	40.3	24.2	4.51	8	22.4
2.5	48.787	39.0	23.7	4.46	8	22.2
2.75	49.245	39.3	24.2	4.49	9	22.2
3.0	47.819	39.6	24.7	4.59	9	22.4
3.25	48.783	40.1	23.6	4.50	10	23.5
3.5	47.951	39.1	23.9	4.51	9	23.7
3.75	48.000	40.0	24.1	4.63	9	23.0
4.0	47.295	39.2	23.6	-	10	-

Table E.12: Experimental readings (37.2 L/h, 50 mA)

Time [h]	Concentration [ppm]	Current [mA]	Potential [V]	pH	Conductivity [μ S]	Temperature [$^{\circ}$ C]
0.0	53.042	50.0	7.53	4.99	6	20.5
0.25	50.851	51.8	13.28	4.42	20	20.8
0.5	50.488	50.4	14.29	4.26	23	22.2
0.75	49.431	50.3	14.56	4.29	26	22.5
1.0	48.521	50.3	13.88	4.24	31	22.3
1.25	49.426	50.8	13.34	4.19	36	23.7
1.5	47.714	49.6	13.66	4.09	38	25.0
1.75	47.537	49.7	12.88	4.06	36	24.2
2.0	49.053	50.1	12.62	4.02	45	25.5
2.25	47.132	49.7	12.73	4.00	46	25.8

Table E.12: (continued)

2.5	46.259	50.1	12.71	3.97	47	24.7
2.75	47.709	49.9	12.67	3.98	49	24.8
3.0	45.977	50.5	12.24	3.93	51	25.0
3.25	47.375	50.6	12.26	3.92	51	25.0
3.5	45.775	49.0	12.24	3.93	55	25.3
3.75	45.339	50.3	12.52	3.93	55	26.0
4.0	44.361	50.2	11.93	-	56	-

Table E.13: Experimental readings (25.7 L/h, 20 mA)

Time [h]	Concentration [ppm]	Current [mA]	Potential [V]	pH	Conductivity [μ S]	Temperature [$^{\circ}$ C]
0.0	52.733	20.0	-	4.76	4	18.3
0.25	50.544	18.9	13.76	4.52	7	18.0
0.5	50.495	19.4	13.82	4.58	7	18.2
0.75	50.125	19.3	13.67	4.70	7	19.2
1.0	-	19.5	13.43	4.88	8	19.7
1.25	51.389	19.1	13.47	4.84	8.7	20.2
1.5	49.506	18.6	13.27	4.82	8	20.8
1.75	49.219	19.5	13.52	4.89	8	21.0
2.0	48.769	20.0	13.57	4.83	9	21.0
2.25	48.414	19.1	13.47	4.84	10	21.3
2.5	48.441	19.2	13.39	4.91	10	21.9
2.75	47.895	20.6	13.67	4.81	10	21.8
3.0	47.547	20.3	13.57	4.80	10	22.4
3.25	47.372	19.8	13.37	4.90	11	22.5
3.5	47.356	20.4	13.49	4.81	12	22.7
3.75	46.915	19.6	12.96	4.87	12	22.8
4.0	46.730	19.4	13.11	4.89	12	22.7

Table E.14: Experimental readings (25.7 L/h, 30 mA)

Time [h]	Concentration [ppm]	Current [mA]	Potential [V]	pH	Conductivity [μ S]	Temperature [$^{\circ}$ C]
0.0	50.000	30.0	-	5.57	4	17.9
0.25	50.607	30.3	19.40	5.27	4	17.3
0.5	49.522	29.7	19.10	5.16	5	17.5
0.75	49.402	30.4	18.99	5.29	5	17.8
1.0	48.814	30.0	18.82	5.27	5	18.0
1.25	48.641	29.8	18.63	5.23	5	18.7
1.5	48.753	29.5	18.80	5.17	5	18.2
1.75	48.968	29.9	18.89	5.16	5	18.3
2.0	48.203	30.3	18.79	5.23	5	17.9
2.25	47.983	30.2	18.85	5.21	4	17.5
2.5	48.141	30.2	18.94	5.24	4	17.4
2.75	47.456	30.1	18.53	5.40	5	17.3
3.0	47.666	29.8	18.46	5.29	5	17.9
3.25	47.122	29.6	18.17	5.42	4	18.0
3.5	47.290	29.7	18.07	5.27	5	18.2
3.75	46.974	30.4	18.56	5.39	5	17.8
4.0	46.940	30.8	18.88	5.42	5	17.9

Table E.15: Experimental readings (25.7 L/h, 40 mA)

Time [h]	Concentration [ppm]	Current [mA]	Potential [V]	pH	Conductivity [μ S]	Temperature [$^{\circ}$ C]
0.0	51.055	40.0	-	4.86	4	18.3
0.25	50.415	40.4	22.2	4.57	7	17.9
0.5	49.891	40.8	20.8	4.75	8	18.0
0.75	50.475	40.2	20.8	4.75	8	18.8
1.0	49.602	40.6	20.4	4.80	8	19.3
1.25	49.435	39.4	20.1	4.80	9	19.8
1.5	49.094	40.5	20.0	4.96	9	20.4
1.75	49.153	40.3	10.9	4.97	9	20.7
2.0	49.057	39.9	19.8	4.96	9	20.9
2.25	48.888	39.2	19.7	5.00	9	21.2

Table E.15: (continued)

2.5	49.025	40.6	19.7	4.99	9	21.0
2.75	48.068	40.5	19.3	5.03	9	21.0
3.0	48.145	39.5	19.46	5.10	9	21.0
3.25	48.254	40.5	19.44	5.15	9	21.2
3.5	47.774	40.8	19.23	5.08	9	21.4
3.75	47.525	40.2	19.22	5.10	9	21.2
4.0	47.616	39.5	19.14	5.06	9	21.2

Table E.16: Experimental readings (25.7 L/h, 50 mA)

Time [h]	Concentration [ppm]	Current [mA]	Potential [V]	pH	Conductivity [μ S]	Temperature [$^{\circ}$ C]
0.0	49.895	50.0	-	5.88	2	16.5
0.25	48.802	50.2	27.6	5.35	4	16.5
0.5	48.756	50.6	26.3	5.27	3	17.5
0.75	48.322	50.3	26.2	5.33	4	17.8
1.0	48.041	50.3	26.3	5.35	4	18.8
1.25	48.027	50.8	25.9	5.41	4	19.4
1.5	47.918	49.7	25.2	5.25	4	19.3
1.75	47.454	50.3	25.4	5.33	4	19.0
2.0	47.292	50.0	24.8	5.33	4	19.0
2.25	46.668	50.5	25.9	5.42	4	18.8
2.5	46.473	50.5	25.7	5.32	5	18.8
2.75	46.807	50.5	25.2	5.29	4	18.9
3.0	46.155	50.7	25.3	5.46	5	18.9
3.25	45.790	50.5	25.5	5.31	5	19.3
3.5	45.570	50.2	24.9	5.41	5	19.2
3.75	45.570	50.6	24.8	5.28	5	18.9
4.0	45.008	49.9	25.2	5.28	5	18.9

Table E.17: Experimental readings (11.5 L/h, 20 mA)

Time [h]	Concentration [ppm]	Current [mA]	Potential [V]	pH	Conductivity [μ S]	Temperature [$^{\circ}$ C]
0.0	52.144	20.9	-	4.59	3	19.8
0.25	50.961	19.5	14.70	4.58	6	19.5
0.5	50.404	20.9	15.42	4.60	8	19.8
0.75	50.161	20.0	15.41	4.58	8	20.5
1.0	49.753	20.2	15.35	4.64	9	21.4
1.25	49.969	20.2	15.19	4.70	10	21.8
1.5	49.612	20.1	15.11	4.74	10	22.0
1.75	49.205	19.9	14.91	4.79	11	22.5
2.0	48.977	20.0	14.87	4.87	10	22.8
2.25	48.728	19.6	14.87	4.90	10	22.5
2.5	47.864	20.0	14.79	4.93	10	22.7
2.75	48.152	19.6	14.95	4.94	11	22.8
3.0	47.904	19.3	14.87	5.01	11	22.8
3.25	47.565	19.5	14.78	4.96	11	23.0
3.5	47.703	19.5	14.84	5.00	12	22.9
3.75	47.566	20.2	15.08	5.00	11	24.0
4.0	47.246	19.7	15.08	5.01	11	24.3

Table E.18: Experimental readings (11.5 L/h, 30 mA)

Time [h]	Concentration [ppm]	Current [mA]	Potential [V]	pH	Conductivity [μ S]	Temperature [$^{\circ}$ C]
0.0	50.088	30.0	-	5.21	3	22.2
0.25	49.356	30.3	19.48	4.99	3	21.4
0.5	49.520	29.5	19.51	5.25	4	21.5
0.75	49.351	30.8	20.0	5.18	4	21.8
1.0	49.410	30.6	20.2	5.25	5	22.2
1.25	48.878	30.4	20.3	5.18	5	22.5
1.5	-	-	-	-	-	-
1.75	48.810	29.5	20.1	5.19	5	22.5
2.0	48.257	29.9	20.3	5.23	5	22.2
2.25	48.148	30.1	20.5	5.18	5	21.7

Table E.18: (continued)

2.5	48.284	29.7	20.7	5.25	5	21.8
2.75	-	-	-	-	-	-
3.0	-	30.0	20.7	5.33	5	22.3
3.25	48.202	30.3	20.7	5.36	5	22.4
3.5	47.449	30.9	20.8	5.32	5	22.2
3.75	47.592	29.8	20.5	5.39	6	22.3
4.0	47.494	30.7	20.6	5.45	6	21.8

Table E.19: Experimental readings (11.5 L/h, 40 mA)

Time [h]	Concentration [ppm]	Current [mA]	Potential [V]	pH	Conductivity [μ S]	Temperature [$^{\circ}$ C]
0.0	50.000	40.0	-	4.62	3	18.0
0.25	48.607	39.7	28.4	4.59	6	17.8
0.5	48.277	40.2	27.9	4.66	8	18.3
0.75	-	40.5	27.6	4.65	9	18.7
1.0	47.667	40.1	27.1	4.80	9	19.3
1.25	47.567	39.8	27.0	4.74	10	19.8
1.5	47.571	39.7	26.8	4.75	10	20.4
1.75	46.629	39.9	26.7	4.82	11	20.9
2.0	46.147	40.5	26.6	4.80	11	20.9
2.25	46.651	39.5	26.6	4.90	11	20.8
2.5	46.314	39.6	26.4	4.88	12	21.2
2.75	46.828	40.3	26.3	4.87	11	20.8
3.0	46.579	39.8	26.1	5.02	11	20.8
3.25	-	-	-	-	-	-
3.5	45.627	39.8	26.1	5.04	11	20.5
3.75	45.592	40.3	26.2	5.02	11	20.8
4.0	45.267	40.3	25.9	5.08	11	21.3

Table E.20: Experimental readings (11.5 L/h, 50 mA)

Time [h]	Concentration [ppm]	Current [mA]	Potential [V]	pH	Conductivity [μ S]	Temperature [$^{\circ}$ C]
0.0	50.635	50.0	-	4.67	3	17.5
0.25	-	50.0	24.8	4.57	6	17.3
0.5	50.472	49.6	24.5	4.63	7	17.4
0.75	49.960	50.6	24.3	4.69	8	17.9
1.0	52.542	50.4	24.2	4.75	8	18.7
1.25	49.925	50.3	24.0	4.78	9	18.5
1.5	49.461	50.5	23.9	4.95	9	18.9
1.75	49.493	50.3	23.5	4.95	9	18.8
2.0	49.146	50.3	23.6	4.96	9	18.8
2.25	49.156	50.8	23.7	4.98	9	18.5
2.5	48.989	50.1	23.4	5.02	9	18.3
2.75	48.637	51.2	23.3	5.06	9	18.5
3.0	48.331	50.9	23.1	5.13	9	18.9
3.25	48.047	50.8	22.9	5.25	9	19.3
3.5	48.060	50.9	22.8	5.22	9	19.7
3.75	47.930	50.4	22.8	5.25	9	19.4
4.0	47.769	50.6	22.7	5.34	9	19.4

Table E.21: Experimental readings (37.2 L/h, 50 mA, 60 ppm)

Time [h]	Concentration [ppm]	Current [mA]	Potential [V]	pH	Conductivity [μ S]	Temperature [$^{\circ}$ C]
0.0	58.249	51.0	-	4.47	3	17.8
0.25	59.375	51.7	19.00	3.97	34	19.8
0.5	59.336	51.2	20.7	3.81	58	20.8
0.75	58.564	50.7	20.3	4.20	35	21.3
1.0	57.666	50.1	19.9	4.08	51	22.3
1.25	59.489	50.7	19.4	4.03	50	23.2
1.5	56.121	51.2	19.12	3.88	40	22.3
1.75	54.695	50.0	19.00	3.98	76	23.2
2.0	56.925	51.2	19.07	3.98	64	23.9

Table E.21: (continued)

2.25	56.822	51.3	18.98	4.04	45	24.4
2.5	55.020	49.5	19.31	4.02	51	24.8
2.75	55.750	50.7	19.53	3.98	72	24.5
3.0	57.074	51.3	19.05	3.98	59	24.8
3.25	55.058	49.6	19.32	3.94	55	24.2
3.5	54.454	50.3	19.42	3.95	55	26.2
3.75	53.657	50.2	19.13	3.91	59	24.9
4.0	54.835	50.4	19.15	3.94	65	25.3

Table E.22: Experimental readings (37.2 L/h, 50 mA, 40 ppm)

Time [h]	Concentration [ppm]	Current [mA]	Potential [V]	pH	Conductivity [μ S]	Temperature [$^{\circ}$ C]
0.0	40.732	50.0	-	4.38	26	16.3
0.25	41.814	50.9	19.9	4.26	27	18.4
0.5	39.246	51.8	24.7	4.18	30	20.3
0.75	40.963	50.4	25.5	4.07	31	20.8
1.0	39.890	51.3	25.6	4.02	33	22.0
1.25	38.989	51.7	24.5	4.04	33	23.7
1.5	38.756	50.8	25.8	4.03	35	22.8
1.75	38.107	50.8	25.8	4.02	34	23.7
2.0	38.786	50.0	25.6	4.02	34	24.5
2.25	37.247	50.1	25.3	4.03	34	24.4
2.5	38.880	50.4	25.3	4.04	34	24.5
2.75	37.288	50.5	25.0	4.04	33	24.4
3.0	37.390	49.9	25.4	4.04	34	23.9
3.25	37.178	50.7	25.3	4.05	34	25.3
3.5	37.686	50.5	25.2	4.07	33	25.7
3.75	36.525	50.4	24.8	4.06	34	25.2
4.0	37.554	50.9	24.7	-	34	-